Nucleic Acids, Water and Protons: Triplexes, Duplexes and Uniplexes

Laurence Lavelle

A Dissertation Presented to the Faculty of Princeton University

in Candidacy for the Degree of Doctor of Philosophy

Recommended for Acceptance by the Department of Chemistry

Program in Molecular Biophysics

June 1996

ACKNOWLEDGMENTS

My parents, Eileen and John, who have been wonderful in giving me the personal freedom to pursue my desire to understand this world through the eyes of science. No matter how unfamiliar the terrain, to them or me, their love and acceptance made it possible.

The same must be said of all my family, friends and former colleagues who I have missed but not forgotten as I studied overseas.

Tanya, a special thank you, you have supported me with much understanding and love through everything.

To my thesis committee, Bob Austin, Ted Cox, Jack Fresco and Clarence Schutt, it was a maturing and pleasant experience to have a supportive committee.

To a friend through thick and thin, Bob Austin, and the best second reader any student could ask for.

To my supervisor, Jack Fresco, who has convinced me that nucleic acids have far greater structural diversity than that depicted by the double helix.

ABSTRACT

Analysis of the spectral change on melting the triplex, $d(C^+\text{-}T)_6{:}d(A\text{-}G)_6{\cdot}d(C\text{-}T)_6$, in neutral and acidic solution shows that the third strand dC residues are protonated at pH 7.0, far above their intrinsic pK_a. Involvement of these residues in ion-dipole interactions is shown by reduced triplex stability above 0.9M Na^+, and enhanced triplex stability with increasing $[H^+]$. Energy minimization of C:G·C and C^+:G·C triplets shows only the latter are feasible. Manning condensation-screening theory was extended to pH-dependent third strand binding to include the H^+ contribution to the electrostatic free energy, giving $\frac{\partial T_m}{\partial(\ln[H^+])} = \frac{1}{2}\frac{\Delta n_2}{Z_2}\frac{R(T_m)^2}{\Delta H_2}$ and a value of $\Delta n_2 = 5.5$ at pH 7, in good agreement with ~6 third strand dC residues/ mole triplex. For triplexes with C^+:G·C triplets, formation and dissociation is thus mediated by proton uptake and release, i.e., a proton switch. Using CD spectroscopy, it was found that at low pH the Watson-Crick antiparallel duplex $d(A\text{-}G)_6{\cdot}d(C\text{-}T)_6$ converts to a parallel Hoogsteen duplex $d(A\text{-}G)_6{\cdot}d(C^+\text{-}T)_6$. The effect of a variety of salts and organic compounds on the stability of several triplexes and their core duplexes was studied. Triplex stability follows the Hofmeister series for anions and the water structure-making ability of organic cations and low molecular weight alcohols. These findings suggest that solutes that favor water structure induce partial target duplex unwinding and removal of water therefrom, facilitating the binding of a third strand in the major groove. Modeling of a novel nucleic acid secondary structure (α-DNA) formed by $d(A\text{-}G)_{6\text{-}20}$ as a result of an *intramolecular*, acid-induced, coil → helix transition confirms that this helix lacks base stacking and pairing, and shows it is maintained by hydrogen

and ionic bonds between the dA^+ residues, which lie approximately parallel to the helix axis, and the n-1 backbone phosphates, somewhat like the -C=O···H-N- longitudinal interactions in a protein α-helix. Modeling of $d(C^+\text{-}T)_5$ confirms that this repeating sequence is also capable of forming the α-DNA structure.

CONTENTS

V. Other possible α-DNA analogs, e.g., $d(C^+-T)_n$

I. Introduction

This thesis contains spectroscopic and modeling studies of unusual nucleic acid structures (non Watson-Crick duplexes) and extensive thermodynamic analysis of the solution conditions that affect their stability. As each chapter is self-contained, this introduction provides an overview and guide to the thesis contents and discusses the relevance of the results of each chapter to current and future research. The structures investigated are very different, ranging from three-stranded helices (triplexes) to single stranded ones (uniplexes). These structures share a commonality in that the stability and hence the existence of each structure is more strongly dependent on its environment than the Watson-Crick duplex, which is known to be structurally viable under a wider variety of solution conditions.

Chapter 2 shows that formation of the triplex, $d(C^+\text{-}T)_6{:}d(A\text{-}G)_6{\cdot}d(C\text{-}T)_6$, is only possible as long as the third strand dC residues are protonated. That is, triplex formation and dissociation are mediated by proton uptake and release, i.e., a proton switch. The difference spectral analysis utilized in chapters 2 and 3 is applicable to other nucleic acid structures that are believed to involve protonated C residues above ~pH 4.5, including parallel Hoogsteen duplexes (1,2), various non-Watson-Crick multistranded structures such as poly[d(C)] and poly[r(C)] (3), $d(C\text{-}T)_n$, and $d(C_nT_n)$ (4-6) in which dC residues are required in the base pairs $C^+{\cdot}C$, $C^+{\cdot}T$, and $C{\cdot}T$ for a number of proposed novel structures (parallel and antiparallel duplexes, tetraplexes).

Chapter 3 continues the analysis of solution conditions on triplex stability, with an extensive experimental study of the triplexes, $d(C^{+}\text{-}T)_6$:$d(A\text{-}G)_6$·$d(C\text{-}T)_6$, $d(T)_{21}$:$d(A)_{21}$·$d(T)_{21}$, Poly r(U:A·U) and their respective core duplexes in the presence of varying concentrations of a variety of inorganic and organic anions and cations, cationic lipids, low molecular weight alcohols, SDS, coralyne, trehalose, glycerol, low molecular weight polyethylene glycols, and DMSO. The results show that water structure-breaking solutes decrease the stability of triplexes, while water structure-making solutes enhance their stability. This work provides a basis for understanding solution conditions that affect triplex stability, and should prove useful in the development of third-stand binding for diagnostic and possible therapeutic applications. In addition, as it thereby becomes possible to significantly enhance stability of short oligonucleotide triplexes, suitable solution conditions may be found to obtain crystals of a triplex in a well ordered lattice, currently a major obstacle in obtaining single crystal structural information on triplexes.

One of the findings of chapter 3 is that triplex stability is enhanced by compounds that are known to dehydrate duplexes. Possibly, then, much greater triplex stabilization can be achieved by direct covalent linkage of hydrophobic groups to the bases and/or phosphodiester backbone of the third strand. In fact, a phosphodiester backbone derivative with a covalently attatched organic cation should facilitate third strand binding by favorable electrostatic interactions between the positively charged nitrogen and the high negative charge density of the other strands, and exclusion of water in the local environment by the alkyl group.

Chapter 4 discusses the modeling of a novel nucleic acid secondary structure (α-DNA) formed by the sequence $d(A^+\text{-}G)_{6\text{-}20}$. As shown by solution studies, this uniplex forms by an intramolecular, cooperative, acid-induced, coil $\rightarrow$ helix transition, is apparently left-handed, lacks base stacking and pairing, and maintained by hydrogen and ionic bonds between dA^+ residues and the phosphodiester backbone. Besides predicting some of these observations, the modeling showed that the dA^+ residues lie approximately parallel to the helix axis, interacting with the n-1 backbone phosphates, somewhat like the -C=O···H-N- longitudinal interactions in a protein α-helix. The dG residues, on the other hand, have no apparent interaction with any other component of the helix; rather, they are unrestricted and accessible to bulk solvent.

Continuing studies of this unique structure are in progress and initial diffraction data have been collected on concentrated samples of $d(A^+\text{-}G)_{10}$ (gels) at different temperatures. The objective is to obtain diffraction data on this sample at pH 4.0 and 7.0 with the expectation that under acidic conditions the dA^+-phosphate repeat will be seen, while at neutrality the expected 3.4 Å interplaner distance between the stacked base tetrads will be seen. If other structural information can also be obtained, it can be used as further constraints in subsequent modeling efforts.

Chapter 5 discusses the modeling of $d(C^+\text{-}T)_5$ and confirms that additional uniplexes (α-DNA analogs) are stereochemically possible and energetically feasible.

Clearly, the ability of the hydrogen cation to induce non-Watson-Crick nucleic acid structures should not be underestimated. It is indeed conceivable that a proton switch

between significantly different conformations can modulate the accessible informational content of various nucleic acid-containing structures.

References

1. Liu, K., Miles, H. T., Frazier, J. and Sasisekharan, V. (1993) *Biochemistry.* **32,** 11802-9.
2. Lavelle, L., and Fresco, J. R. (1995) *Nucleic. Acids. Res.* **23**, No.14, 2692-2705.
3. Antao, V. P. and Gray, D. M. (1993) *J. Biomol. Struct. Dyn.* **10**, 819-39.
4. Gehring, K., Leroy, J. L. and Gueron, M. (1993) *Nature.* **363**, 561-5.
5. Jaishree, T. N. and Wang, A. H. J. (1993) *Nucleic. Acids. Res.* **21**, 3839-44.
6. Leroy, J. L., Gehring, K., Kettani, A. and Gueron, M. (1993) *Biochemistry.* **32,** 6019- 31.

II. UV spectroscopic identification and thermodynamic analysis of protonated third strand deoxycytidine residues at neutrality in the triplex $d(C^+-T)_6$:[$d(A-G)_6$·$d(C-T)_6$]; evidence for a proton switch

Laurence Lavelle and Jacques R. Fresco

published in Nucleic Acids Research (1995) **23**, 2692-2705

Near-UV difference spectral analysis of the triplex formed from $d(C-T)_6$ and $d(A-G)_6$·$d(C-T)_6$ in neutral and acidic solution shows that the third strand dC residues are protonated at pH 7.0, far above their intrinsic pK_a. Additional support for ion-dipole interactions between the third strand dC residues and the G·C target base pairs comes from reduced positive dependence of triplet stability on ionic strength below 0.9M Na^+, inverse dependence above 0.9M Na^+, and strong positive dependence on hydrogen ion concentration. Molecular modeling (AMBER) of C:G·C and C^+:G·C base triplets with the third strand base bound in the Hoogsteen geometry shows that only the C^+:G·C triplet is energetically feasible. van't Hoff analysis of the melting of the triplex and target duplex shows that between pH 5.0 and 8.5 in 0.15M NaCl / 0.005M $MgCl_2$ the enthalpy of melting ($\Delta H°_{obs}$) varies from 5.7 to 6.6 kcal.mol^{-1} for the duplex in a duplex mixture, and from 7.3 to 9.7 kcal.mol^{-1} for third strand dissociation in the triplex mixture. We have extended the condensation-screening theory of Manning to pH-dependent third strand binding. In this development we explicitly include the H^+ contribution to the electrostatic free energy and obtain $\frac{\partial T_m}{\partial(\ln[H^+])} = \frac{1}{2}\frac{\Delta n_2}{Z_2}\frac{R(T_m)^2}{\Delta H_2}$. The number of protons released in the dissociation of the third strand from the target duplex at pH 7.0, Δn_2, is thereby calculated to be 5.5, in good agreement with ~6 third strand dC residues per mole of triplex. This work shows that when third strand binding requires protonated residues that would otherwise be neutral, triplex formation and dissociation are mediated by proton uptake and release, i.e., a proton switch. As a by-product of this study, we have found that at low pH the Watson-Crick duplex $d(A-G)_6$·$d(C-T)_6$ undergoes a transition to a parallel Hoogsteen duplex $d(A-G)_6$·$d(C^+-T)_6$.

2.1 Introduction

Nucleic acid triplexes hold much current attention, in large measure because of the possibilities for exploiting third strand binding as an artificial mechanism for the control of gene expression (reviewed in 1,2) and as a tool for site specific delivery of reagents to genomes (e.g.,3). It is therefore important to understand the molecular mechanisms that underlie recognition of target base pairs by third strand residues. The targets of interest for third strand binding are Watson-Crick helices with the base pairs A•T/U and G•C, arranged in homopurine•homopyrimidine segments, since it is in such sequences that the target pairs are most strongly and accurately recognized, i.e., bound specifically by third strand residues. In the present work, the issue of primary concern is the way a G•C target pair is recognized by a third strand cytidine residue.

The G•C base pair was originally shown to be bound by third strand C or G residues in studies with polyribonucleotides (4,5). In those studies it was shown that the interaction of C with G•C base pairs is at best weak at neutrality, being considerably stabilized as the pH is decreased. These observations were reinforced in the later studies of Morgan and Wells (6) and Thiele and Guschlbauer (7); the rationale was given clear expression in the model building study of Arnott et al. (8), who showed that addition of a proton to N3 of C enables that base to form two rather than one hydrogen bond (H-bond) with G (or I) of a target base pair in the Hoogsteen arrangement, thus forming a base triplet that is isostructural with U:A•U and T:A•T. It is this rationale that has been used to explain the stabilization at low pH of intramolecular triplexes with homopyrimidine third strands i.e. H-DNA (9) and intermolecular triplexes with poly(C) third strands (10).

Since the pK_a of CMP and dCMP are 4.3 and 4.6 respectively at 25 °C, this raises the question of the structure of the C:G•C triplet at neutrality or above, where biologically relevant triplex formation is likely to occur *in vivo*. The question receives added impetus from reports that some dC-rich third strands can bind productively to targets at neutrality or above (11-13). It is also of interest to know whether under physiological conditions C:G•C triplets involve two H-bonds between third strand dC residues and their target dG residues, as has been observed only below pH 6 at very high third strand concentration by NMR (14,15), or instead only one H-bond as the conventional wisdom suggests (e.g., 13,16), i.e., at neutrality the dC residue is neutral. An effort to address this question was made using NMR on a sequence forming a short intramolecular triplex with C:G•C triplets (17). While imino protons on dC residues were observed at neutrality, they could not be quantitated, so that the data was not amenable to thermodynamic analysis. Hence, we undertook a different spectroscopic approach to address these issues.

Thus we have employed UV spectroscopy to compare the states of protonation of dC residues in the third strand $d(C\text{-}T)_6$, when it binds to the target duplex $d(A\text{-}G)_6 \cdot d(C\text{-}T)_6$. Stretches of such duplex sequences are well known in eukaryotic genomes, particularly in promoter and gene switch regions, where they are thought to be prone to intramolecular triplex formation (H-DNA) (1,9). The approach taken depends on two considerations. One, when the third strand dissociates from the target strands well above the pK_a for dC, the nature of the accompanying spectral change will depend on whether or not the third strand dC residues in the triplex are protonated. This is because the spectra of neutral and protonated dC are markedly different, so that upon dissociation of the third strand the dC

residues will lose a proton if bound by two H-bonds, but undergo no such large characteristic spectral change if held by just one H-bond. The second consideration stems from the fact that if the third strand dC residues are protonated at neutrality, then the stability of the triplex should show inverse dependence of stability on ionic strength.

The observations presented below are consistent with a two H-bond interaction at neutrality and above. Moreover, a thermodynamic analysis of the pH and ionic strength dependencies provides quantitative insights into the nature and properties of the C^+:G•C base triplet. Finally, molecular modeling of the base triplets C:G•C, C^+:G•C and T:A•T show C^+:G•C to be the most stable and the probability of formation of a C:G•C triplet with one H-bond to be extremely low, due to significant repulsion between the lone pairs on N7 of dG and N3 of dC in the third strand. These results imply that the limited availability of free protons within a cell can serve as a switch for binding of third strands with neutral residues that must be protonated in the triplex.

2.2 Materials and Methods

Samples

$d(A\text{-}G)_6$ and $d(C\text{-}T)_6$ were synthesized using standard phosphoramidite chemistry on an Applied Biosytems 380B synthesizer. The oligomers were purified by reverse phase HPLC (0.1M triethylammonium acetate pH 7.0 / acetonitrile) and ion exchange HPLC (5M urea, 20mM sodium phosphate pH 6.0 / 5M urea, 20mM sodium phosphate, 1M sodium sulfate pH 6.0) and desalted by reverse phase chromatography using C18 Sep-Pak. Purity was checked using reverse phase HPLC and PAGE on 16% denaturing gels

after ^{32}P 5'-end labeling the oligomers, confirming their homogeneity. The purified oligomers were stored dry at -20 °C. Molar extinction coefficients determined after phosphodiesterase I digestion $\varepsilon_{260} = 9890$ for $d(A\text{-}G)_6$ and $\varepsilon_{260} = 8510$ for $d(C\text{-}T)_6$ at 25 °C in 2.6 x 10^{-5}M Tris pH 7.4 / 2.4 x 10^{-5}M $MgCl_2$, were used to determine oligomer concentration.

Unless otherwise stated, triplexes were prepared in a *mixing buffer* of 0.15M NaCl/ 0.005M $MgCl_2$/0.01M cacodylate, titrated to the desired pH. Triplex mixtures were made with equimolar stocks of the two strands; after forming the duplex, a stoichiometric amount of the third strand was added.

UV Spectroscopy and Melting Profiles

Absorption spectra and thermal melting profiles were determined in a computer driven AVIV 14DS spectrophotometer equipped with a thermoelectrically controlled holder. All samples were made with ddH_2O and degassed by bubbling helium through the solution. Filtered, dry air was passed through the cell compartment to prevent condensation on the cells at low temperatures. Flow rate was set low enough so as not to create a temperature gradient between the sample and the cell holder, which was confirmed by monitoring the temperature in the sample and cell holder during trial melting profiles. For melting experiments, spectral data were measured every 1 nm at 1 °C intervals. Temperature was raised slowly enough to provide equilibrium melting profiles. T_m values obtained from the transition midpoint ($\alpha = ½$) and from the maximum of the first derivative were the

same. Sample integrity and hysteresis were checked by measuring each melting profile at least twice, with no significant differences observed ($T_m \pm 0.5$ °C).

The melting of duplex and triplex structures are each represented as a series of difference spectra between the spectrum at any temperature, T, and that at 1 °C, projected in 3-D to make evident component transitions over a broad wavelength range. These 3-D melting representations were generated using AXUM 3.0 (18) and are plotted in Figures 1A-C, on the same scale, with wavelength every 1 nm (x-axis); temperature every 5 °C (y-axis); absorbance difference (z-axis).

CD Spectroscopy

CD spectra from 320 to 200 nm, every 0.2 nm (1 sec. average), with a 1.5 nm bandwidth were recorded at 1 °C on a computer-driven AVIV 62DS CD spectrometer with a thermoelectrically controlled cell holder. The cell compartment was continuously purged with dry N_2. The data was smoothed by a least-squares polynomial fit of 7th order.

Molecular Modeling

This was done on a PC (Intel 486DX, 33MHZ, 16MB RAM) with the program Amber as part of HyperChem (19). All parameters are those of Amber 3.0A (20), using the standard unmodified all-atom force field. For the protonated form of N1-methylcytosine, all the base charges are those of Amber 3.0A but for a proton on N3. Energy minimization of each base triplet alone, T:A•T, C^+:G•C and C:G•C, with a methyl substituent at the glycosyl bond position of each base, was performed using a conjugate gradient method

(Polak-Ribiere) and convergence was set at 0.1 kcal.Å^{-1}.mol^{-1} for the rms gradient. No cutoff distance was used for nonbonded interactions and a distance dependent dielectric constant was used as a model solvent. No constraints were used in the energy minimizations.

2.3 Theory

Thermodynamic Analysis of the Triplex Transition

The melting profile for the triplex shows two well resolved transitions corresponding to the dissociation of the third strand from the core duplex, and for the melting of duplex at much higher temperature. Assuming there is no strand overlap at the low strand concentration at which the triplexes were formed (10^{-5} M), the transitions can be treated as separate intermolecular transitions; and because the strands are only 12 residues in size, each transition can be treated using a two-state analysis. This is consistent with the spectral data showing wavelength independence of T_m (Figures 1A-F). The first transition, i.e., the dissociation of the third strand from the core duplex can be described by the equilibrium:

$$\mathcal{T} \leftrightarrow \mathcal{D} + S$$

where, $\mathcal{T} \equiv$ triplex = d(C$^+$-T)$_6$:[d(A-G)$_6$·d(C-T)$_6$]; $\mathcal{D} \equiv$ duplex = [d(A-G)$_6$·d(C-T)$_6$] and $S \equiv$ single strand = d(C-T)$_6$.

If C_t is the total concentration of $\mathcal{D}+S$ available to form T; α is the fraction of third strand in triplex; $\mathcal{D}$ and S are each always present at the same concentration $(1-\alpha)\frac{C_t}{2}$; and $(\alpha)\frac{C_t}{2}$ is the concentration of T; then the observed equilibrium constant is

$$K_{obs} = \frac{[\mathcal{D}][S]}{[T]} = \frac{(1-\alpha)^2 \frac{C_t}{2}}{\alpha} \qquad \text{with } \alpha = \frac{A(\text{duplex + coil})_{255} - A_{255}}{A(\text{duplex + coil})_{255} - A(\text{triplex})_{255}} \qquad [1]$$

where, K_{obs} is obtained from the equilibrium between the triplex and the core duplex + third strand, in contrast to K_{expl} that *explicitly* includes Na^+ and H^+ in the equilibrium (see below); the hyperchromic change at 255nm is a measure of the dissociation of triplex; $A(\text{triplex})_{255}$ is the absorbance of intact triplex; $A(\text{duplex + coil})_{255}$ is the sum of the absorbances of duplex and single strand; A_{255} is the absorbance at any temperature within the transition.

Values for the observed van't Hoff enthalpy for the transition, $\Delta H°_{obs}$, were obtained according to [2], from a plot of $\ln K_{obs}$ vs 1/T

$$\ln K_{obs} = \frac{-\Delta H°_{obs}}{RT} + \frac{\Delta S°_{obs}}{R} \qquad [2]$$

where, R is the gas constant (1.989 $cal.K^{-1}.mol^{-1}$) and T is the absolute temperature interval over which the transition occurs.

The value for the observed transition entropy, $\Delta S°_{obs}$, was then calculated at $T = T_m$.

Values for the observed transition free energy at 25 °C, $\Delta G°_{obs}$, were obtained from

$$\Delta G°_{obs} = \Delta H°_{obs} \left(1 - \frac{T_{298}}{T_m}\right). \qquad [3]$$

To evaluate the effects of the ionic environment on triplex stability, both electrostatic shielding (Debye-Hückel) by the counterion atmosphere and condensation of counterions (Na^+) onto the nucleic acid polyelectrolyte are considered. To these are added site binding of H^+ on a ring N of a base, which may be viewed as a special type of condensation. This analysis assumes the site binding of the H^+ ions bound to N3 of the third strand dC residues in the triplex can be treated in a manner comparable to that used for condensed Na^+ ions, which seems justified because those H^+ ions reduce the net negative charge in the triplex structure, thereby effectively reducing the amount of Na^+ condensation. This approach is supported by the observed inverse ionic strength dependence of triplex stability, and as seen below, gives a chemically meaningful value for the number of protons bound by the third strand in the triplex.

Following Manning's approach (21,22) [1/], let Z be the negative charge per phosphate separated by their average spacing b. Then, the extent of counter ion binding is given by the dimensionless parameter

$$\xi = \frac{e^2}{b\varepsilon kT} \qquad [4]$$

where e is the charge of the electron, ε is the solvent dielectric constant, k is the Boltzmann constant and T is the absolute temperature.

The fraction of counterion condensation per charge

$$\theta_m = 1 - \frac{1}{\xi}. \qquad [5]$$

That is, after counterion condensation, a net negative charge of $1 - \theta_m$ remains on each phosphate, and must be screened by the counterion atmosphere. Using a shielded

potential, the electrostatic free energy per mole of phosphate associated with counterion screening

$$G_{el} = -RT\frac{1}{\xi} \ln \kappa b \qquad [6]$$

where the Debye-Hückel screening parameter for a cylindrical geometry

$$\kappa = \left(\frac{4\pi e^2}{\varepsilon kT}\right)^{1/2} I^{1/2} \qquad [7]$$

and the ionic strength of the solution

$$I = \Sigma_i \frac{C_i z_i^2}{2} \qquad [8]$$

where C_i is the molar concentration of the ith counterion species with charge z_i.

Having developed a general form of the electrostatics, we now explicitly introduce Na^+ and H^+ into the equilibrium for the dissociation of triplex to duplex and third strand, thus:

$$\mathcal{T} \leftrightarrow \mathcal{D} + S + \Delta n_1 Na^+ + \Delta n_2 H^+ \quad \text{and} \quad K_{expl} = \frac{[\mathcal{D}][S][Na^+]^{\Delta n_1}[H^+]^{\Delta n_2}}{[\mathcal{T}]} \qquad [9]$$

where Δn_1 is the number of Na^+ released or bound, Δn_2 is the number of H^+ released or bound, and $\mathcal{T}$, $\mathcal{D}$ and S are triplex, duplex and single strand, respectively.

The explicit Gibbs free energy change associated with release of third strand, ΔG_{expl}, has the following components: $\Delta G_{structure}$, the change associated with separation of third strand and duplex (i.e., ΔH due to loss or gain of H-bonding and base stacking, ΔS due to loss or gain of conformational and vibrational freedom of the system); ΔG_{Na^+}, the change associated with release or uptake of Na^+; ΔG_{H^+}, the change associated with

release or uptake of H^+; $\Delta G_{el\ Na^+}$, the change associated with the different ion-atmosphere shielding by Na^+ of the triplex vs duplex plus single strand; $\Delta G_{el\ H^+}$, the change associated with the different ion-atmosphere shielding of the triplex vs duplex plus single strand for H^+. Since only the triplex contains H^+ ions, this effect comes from their contribution to electrostatic shielding by way of reducing the net charge on the triplex.

For completeness, a sixth free energy change associated with the difference in water binding or hydration of the triplex vs that of the duplex plus single strand should be included. However, we do not address the water explicitly and this factor is considered as part of $\Delta G°$.

For a triplex with Z_1 phosphates, the change in the number of condensed Na^+ on dissociation of the third strand is

$$\Delta n_1 = n_1\mathcal{T} - n_1\mathcal{D} - n_1\mathcal{S} = Z_1(1[1 - \frac{1}{\xi(\mathcal{T})}] - \frac{2}{3}[1 - \frac{1}{\xi(\mathcal{D})}] - \frac{1}{3}[1 - \frac{1}{\xi(\mathcal{S})}])$$

$$= Z_1(\frac{2}{3\xi(\mathcal{D})} + \frac{1}{3\xi(\mathcal{S})} - \frac{1}{\xi(\mathcal{T})}) \qquad [10]$$

where $n_1\mathcal{T}$ is the average number of Na^+ bound to triplex; $n_1\mathcal{D}$ is the average number of Na^+ bound to duplex; $n_1\mathcal{S}$ is the average number of Na^+ bound to single strand. Knowing that Na^+ and H^+ must both contribute to electrostatic shielding of the triplex, we use the Debye-Hückel approximation for a shielded potential and obtain expressions for the Na^+ and H^+ dependence.

For a solution with Na^+ concentration M_1, the entropic contribution of the Na^+ counterions to the free energy of third strand dissociation

$$\Delta G_{Na+} = -RT\, Z_1\left(\frac{2}{3\xi_{(D)}} + \frac{1}{3\xi_{(S)}} - \frac{1}{\xi_{(T)}}\right) \ln[M_1] = -RT\, \Delta n_1 \ln[M_1] \qquad [11]$$

and for a triplex with Z_1 phosphates, using [6], the shielding contribution (enthalpic contribution) of the Na^+ counterions to the free energy of third strand dissociation

$$\Delta G_{el\ Na+} = -RT\, Z_1 \{[\frac{1}{\xi_{(T)}} \ln \kappa b_{(T)}] - [\frac{2}{3\xi_{(D)}} \ln \kappa b_{(D)}] - [\frac{1}{3\xi_{(S)}} \ln \kappa b_{(S)}]\} \qquad [12]$$

Assuming the fraction[2] of H^+ bound per third strand dC residue to be given by $1-\frac{1}{\xi}$, and that their contribution to the electrostatic shielding can be modeled by a shielded potential, then the H^+ contribution to the free energy of third strand dissociation has the following entropic [14] and enthalpic [15] components, with the change in the number of H^+ on third strand dissociation, Δn_2, given by:

$$\Delta n_2 = n_{2T} - n_{2S} = Z_2(1[1 - \frac{1}{\xi_{(T)}}] - 1[1 - \frac{1}{\xi_{(S)}}]) = Z_2(\frac{1}{\xi_{(S)}} - \frac{1}{\xi_{(T)}}) \qquad [13]$$

where n_{2T} is the average number of H^+ site bound to triplex; n_{2S} is the average number of H^+ site bound to single strand; and Z_2 is the total number of potential H^+ binding sites in the triplex.

Then, for a solution with H^+ concentration M_2, the entropic contribution of the bound H^+ to the free energy of third strand dissociation

$$\Delta G_{H+} = -RT\, Z_2\left(\frac{1}{\xi_{(S)}} - \frac{1}{\xi_{(T)}}\right) \ln[M_2] = -RT\, \Delta n_2 \ln[M_2] \qquad [14]$$

and for a triplex with protonated dC residues, from [6], the shielding contribution (enthalpic contribution) to the free energy of third strand dissociation

$$\Delta G_{el\ H^+} = -RT\ Z_2\{[\frac{1}{\xi_{(T)}} \ln \kappa b_{(T)}] - [\frac{1}{\xi_{(S)}} \ln \kappa b_{(S)}]\}. \qquad [15]$$

Substituting [11], [12], [14] and [15] into

$$\Delta G_{expl} = (\Delta G_{structure}) + (\Delta G_{Na^+}) + (\Delta G_{el\ Na^+}) + (\Delta G_{H^+}) + (\Delta G_{el\ H^+})$$

and using $\ln K_{expl} = \frac{-\Delta G_{expl}}{RT}$ we obtain

$$\ln K_{expl} = \ln K_{structure} + Z_1(\frac{2}{3\xi_{(D)}} + \frac{1}{3\xi_{(S)}} - \frac{1}{\xi_{(T)}}) \ln[M_1]$$

$$+Z_1\{[\frac{1}{\xi_{(T)}} \ln \kappa b_{(T)}] - [\frac{2}{3\xi_{(D)}} \ln \kappa b_{(D)}] - [\frac{1}{3\xi_{(S)}} \ln \kappa b_{(S)}]\}$$

$$+ Z_2(\frac{1}{\xi_{(S)}} - \frac{1}{\xi_{(T)}}) \ln[M_2] + Z_2\{[\frac{1}{\xi_{(T)}} \ln \kappa b_{(T)}] - [\frac{1}{\xi_{(S)}} \ln \kappa b_{(S)}]\}. \qquad [16a]$$

For a monovalent electrolyte, $\kappa = \left(\frac{4\pi e^2}{\varepsilon kT}\right)^{1/2} [M]^{1/2} = \kappa' [M]^{1/2}$. Substituting for κ and simplifying, we obtain

$$\ln K_{expl} = \ln K_{structure} + \frac{1}{2} Z_1(\frac{2}{3\xi_{(D)}} + \frac{1}{3\xi_{(S)}} - \frac{1}{\xi_{(T)}}) \ln[M_1]$$

$$+ Z_1\frac{1}{\xi_{(T)}} \ln \kappa' b_{(T)} - Z_1\frac{2}{3\xi_{(D)}} \ln \kappa' b_{(D)} - Z_1\frac{1}{3\xi_{(S)}} \ln \kappa' b_{(S)}$$

$$+ \frac{1}{2} Z_2 (\frac{1}{\xi_{(S)}} - \frac{1}{\xi_{(T)}}) \ln[M_2] + Z_2\frac{1}{\xi_{(T)}} \ln \kappa' b_{(T)} - Z_2[\frac{1}{\xi_{(S)}} \ln \kappa' b_{(S)}]\}. \qquad [16b]$$

Thus, the effect of Na^+ concentration (M_1) on the explicit equilibrium constant is

$$\frac{\partial(\ln K_{expl})}{\partial(\ln [Na^+])} = \frac{1}{2} Z_1 \left(\frac{2}{3\xi_{(D)}} + \frac{1}{3\xi_{(S)}} - \frac{1}{\xi_{(T)}} \right) = \frac{1}{2} \Delta n_1 \qquad [17]$$

and the effect of H^+ concentration (M_2) on the explicit equilibrium constant is

$$\frac{\partial(\ln K_{expl})}{\partial(\ln [H^+])} = \frac{1}{2} Z_2 \left(\frac{1}{\xi_{(S)}} - \frac{1}{\xi_{(T)}} \right) = \frac{1}{2} \Delta n_2 \, . \qquad [18]$$

The temperature dependence of ln K_{expl} is

$$\frac{\partial(\ln K_{expl})}{\partial T} = \frac{\partial}{\partial T} \left(\frac{-\Delta G}{RT} \right) = \frac{\Delta H}{RT^2} \, . \qquad [19]$$

Finally, we obtain expressions giving the effect of counterion concentration on triplex stability, as reflected by observed T_m values. Thus

$$\frac{\partial T_m}{\partial(\ln[Na^+])} = \frac{\partial(\ln K_{expl})}{\partial(\ln[Na^+])} \times \frac{\partial T_m}{\partial(\ln K_{expl})} = \frac{1}{2} \frac{\Delta n_1}{Z_1} \frac{R(T_m)^2}{\Delta H_1} \qquad [20]$$

$$\frac{\partial T_m}{\partial(\ln[H^+])} = \frac{\partial(\ln K_{expl})}{\partial(\ln[H^+])} \times \frac{\partial T_m}{\partial(\ln K_{expl})} = \frac{1}{2} \frac{\Delta n_2}{Z_2} \frac{R(T_m)^2}{\Delta H_2} \qquad [21]$$

Integration and simplification of [20] and [21] yields respectively

$$\Delta\left[\frac{1}{T_m}\right] = -\frac{1}{2} \left(\frac{2}{3\xi_{(D)}} + \frac{1}{3\xi_{(S)}} - \frac{1}{\xi_{(T)}} \right) \frac{2.303R}{\Delta H_1} \Delta(\log[Na^+]) \qquad [22]$$

$$\Delta\left[\frac{1}{T_m}\right] = -\frac{1}{2} \left(\frac{1}{\xi_{(S)}} - \frac{1}{\xi_{(T)}} \right) \frac{2.303R}{\Delta H_2} \Delta(-pH) \qquad [23]$$

where $\frac{\Delta n_1}{Z_1}$ is the stoichiometric change in Na^+ bound per phosphate; ΔH_1 is the enthalpy change per mole phosphate; Δn_1 is the stoichiometric change in Na^+ bound on triplex dissociation, and $\frac{\Delta n_2}{Z_2}$ is the stoichiometric change in H^+ bound per third strand dC

residue; ΔH_2 is the enthalpy change per mole third strand dC residue; Δn_2 is the stoichiometric change in H^+ bound on triplex dissociation.

While Manning's approach to include ionization of the nucleic acid bases and the effect that this has on the Na^+ and H^+ dependence has previously been extended by Record et al. (23), there are distinct differences between their results and ours (see Discussion).

Thermodynamic Analysis of the Duplex Transition

The melting of the duplex in both the duplex and triplex mixtures is described by the following equilibrium: $\mathcal{D} \leftrightarrow S_1 + S_2$

where $\mathcal{D} \equiv$ duplex = d(A-G)$_6$:d(C-T)$_6$; $S_1 \equiv$ single strand = d(C-T)$_6$ and $S_2 \equiv$ single strand = d(A-G)$_6$.

For these non-self complementary strands, the observed equilibrium constant

$$K_{obs} = \frac{[S_1][S_2]}{[\mathcal{D}]} = \frac{(1-\alpha)^2 \frac{C_t}{2}}{\alpha} \qquad \text{for the duplex mixture} \qquad [24]$$

$$\text{with } \alpha = \frac{A(coil)_{255} - A_{255}}{A(coil)_{255} - A(duplex)_{255}}$$

$$K_{obs} = \frac{2[S_1][S_2]}{[\mathcal{D}]} = \frac{(1-\alpha)^2 \frac{2C_t}{3}}{\alpha} \qquad \text{for the triplex mixture} \qquad [25]$$

$$\text{with } \alpha = \frac{A(coil)_{255} - A_{255}}{A(coil)_{255} - A(duplex + coil)_{255}}$$

where α is the fraction of single strand in duplex; C_t is the total concentration of single strands. The fraction of dissociated duplex is measured in terms of the quantities $A(duplex)_{255}$, the absorbance of the duplex; $A(coil)_{255}$, the absorbance of the separated strands; A_{255}, the absorbance at some temperature within the transition; and $A(duplex + coil)_{255}$, the absorbance of the duplex and dissociated single strand.

2.4 Results

Identifying the Triplex and Duplex Transitions

Melting of the triplex formed from $d(C\text{-}T)_6$ and $[d(A\text{-}G)_6 \cdot d(C\text{-}T)_6]$ at pH 7.0, is shown in Figure 1B, where the absorbance difference spectrum ($\Delta A_\lambda = \Delta\varepsilon CL$) over a range of wavelengths, λ, at any temperature, T, is given by $\Delta A_{\lambda,T}$ (triplex mixture) = $A_{\lambda,T} - A_{\lambda,1^\circ}$. Two transitions are apparent, one between 5 - 15 °C and the second between 40 - 60 °C. The first transition must represent dissociation of the third strand from the core duplex of the triplex since the second transition clearly coincides with that for the duplex alone at the same pH (Figure 1A). Similarly, Figure 1C shows the comparable melting pattern of the triplex at pH 4.2, with the first transition occurring from 25 - 35 °C and the second from 55 - 70 °C.

Melting profiles at individual wavelengths between 240 and 280 nm for the duplex mixture at pH 7.0 (e.g., Figure 1D) and the triplex mixture at pH 7.0 (e.g., Figure 1E) and pH 4.2 (e.g., Figure 1F), clearly illustrate the features of the thermal transition(s) and confirm that T_m is wavelength independent. This behavior is consistent with *cooperative* transition(s) as all the chromophores undergo spectral changes simultaneously.

An analysis of the difference in spectral changes on triplex melting at the two pH values is given below; so is a thermodynamic analysis of the pH dependence of T_m for the transition.

Figure 1:

(A) Melting spectra, $\Delta A_{\lambda,T}$ (duplex mixture) = $A_{\lambda,T}$ (duplex mixture) - $A_{\lambda,1°}$ (duplex mixture), of duplex mixture in mixing buffer at pH 7.0. The scan at 1 °C was subtracted from all subsequent scans, so the plot represents a series of temperature dependent difference spectra.

(B) Melting spectra, $\Delta A_{\lambda,T}$ (triplex mixture) = $A_{\lambda,T}$ (triplex mixture) - $A_{\lambda,1°}$ (triplex mixture), of triplex mixture in mixing buffer at pH 7.0 [y-axis labels omitted for clarity].

(C) Melting spectra, $\Delta A_{\lambda,T}$ (triplex mixture) = $A_{\lambda,T}$ (triplex mixture) - $A_{\lambda,1°}$ (triplex mixture), of triplex mixture in mixing buffer at pH 4.2.

(D) Melting profiles of duplex mixture in mixing buffer at pH 7.0, measured at 245 nm (—) and 275 nm (···). T_m is wavelength independent, consistent with a cooperative transition.

(E) Melting profiles of triplex mixture in mixing buffer at pH 7.0, measured at 245 nm (—) and 275 nm (···). T_m values are wavelength independent for both transitions.

(F) Melting profiles of triplex mixture in mixing buffer at pH 4.2, measured at 245 nm (—) and 275 nm (···). T_m values are wavelength independent for both transitions.

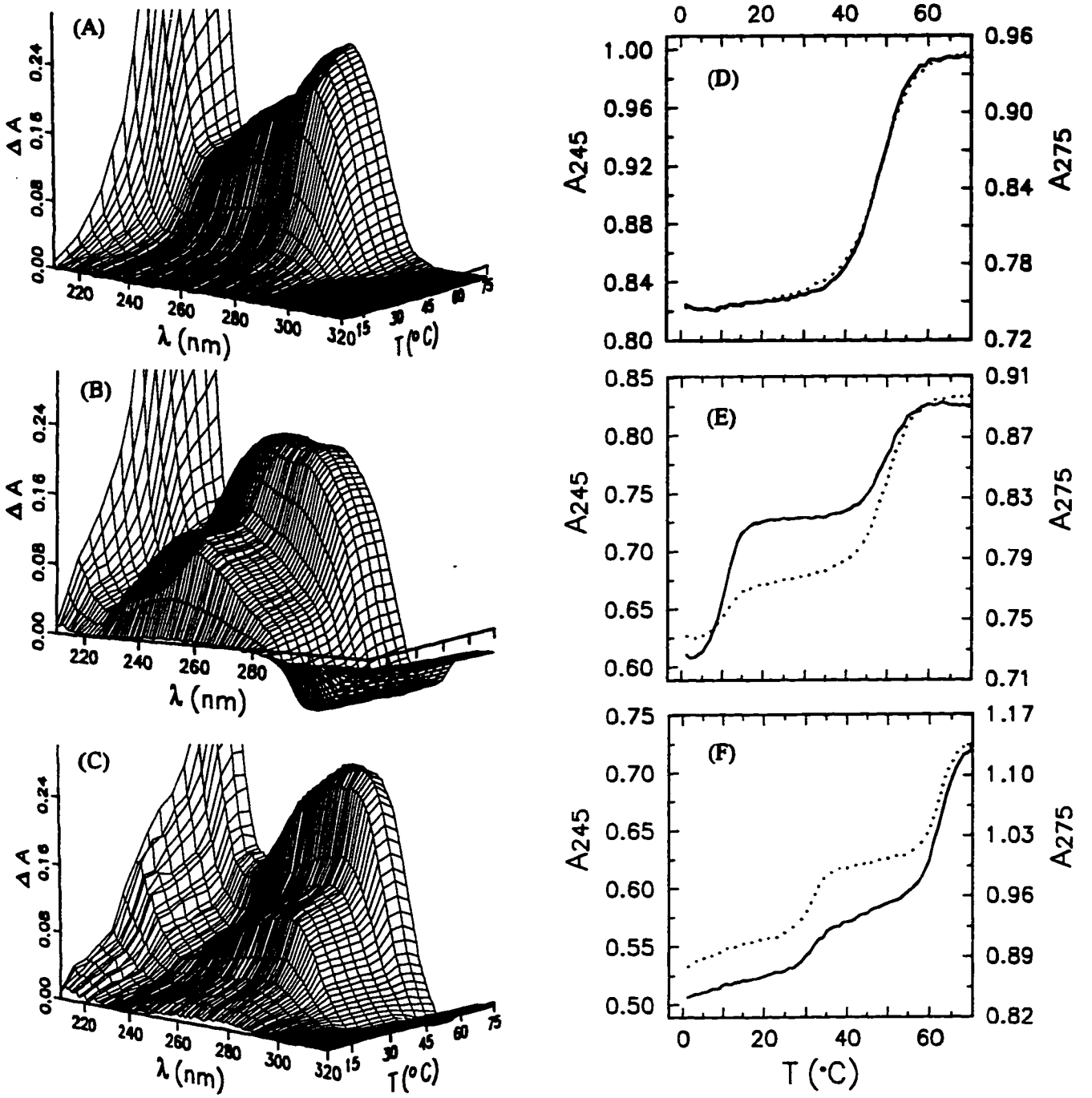
(A)
(B)
(C)
(D)
(E)
(F)
ΔA
λ (nm)
T(°C)
A245
A275
T (°C)

Spectroscopic Characterization of the Triplex → Duplex Transition

Of the four residues contained in the triplex, only dC shows significant near-UV spectral differences under relevant acidic and neutral conditions. On dissociating a proton from 5'dC^+MP (pK_a 4.6), these differences take the form of a positive peak between 220 and 265 nm and a negative peak centered at 288 nm (Figure 2A). Hoogsteen pairing of a third strand dC residue to the dG residue of a target G·C base pair results in a base triplet that is isostructural to T:A·T (Figure 9A), the third strand dC residue interacting with the target dG via two H-bonds if it is protonated at N3 (Figure 9B), and via one H-bond if it is not. Moreover, if the third strand dC residues are protonated at all pH values where the triplex exists, the fraction that should lose their protons on third strand dissociation at any given pH can be estimated by assuming that the pK_a of dC in $d(C^+\text{-}T)_6$ is the same as for dCMP, i.e., 28% at pH 4.2 and 100% at pH 7.0. This means that at pH 4.2 the characteristic spectral change for $dC^+ \rightarrow dC$ should contribute to the total spectral change upon third strand dissociation from the core duplex only to a small extent, whereas at pH 7.0 the contribution should be very pronounced. We have therefore particularly evaluated the observed spectral change on third stand dissociation for evidence of that characteristic contribution for $dC^+ \rightarrow dC$ at pH 7.0.

To do so we ask whether the total spectral change, ΔA_λ, observed on dissociating the putative third strand $d(C^+\text{-}T)_6$ from the core duplex $d(A\text{-}G)_6 \cdot d(C\text{-}T)_6$ at pH 7.0 is a linear combination of the following "library" spectral contributions: 1. the dissociation and unstacking of dT from A·T target base pairs (ΔA_λ, $T{:}A{\cdot}T \rightarrow T + A{\cdot}T$); 2. the dissociation and unstacking of dC^+ from G·C target base pairs (ΔA_λ, $C^+{:}G{\cdot}C \rightarrow C^+ + G{\cdot}C$);

3. the consecutive deprotonation of $dC^+ \rightarrow dC$ at pH 7.0 ($\Delta A_{\lambda,\ C^+ \rightarrow C}$).

The first spectral library component, $\Delta A_{\lambda,\ T:A\cdot T \rightarrow T + A\cdot T}$, was obtained from the difference spectrum [(duplex + single strand) - (triplex)] for the dissociation of the third strand $(dT)_{21}$ from the core duplex $(dA)_{21}\cdot(dT)_{21}$ in neutral mixing buffer. That difference spectrum (Figure 2B) shows a broad peak centered at 265 nm.

The second spectral library component, $\Delta A_{\lambda,\ C^+:G\cdot C \rightarrow C^+ + G\cdot C}$, was approximated from the difference spectrum [(poly(dC), 80 °C) - (poly(dC), 1 °C)], i.e., for the melting of poly(dC) in neutral mixing buffer. This component (Figure 2C) shows the double peak characteristic of unstacking dC residues, and its use implies that it is very similar for unstacking dC^+ residues.

The third spectral library component, $\Delta A_{\lambda,\ C^+ \rightarrow C}$, was obtained from dCMP, pH 7.0 - dC^+MP, pH 2.0 in 0.05M sodium phosphate buffer at 25 °C, as described above (Figure 2A). The sum of the three library spectra is shown in Figure 2D along with the observed difference spectrum for third strand dissociation at pH 7.0. While the two spectra do not coincide, it can be seen that they do so when the summated one is displaced on the wavelength axis +6 nm, as can be seen in Figure 2E. That the sum of the library spectra needs to be red shifted 6 nm is not unreasonable given that the library spectra do not account for the characteristic red shift that occurs on breaking H-bonds between bases (24), in this case between the third strand dC^+ residues and the target dG residues. Moreover, the second spectral library component accounts for the unstacking of dC rather than dC^+ residues, the latter being inaccessible because poly(dC^+) forms a hemiprotonated double stranded helix under acidic conditions (25,26). These two

limitations notwithstanding, it is apparent that the spectral components contributing to third strand dissociation from the duplex are quite well approximated, and that the *major contribution* to the difference spectrum at pH 7.0 derives from deprotonation of the third strand dC^+ residues. That being the case, the third strand dC residues must be fully protonated in the triplex.

Figure 3 shows difference spectra for third strand dissociation as a function of pH. The reason for the large blue shift as pH rises is that the library component for $dC^+ \rightarrow dC$ (Figure 2A) makes an increasingly greater contribution, resulting in increasing enhancement of the peak at 245 nm and the trough at 294 nm, while the contribution from the two other spectral components is unchanging. At pH 4.2, for example, the difference spectrum shows a broad peak centered at 275 nm due to the dissociation and unstacking of the dT residues from the A·T target base pairs. That peak is seen only as a shoulder of the main peak at pH 5.0 and 7.0, due to the superposition of the large contribution of the $dC^+ \rightarrow dC$ difference spectrum.

In sum, UV spectroscopic evidence shows that at pH 7.0 the third strand dC residues are protonated in the triplex, and therefore the presence of two H-bonds in the Hoogsteen C^+:G base pair component. If the Hoogsteen pair of the C:G·C base triplet could form with only one H-bond, then that pair should remain stable so long as the target base pair is stable. Yet, the hyperchromic change at 255 nm on dissociating the third strand drops from 12% at both pH 5.0 and pH 7.0 to 4% at pH 7.5. This 2/3 loss of hyperchromic change indicates a comparably reduced proportion of triplex formation, a reduction which

can be ascribed to the limited availability of H^+ ions, which are required to drive the equilibrium toward triplex formation, thus:

$$H^+ + d(C\text{-}T)_6 + d(A\text{-}G)_6 \cdot d(C\text{-}T)_6 \leftrightarrow d(C^+\text{-}T)_6 : [d(A\text{-}G)_6 \cdot d(C\text{-}T)_6].$$

In this respect, hydrogen ion concentration may be seen as a switch for triplex formation.

Figure 2: Library spectral components for analysis of dissociation of the triplex at different pH values.

(A) Spectral change associated with deprotonation of dC^+MP, i.e., $\Delta A = A\lambda$, pH 7.0 - $A\lambda$, pH 2.0) in 0.05 M sodium phosphate buffer at 25 °C. This is taken to represent the spectral change associated with deprotonation of dC^+ residues in the third strand, i.e., $\Delta A\lambda$, $C^+ \rightarrow C$·

(B) Spectral change associated with both dissociation and unstacking of dT residues from A·T target base pairs ($\Delta A\lambda$, $T{:}A{\cdot}T \rightarrow T + A{\cdot}T$). It was obtained from the difference spectrum [(duplex + melted single strand) - (triplex)] for the dissociation of the third strand $(dT)_{21}$ from the core duplex $(dA)_{21}{\cdot}(dT)_{21}$ in neutral mixing buffer.

(C) Spectral change associated with unstacking of dC residues of poly(dC), i.e., $\Delta A\lambda$, 80° - 1°C, in neutral mixing buffer. This difference spectrum was used to mimic the change due to unstacking of third strand dC^+ residues upon dissociation from G·C target base pairs ($\Delta A\lambda$, $C^+{:}G{\cdot}C \rightarrow C^+ + G{\cdot}C$).

(D) Spectral change calculated for the dissociation at pH 7.0 of $d(C\text{-}T)_6$ from the target duplex by linear summation of the difference spectra in (A), (B) and (C).

(E) Comparison of the calculated difference spectrum in (D), displaced +6 nm (—), with the melting difference spectrum (20 - 1 °C) of the triplex at pH 7.0 (···).

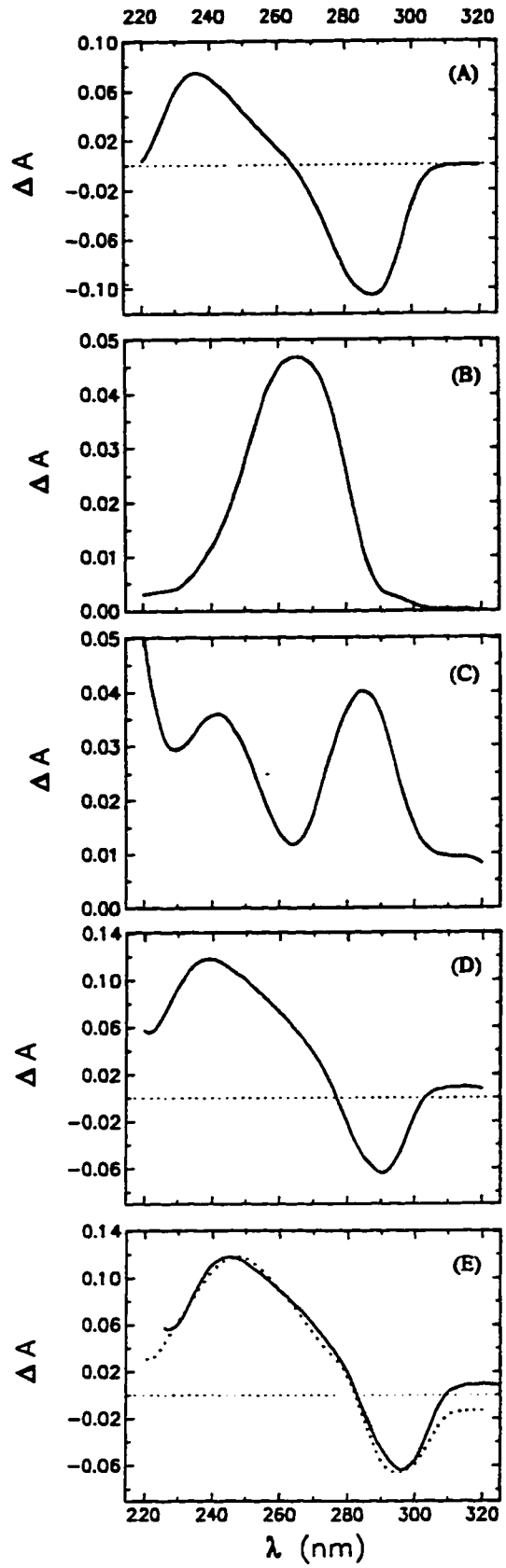
220
240
260
280
300
320
(A)
(B)
(C)
(D)
(E)
ΔA
λ (nm)

Figure 3: Difference spectra (20 - 1 °C) for the triplex mixture at pH 4.2 (—), 5.0 (·--·) and 7.0 (···) in mixing buffer.

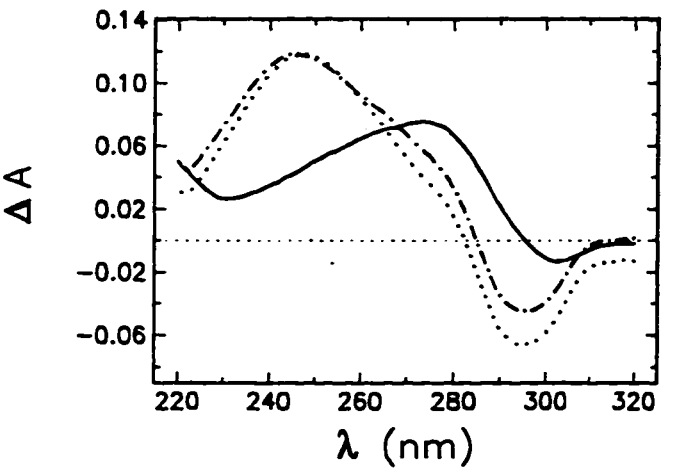
0.14
0.10
0.06
0.02
−0.02
−0.06
ΔA
220
240
260
280
300
320
λ (nm)

Thermodynamic Parameters for the Triplex and Duplex Transitions

It is evident from the linearity of the van't Hoff plots in Figures 4, 5 and 6 that the data obtained from the UV melting profiles are in accord with that type of analysis, i.e., the enthalpy change over the temperature range of each transition is essentially constant. This enables the accumulation of the standard molar thermodynamic parameters given in Table 1. The average ΔH°_{obs} per mole base pair were obtained by dividing ΔH°_{obs} per mole oligomer by 12, the number of residues per strand that are unstacking in the transition. This analysis was possible as the transitions are well separated, cooperative and have good baselines. The one exception to this were the triplex and duplex profiles at pH 4.2, which had poor baselines and gave anomalously high enthalpy values.

The unique occurrence of high T_m values for the *duplex* at pH 4.2 in both the duplex (57 °C) and triplex (62 °C) mixtures suggested the presence of some species other than a Watson-Crick duplex (48 °C). Since protonation of dC at N_3 must lead to disruption of a Watson-Crick G·C base pair, and both protonated dC and neutral dT residues are amenable to isostructural Hoogsteen pairing with dG and dA respectively, we inferred that at low pH $d(C^{+}\text{-}T)_6 + d(A\text{-}G)_6$ must form a parallel Hoogsteen rather than an antiparallel Watson-Crick duplex. In fact, such a duplex has been observed at low pH (27) for a similar 20 mer sequence. The CD spectra of this duplex at pH 4.2 and 7.0 (Figure 10), in comparison to those in (27), confirm the formation of a parallel Hoogsteen duplex under acidic conditions.

The *enthalpy* values show that under all conditions studied the Hoogsteen-bound third strand in the triplex is more tightly held than the comparable Watson-Crick strand (in the

duplex). For example, at pH 7.0 in mixing buffer, $\Delta H^{\circ}_{obs} = 6.4$ kcal.mol^{-1} base pair for duplex dissociation, and 9.7 kcal.mol^{-1} base pair for third strand dissociation. In addition, the formation of a parallel Hoogsteen duplex at pH 4.2 with eleven base pair interactions and a significantly higher T_m than that of the Watson-Crick duplex with twelve base pair interactions clearly confirms the greater stability of the Hoogsteen interactions. This finding is consistent with several earlier observations:

1. Hoogsteen (28) found that 1-methylthymine and 9-methyladenine cocrystallize only in an H-bonding geometry that is different ("Hoogsteen") from that of the Watson-Crick A·T base pair.

2. Ornstein and Fresco (29) calculated that the Hoogsteen T:A base pair is more stable by -1.03 kcal.mol^{-1} than the Watson-Crick A·T base pair.

3. In contrast, the monomers of C and G only co-crystallize in the Watson-Crick G·C geometry, and not in the *neutral* Hoogsteen C:G geometry.

4. The total H-bond interaction energy for a neutral H-bond consists of dispersion, polarization and electrostatic components, with the latter contributing about 80% of the total energy. Hence, for the Hoogsteen C^+:G base pair with an ionic H-bond, the interaction energy is higher. In fact, doubling and tripling of the interaction energy for ionic H-bonds has been both calculated and experimentally observed (30,31). Further, Pullman et al. (32) calculated interaction energies (kcal.mol^{-1}) for base pairs and triplets as follows: UAU -12, Watson-Crick GC -19, Hoogsteen CC +13, Hoogsteen C^+C -35, C^+GC -48, with the latter triplet the most stable.

The foregoing trends in the enthalpy values notwithstanding, under all conditions studied, the free energy of *formation* of triplex at 25 °C is less than that for the comparable Watson-Crick duplex. For example, at pH 7.0 in mixing buffer, $\Delta G^{\circ}_{obs,298}$ = -5.5 kcal.mol^{-1} oligomer for duplex *formation* but 5.7 kcal.mol^{-1} oligomer for triplex *formation*. The less favorable free energy values for formation of the triplex obviously result from their more negative ΔS°_{obs} values than those for the duplex under comparable conditions (Table 1). Thus, for this triplex, *association* of the third strand to the duplex is enthalpicaly driven (favorable) and entropicaly unfavorable. This behavior is consistent with proton uptake by the third strand dC residues.

For triplex formation the free energy at 25 °C becomes increasingly negative with decreasing pH, as is expected with the requirement that third strand dC residues be protonated ($\Delta G^{\circ}_{obs,298}$ = 8.5 kcal.mol^{-1} oligomer at pH 7.5, 5.7 at pH 7.0, -1.2 at pH 5.0, and -2.5 at pH 4.2 (Table 1). Finally, the endergonic values at pH 7.0 and 7.5 are consistent with the fact that the triplex does not exist at 25 °C, its T_m values under these conditions being 11 and 1 °C, respectively.

The high values of ΔH°_{obs}, ΔS°_{obs} and ΔG°_{obs} for the triplex in 3M NaCl merit additional comment. The large positive ΔH°_{obs} of 15.4 kcal.mol^{-1} base pair dissociation shows the third strand binding interactions to be favorable. At the same time, the large positive ΔS°_{obs} (0.67 kcal.mol^{-1}.K^{-1} oligomer) is significant in that it compensates for this positive enthalpy change, resulting in a negative ΔG°_{obs} (-13.3 kcal.mol^{-1} oligomer). The significantly larger ΔS°_{obs} for dissociation of third strand at 3M NaCl must to a significant extent result from an increase in entropy of the water, as the dissociated

duplex and single strand have a net gain of 9 Na^+ (see next section). That is, removal of ions from the solution results in the release of H_2O from the ion-H_2O clusters that were in solution. This is also the case for 2M NaCl (5 Na^+) and 1M NaCl (4 Na^+), but to a lesser extent. We note also that the % hyperchromicity for the third strand dissociation is significantly less in 3M NaCl: 1.0M NaCl 17%; 2M NaCl 13%; 3M NaCl 2%. This significant reduction in the % hyperchromicity is probably due to the equilibrium being shifted to the right, resulting in less triplex formation under these conditions and therefore an anomalous value of ΔH°_{obs} for the triplex in 3M NaCl.

Table I: Thermodynamic Parameters for Dissociation* of the Third Strand from the Target Duplex and for Dissociation* of the Duplex

Sample	Conditions	ΔH°_{obs} kcal.mol^{-1} of base pair	ΔH°_{obs} kcal.mol^{-1} of oligomer	ΔS°_{obs} kcal.mol^{-1}.K^{-1} of oligomer	$\Delta G^\circ_{obs,298}$ kcal.mol^{-1} of oligomer	T_m °C
Triplex Mixture[a]	pH 4.2	8.9	107	0.35	2.5	32
1st Transition	5.0	7.3	88.1	0.29	1.2	29
	7.0	9.7	116	0.41	-5.7	11
	7.5	8.1	97.5	0.36	-8.5	1
	8.0	-	-	-	-	0
Triplex Mixture[b]	M NaCl 0.1	7.2	86.0	0.31	-5.5	7
1st Transition	0.3	6.6	79.1	0.28	-5.1	7
	0.4	7.1	85.4	0.31	-5.5	7
	0.5	7.3	88.1	0.31	-5.3	8
	0.8	6.4	76.5	0.27	-4.1	10
	0.9	5.9	70.9	0.25	-3.8	10
	1.0	7.3	87.6	0.31	-5.0	9
	2.0	9.2	110	0.39	-7.1	7
	3.0	15.4[†]	185	0.67	-13.3	5
Triplex Mixture[a]	pH 4.2	13.6[†]	163	0.49	18.0	62[†]
2nd Transition	5.0	9.3	112	0.35	8.7	50
	7.0	8.2	98.7	0.31	7.6	50
	7.5	7.6	91.4	0.28	7.1	50
	8.0	8.2	98.4	0.31	7.6	50
	8.5	8.8	106	0.33	7.9	49
Triplex Mixture[b]	M NaCl 0.1	6.8	82.0	0.26	5.6	47
2nd Transition	0.3	7.6	91.3	0.28	7.3	51
	0.4	7.8	93.3	0.29	8.0	53
	0.5	6.6	78.9	0.24	7.0	54
	0.8	7.4	88.8	0.27	8.4	56
	0.9	7.8	93.1	0.28	8.8	56
	1.0	6.8	82.0	0.25	7.3	54
	2.0	7.8	93.7	0.29	8.3	54
	3.0	8.7	104	0.32	10.1	57
Duplex Mixture[a]	pH 4.2	8.4[†]	101	0.31	9.8	57[†]
	5.0	5.7	67.9	0.21	4.9	48
	7.0	6.4	76.9	0.24	5.5	48
	7.5	6.2	74.8	0.23	5.4	48
	8.0	6.6	79.1	0.25	5.7	48
	8.5	6.3	75.6	0.24	5.4	48
Duplex Mixture[b]	M NaCl 0.1	5.6	67.3	0.21	4.0	44
	0.3	5.8	69.0	0.21	5.3	50
	0.4	6.1	72.9	0.22	5.9	51
	0.5	5.7	68.3	0.21	5.7	52
	0.8	5.8	69.4	0.21	6.1	54
	0.9	5.8	69.6	0.21	6.2	54
	1.0	6.0	72.0	0.22	6.2	53
	2.0	5.7	68.7	0.21	5.7	52
	3.0	5.7	68.8	0.21	5.7	52

*The more positive the ΔG°_{obs} the more stable the triplex or duplex. [a]0.01M Cacodylate/0.15M NaCl/0.005M $MgCl_2$. [b]pH 7.0/0.01M Cacodylate. [†]For discussion of these values see Results section, Thermodynamic Parameters for the Triplex and Duplex Transitions.

Figure 4: van't Hoff plots for the first transition of triplex mixtures (triplex dissociation to third strand + duplex).

(A) mixing buffer, pH 4.2 (●), 5.0 (▲), 7.0 (■), 7.5 (◆).

(B) 0.01 M cacodylate pH 7.0, with 0.1 M NaCl (●), 0.3 M NaCl (▲), 0.4 M NaCl (■), 0.5 M NaCl (◆), 0.8 M NaCl (+), 0.9 M NaCl (x), 1.0 M NaCl (o), 2.0 M NaCl (Δ), 3.0 M NaCl ( ).

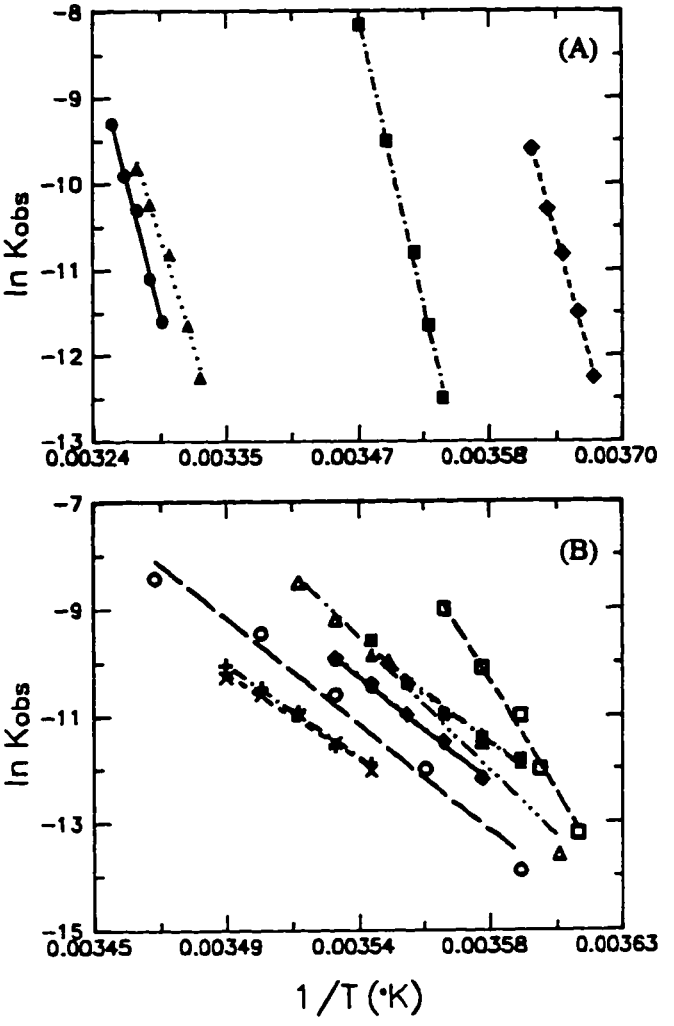
(A)
(B)
ln Kobs
1/T (°K)
-8
-9
-10
-11
-12
-13
-7
-15
0.00324
0.00335
0.00347
0.00358
0.00370
0.00345
0.00349
0.00354
0.00358
0.00363

Figure 5: van't Hoff plots for the second transition of triplex mixtures (duplex dissociation in presence of the third strand).

(A) mixing buffer, pH 4.2 (●), 5.0 (▲), 7.0 (■), 7.5 (◆), 8.0 (+), 8.5 (x). The plots superimpose between pH 5.0 - 8.5, indicating that T_m for the duplex is pH independent over this range.

(B) 0.01 M cacodylate pH 7.0, with 0.1 M NaCl (●), 0.3 M NaCl (▲), 0.4 M NaCl (■), 0.5 M NaCl (◆), 0.8 M NaCl (+), 0.9 M NaCl (x), 1.0 M NaCl (o), 2.0 M NaCl (Δ), 3.0 M NaCl ( ).

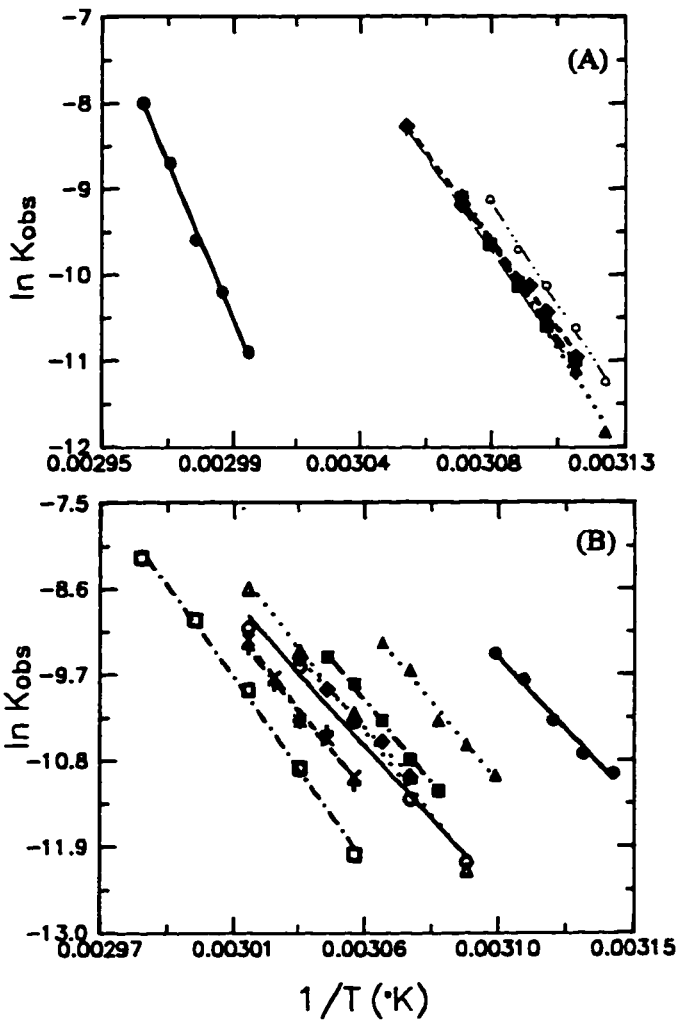
(A)
(B)
ln Kobs
ln Kobs
1/T (°K)
-7
-8
-9
-10
-11
-12
0.00295
0.00299
0.00304
0.00308
0.00313
-7.5
-8.6
-9.7
-10.8
-11.9
-13.0
0.00297
0.00301
0.00306
0.00310
0.00315

Figure 6: van't Hoff plots for melting of duplex.

(A) mixing buffer, pH 4.2 (●), 5.0 (▲), 7.0 (■), 7.5 (◆), 8.0 (+), 8.5 (x). The plots superimpose between pH 5.0 - 8.5, indicating that T_m for the duplex is pH independent over this range.

(B) 0.01 M cacodylate pH 7.0, with 0.1 M NaCl (●), 0.3 M NaCl (▲), 0.4 M NaCl (■), 0.5 M NaCl (◆), 0.8 M NaCl (+), 0.9 M NaCl (x), 1.0 M NaCl (o), 2.0 M NaCl (Δ), 3.0 M NaCl ( ).

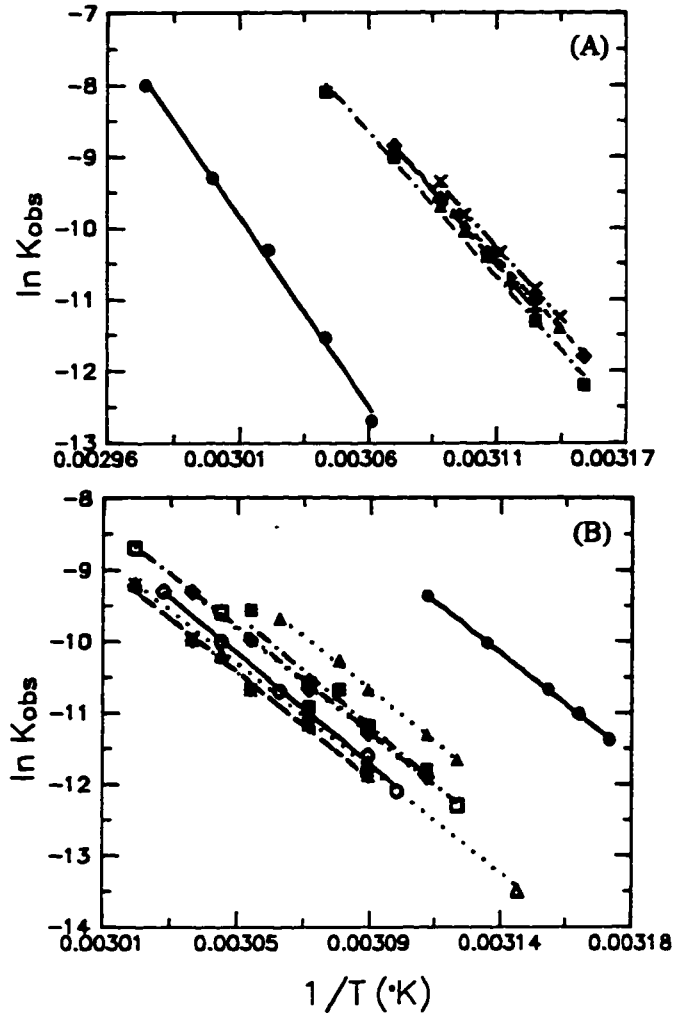
(A)
(B)
ln Kobs
1/T (°K)
-7
-8
-9
-10
-11
-12
-13
-14
0.00296
0.00301
0.00306
0.00311
0.00317
0.00301
0.00305
0.00309
0.00314
0.00318

Sodium Ion Dependence of Third Strand Binding

The thermal stability of the triplex is not affected on increasing NaCl concentration from 0.1 to 0.4M, but above 0.4M *increases* to a maximum at approximately 0.9M (T_m = 10 °C) and then *decreases* to 5 °C at 3M NaCl (Table 1 and Figures 7A-C). That decreasing NaCl concentration below 0.4M has no effect on T_m was repeatedly confirmed. This unusual behavior must result from the protons of dC^+ contributing to the stability of the triplex. That this is not an artifactual result is shown by the T_m for the duplex in the triplex solution decreasing in the normal manner below 0.4M. Thus, Figure 7C shows the log[NaCl] dependence for the duplex in triplex solution and for the duplex in duplex solution, confirming the decreasing ionic strength of these solutions.

Between 0.4 and 0.9M NaCl the dominant effect of increasing Na^+ concentration is presumably to contribute to triplex stability by shielding the negative charges of the three phosphodiester backbones; yet, over that range $\frac{\partial T_m}{\partial \log[Na^+]}$ is 10 °C (Figure 7B), relative to a value of 11 °C (Figure 7C) for the duplex, a value in good agreement for oligomers of this length. Dependence of T_m on $\log[Na^+]$ has been shown to fall off sharply with decreasing strand length, N, in the range $16 \leq N \leq 44$, e.g., for $d(T\text{-}A)_9$, $\frac{\partial T_m}{\partial \log[Na^+]}$ = 12 °C (33). Blake et al. (34) showed much higher salt dependence of triplex stability, $\frac{\partial T_m}{\partial \log[Na^+]}$ = 31 °C, for the analogous polymer triplex with uncharged homopyrimidine third strand *residues* [poly(U:A·U)] in comparison to "average" duplex polymer DNA that has a value of 18 °C (35,36). It must be that the salt dependence of our

triplex is reduced because the net repulsive energy in the backbone is partially counterbalanced by the positive charges on the third strand dC residues. Moreover, saturation is not observed at higher NaCl concentration, as is the case for poly(U:A·U), presumably because the ionic interaction between the Hoogsteen C^+:G base pair is destabilized by still higher monovalent cation concentration, $\frac{\partial T_m}{\partial \log[Na^+]_{0.9 \text{ to } 3M}} = -9$ °C (Figure 7B). This inverse salt dependence has not been observed previously (37, 38) as earlier work only examined salt dependence below 1M NaCl. Plum et al. (37) determined $\frac{\partial T_m}{\partial \log[Na^+]_{0.2 \text{ to } 1M}} = 12$ °C for melting of the third strand 5-'TTTTTCTCTCTCTCT-3' from a core homopurine-homopyrimidine duplex with 21 base pairs. Our value of 10 °C over an equivalent salt range is similar.

From equation [22] a plot of $\frac{1}{T_m}$ vs $\log[NaCl]_{0.9 \text{ to } 3M}$ (Figure 7A) shows positive logarithmic dependence at pH 7.0 ($Y = 1.1 \times 10^{-4} K^{-1} X$). Substituting for $Z_1 = 33$ and $\Delta H°_1 = 2.7$ kcal.mol^{-1} phosphate at 1M NaCl into [22], one obtains $\Delta n_1 = -4$. Similarly at 2M NaCl with $\Delta H°_1 = 3.3$ kcal.mol^{-1} phosphate, $\Delta n_1 = -5$ and at 3M NaCl with $\Delta H°_1 = 5.6$ kcal.mol^{-1} phosphate, $\Delta n_1 = 9$.

In triplexes without protonated residues in the third strand, Δn_1 is positive as the triplex has a higher charge density than its core duplex; in that event, third strand dissociation should result in release of Na^+. For this triplex, however, the positive charges on the dC residues of the third strand reduce the net negative charge of the triplex. Hence, on third strand dissociation above 0.9M NaCl at pH 7.0, there is a net

uptake of Na^+ by the duplex and single strand. Confirmation that the protons on the dC residues contribute to shielding, i.e., reduce the net negative charge on the triplex, comes from the negative values for Δn_1 (uptake of Na^+) obtained on dissociating the third strand from the core duplex at pH 7.0. Increasing NaCl concentration should favor the dissociation (Le Châteliers principle), which is what is observed in the form of decreasing triplex stability. Thus, the inverse dependence of triplex stability on NaCl concentration above 0.9M NaCl provides additional evidence that the dC residues are protonated at pH 7.0.

Figure 7:

(A) Linear plot according to [22], $\frac{1}{T_m}$ vs $\log[NaCl]_{0.9 \text{ to } 3M}$ at pH 7.0, 0.01M cacodylate, for dissociation of third strand.

(B) Plot of T_m vs $\log[NaCl]_{0.1 \text{ to } 3M}$ at pH 7.0, 0.01M cacodylate, for dissociation of third strand.

(C) Plot of T_m vs $\log[NaCl]_{0.1 \text{ to } 0.8M}$ at pH 7.0, 0.01M cacodylate, for dissociation of duplex in triplex solution (●), and duplex in duplex solution (▲).

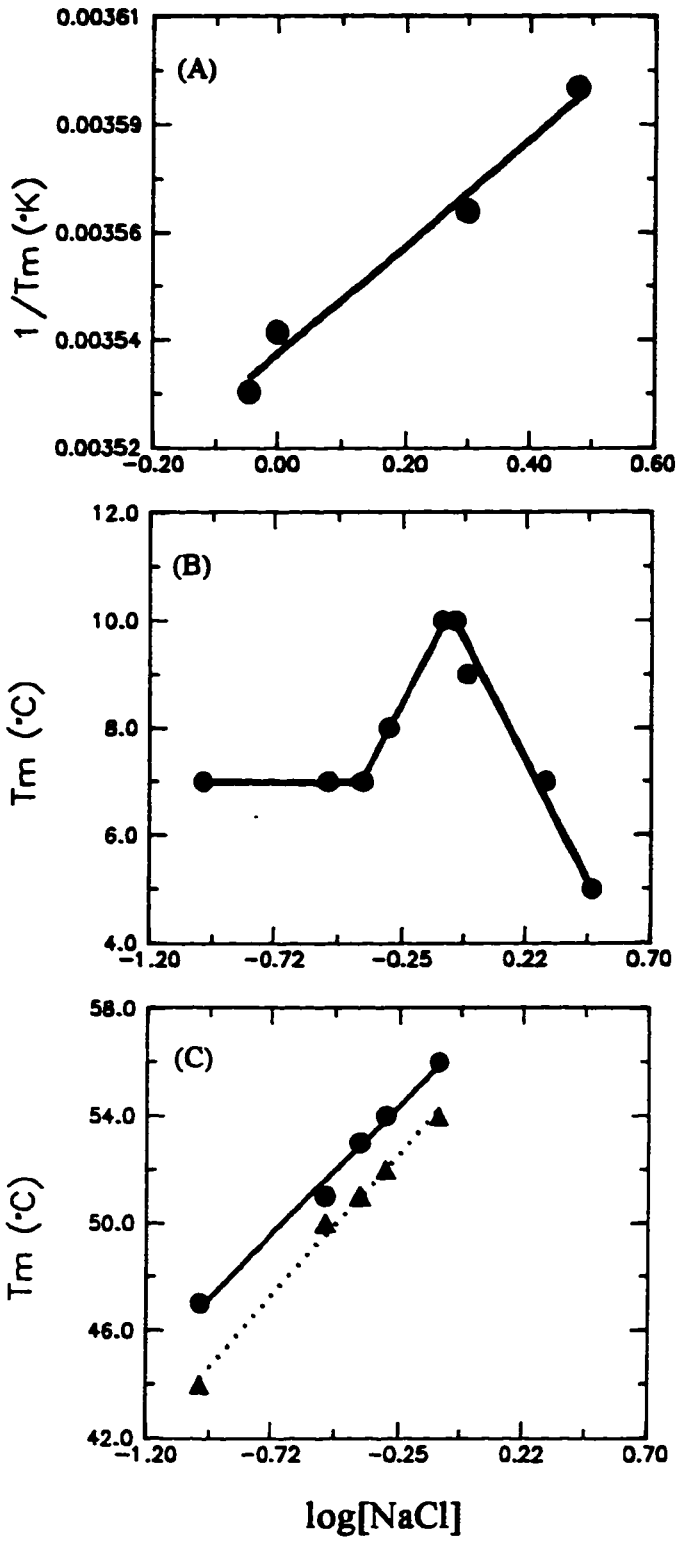
(A)
1/Tm (°K)
0.00361
0.00359
0.00356
0.00354
0.00352
-0.20
0.00
0.20
0.40
0.60
(B)
Tm (°C)
12.0
10.0
8.0
6.0
4.0
-1.20
-0.72
-0.25
0.22
0.70
(C)
Tm (°C)
58.0
54.0
50.0
46.0
42.0
-1.20
-0.72
-0.25
0.22
0.70
log[NaCl]

Hydrogen Ion Dependence of Third Strand Binding

Figure 8 shows negative dependence of T_m for third strand dissociation on pH, i.e., with $\frac{1}{T_m}$ decreasing linearly with -pH ($Y = -1.08 \times 10^{-4} K^{-1} X$). Substituting $\Delta H° =$ 116 kcal.mol^{-1} oligomer at pH 7.0 into equation [23], one obtains $\Delta n_2 = 5.5$, i.e., on dissociating the third strand at pH 7.0, 5.5 protons are released into solution. This value equals 1 H^+ per third strand dC residue if the likelihood of bound third strands with dangling 5' dC and 3' dT residues is the same (see Figure 11 and Discussion). It is not surprising therefore that increasing hydrogen ion concentration favors triplex stability. While this pH dependence has been widely observed, the number of protons involved in the transition has been underestimated previously (11). Quantitation in that work was based upon $\frac{dT_m}{d(pH)} = \Delta H^+ \frac{2.3\, R(T_m)^2}{\Delta H°_{obs}}$ by Record et. al. (23), which differs from our equation [23] by a factor of one half because it does not take into account the shielding contribution of protonated dC residues in the triplex. For example, the binding of d(mCTTmCmCTmC mCTmCT) (mC ≡ d 5-methylC residues) to duplex was calculated (11) to involve three protons whereas use of equation [23] gives a value of six protons, which equals the number of third strand dC residues.

It is possible to calculate the free energy associated with transfer of H^+ from aqueous solution to the third strand dC residues at various pH values using $\Delta G_{pKa} =$ 2.303 $RT\Delta pK_a$, where ΔpK_a is essentially the difference between 4.6 (pK_a of dCMP) and the pH of the bulk solution. This will be favorable if the pH of the solution is below 4.6 or unfavorable if above. At 25 °C, $\Delta G_{pKa} = -0.6$ kcal.mol^{-1} H^+ at pH 4.2, 0.6 at pH 5.0,

3.3 at pH 7.0 and 4.0 at pH 7.5. The increasingly large positive values as pH rises above 5.0 indicate that third strand association with duplex requires significant favorable interactions for triplex to form. For the triplex at pH 7.0, at T_m (11 °C), $\Delta G_{total} = 0 = \Delta G_{pKa} + \Delta G_{structural}$, where $\Delta G_{structural}$ is the favorable free energy contribution resulting from the third strand-duplex interactions. With ΔG_{pKa} = 3.1 kcal.mol^{-1} H^+ at 11 °C, $\Delta G_{structural}$ = -18.6 kcal.mol^{-1} oligomer. Since we have shown that triplex formation requires protonation of the third strand dC residues, a significant contribution to $\Delta G_{structural}$ must come from elimination of the lone pair repulsion between N3 of dC and N7 of dG by formation of an ionic H-bond (Figure 10), and the favorable Coulombic attraction between the protonated dC residues and the surrounding negatively charged phosphodiester backbones of the three strands. These observations provide further evidence for the protonated state of third strand dC residues in C:G·C triplets at neutrality, i.e., C^+:G·C.

Figure 8: Linear plot according to [23], $\frac{1}{T_m}$ vs -pH in mixing buffer, for dissociation of third strand.

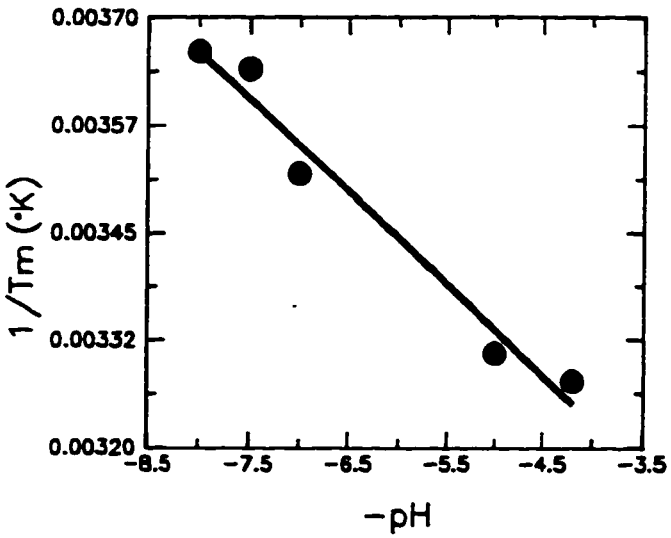
0.00370
0.00357
0.00345
0.00332
0.00320
1/Tm (°K)
-8.5
-7.5
-6.5
-5.5
-4.5
-3.5
-pH

Energy Minimized Structures of T:A·T and C^+:G·C vs C:G·C

The energy minimized structure for the isolated base triplet T:A·T, shown in Figure 9A, was obtained after 309 search directions and 686 single point calculations, resulting in an energy minimum of -90.5 $kcal.mol^{-1}$. The space filling model shows four H-bond 'contacts', all within standard H-bond distances.

The comparable energy minimized structure for C^+:G·C (Figure 9B) was obtained after 265 search directions and 561 single point calculations, resulting in an energy minimum of -169.0 $kcal.mol^{-1}$. The space filling model shows five H-bond 'contacts', all within standard H-bond distances. Noteworthy is the significantly shorter ionic H-bond of 2.66Å vs 2.84 ±0.02 for the others, showing the additional stability arising from the significantly larger electrostatic contribution to this H-bond.

In contrast, no reasonable structure could be obtained for the isolated base triplet C:G·C. Since all the energy minimizations were done with no constraints, the neutral Hoogsteen N1-methylcytosine was apparently forced away from the N9-methylguanine, resulting in no realistic structure. The repulsion between the negatively charged N3 of the Hoogsteen cytosine and the N7 of guanine results in an energetically very unstable Hoogsteen C:G interaction that would require large amounts of compensatory stacking energy not likely to result from the overlap of dT and dC residues in the third strand. As expected, the Watson-Crick G·C base pair in these base triplets remained normal after these minimizations. Thus, there is a clear electrostatic basis for the requirement for protonation of dC in order to form a C^+:G·C base triplet at any pH value.

Figure 9: Energy minimized structures of isostructural base triplets between third strand pyrimidine residues and target Watson-Crick base pairs:

(A) T:A•T. H-bond distances from left to right are 2.81Å, 2.87Å, 2.87Å and 2.83Å;

(B) C^+:G•C. H-bond distances from left to right are 2.66Å, 2.83Å, 2.85Å, 2.86Å and 2.83Å.

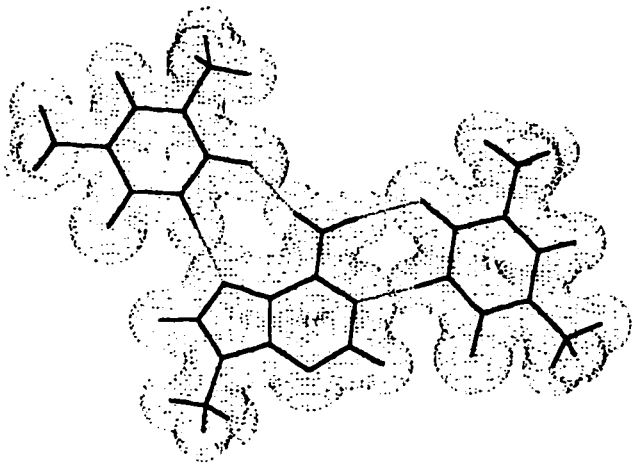

(A)

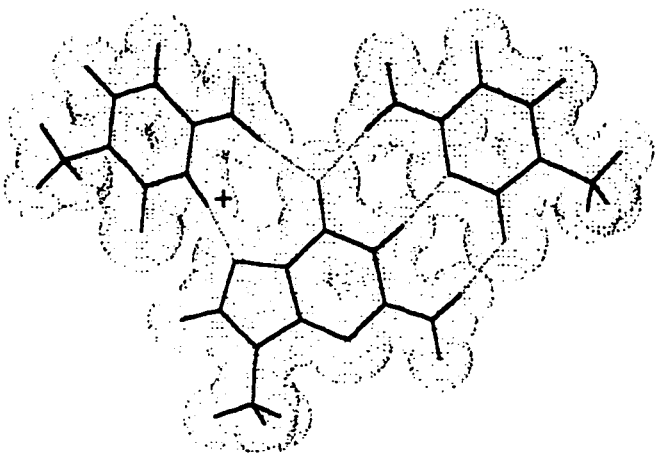

(B)

2.5 Discussion

Condensation-Screening Theory

Our derivation for the salt dependence of T_m without taking protonated residues into account [20] is the same as that obtained by Manning (22)[3/]. When Record et al. (23) analyzed the dependence of T_m on salt concentration for *protonated helices*, they obtained for the dependence of T_m on pH (their equation 22)

$$\frac{dT_m}{d(pH)} = \Delta H^+ \frac{2.3\, R(T_m)^2}{\Delta H°_{obs}} \qquad [A]$$

where ΔH^+ is the number of H^+ involved in the helix-coil transition.

In contrast, we obtain

$$\frac{dT_m}{d(pH)} = \frac{\Delta H^+}{2} \frac{2.3\, R(T_m)^2}{\Delta H°_{obs}} \qquad [B]$$

where the factor of one half results from explicit inclusion of electrostatic shielding by H^+ (i.e. $\Delta G_{el\ H^+}$ of our [15]). Although we have developed our analysis for the triplex at pH 7, it is easily generalized to any coil to helix transition involving proton uptake. For such cases [B] is the same, but the expression for ΔH^+ [13] would be different e.g.,

$$2\ \text{poly(A)} + 2\ H^+ \rightarrow \text{poly}(A^+ \cdot A^+) \qquad \text{and} \qquad \Delta H^+ = Z_2\left(\frac{1}{2\xi(S_1)} + \frac{1}{2\xi(S_2)} - \frac{1}{\xi(D)}\right).$$

As is the case for the triplex we have studied and the similar one studied by Xodo et al. (11), use of [B] results in exact agreement with the number of H^+ involved in third strand binding. These results show that all the third strand dC residues must be protonated, even at pH 7. The importance of all the third strand dC residues requiring H^+ upon binding has

also been shown for dC residues that are adjacent d(TTC$^+$C$^+$C$^+$TC$^+$TTC$^+$C$^+$C$^+$C$^+$C$^+$) (39).

The difference in the number of H^+ released when poly(A^+·A^+) is melted at pH 4.2 and 5.3 is 0.55 (40). Using the data and [A] from (23), ΔH^+ was calculated to be 0.2 (23); however using our equation [B] we obtain $\Delta H^+ = 0.4$, much closer to the value observed experimentally.

UV Spectroscopy

The spectral components contributing to the UV-absorbance difference on third strand dissociation have been identified, and explicitly shown that deprotonation of dC residues is the major spectral component at pH 7.0. This method of spectral analysis should prove useful for current work on the acid induced structures of poly[d(C)] and poly[r(C)] (41) and of d(C-T)$_n$ and d(C$_n$T$_n$) (42-44) in which dC residues are required in the base pairing schemes, C$^+$·C, C$^+$·T, and C·T for a number of proposed novel structures (parallel and antiparallel duplexes, tetraplexes).

Enthalpy Values for Dissociation of Third Strand and Duplex

For the duplex, d(A-G)$_6$·d(C-T)$_6$, in a duplex mixture over a variety of conditions, 0.15 M NaCl/0.005M $MgCl_2$/pH 5.0 to 8.5, and 0.1 to 3.0 M NaCl/pH 7.0, our mean $\Delta H°_{obs}$ value of about -6 kcal.mol^{-1} base pair is in very good agreement with other reported mean $\Delta H°$ values, e.g., for a similar homopurine-homopyrimidine 21 base pair duplex, $\Delta H° = -6$ kcal.mol^{-1} base pair obtained by DSC (37). Unlike the sensitivity to pH

and ionic conditions indicated by the ΔH° values for the triplex, the ΔH° values show that the interactions that stabilize the Watson-Crick duplex are not similarly sensitive.

However, our ΔH°_{obs} values for dissociation of third strand do vary with solution conditions, showing that the interactions of these Hoogsteen base pairs are quite sensitive to ionic strength and pH and that this third strand binding interaction is stronger than that between the strands of a Watson-Crick duplex. Our ΔH°_{obs} values for the dissociation of the third strand include all the enthalpic components that contribute to the transition: dissociation of the Hoogsteen base pairs, T:A and C^+:G; deprotonation of the dC^+ residues (when the solution pH > 4.6) and any additional enthalpy changes occurring in the core Watson-Crick duplex, i.e., A → B transition. The literature contains a variety of ΔH° values for the Hoogsteen base pairs of similar deoxytriplexes: -6.6 by UV and after subtracting the estimated enthalpy contribution from protonation of the dC^+ residues (45), -5.8 by DSC and UV and after subtracting the estimated enthalpy contribution from protonation of the dC^+ residues (46), -5 by UV (47), -4.2 by UV (48), -2.0 by calorimetry and -6 $kcal.mol^{-1}$ Hoogsteen base pair by UV (37). This spread of values may result from differences in oligomer sequence (stacking interactions); end effects due to variation in length of strands, including in some cases differences in the third strand and core duplex length; various solution conditions (pH, ionic strength, different cations); and variations in the methods and models used to obtain the enthalpy values [4]. A recent paper by Wilson et al. (49) has shown that calorimetrically-obtained enthalpy values, **only for third strands with C residues**, vary significantly with the type of buffer used and the pH

(for a third strand (19 mer) containing only three dC residues the enthalpy values vary from -2.9 to -5 kcal.mol^{-1} base triplet).

Ionic Strength Dependence

If the third strand dC residues in the triplex were uncharged at pH 7.0, then one would expect a positive ionic strength dependence of triplex stability over a broad range of ionic strength, due to the high negative charge density arising from the negatively charged phosphates on the three strands. Such ionic strength dependence of stability is the norm for duplexes and triplexes with uncharged bases, e.g., poly(U:A•U) (34). In contrast, inverse salt dependence of T_m at moderate ionic strengths is observed with duplexes stabilized by ionic interactions, as in the case of poly(C^+•C) (25,50) and poly(A^+•A^+) (51). Similarly, we observe that increasing NaCl concentration above 0.9M destabilizes third strand binding, and we attribute this reversal of salt dependence to increased shielding by the Na^+, resulting in a reduced affinity of the dC residues for H^+, and a decrease in the electrostatic attraction between the C^+:G Hoogsteen base pair, and also the dC^+ residues and the phosphodiester backbone of the duplex. We do not attribute this reduction in T_m to the higher concentrations of Cl^-, as the duplex at these high concentrations (1M NaCl to 3M NaCl) shows no reduction in stability (Table 1). In this regard, there is some confusion in the literature as to the effect that high concentrations of anions have on duplex stability. Our results confirm those of Hamaguchi and Geiduschek (52), who showed that DNA has a constant T_m of 90 °C at high ionic strengths of up to 4M NaCl; i.e., there is no T_m dependence on Cl^- concentration, unlike other anions that

were shown to decrease duplex stability and were classed as hydrophobic bond breaking agents and arranged in a chaotropic series by those authors.

Third Strand Orientation and Register

Binding of the homopyrimidine third strand via reverse Hoogsteen base pairing is not known to occur, i.e., with the third strand antiparallel to the Watson-Crick homopurine strand (Figure 11A). Binding of the third strand parallel to the homopurine strand has been proposed from fiber diffraction data and modeling (8,53) and confirmed by NMR for the triplex $d(T\text{-}C)_4$:$d(G\text{-}A)_4$•$d(T\text{-}C)_4$ (15). But even with parallel third strand orientation via Hoogsteen base pairing, two alternative registers are possible. The third strand must be displaced, with either a dangling dC residue at the 5' end (Figure 11B) or a dangling dT residue at the 3' end (Figure 11C). While both of these binding arrangements have 11 base pair interactions, the structure with the 3' overhang is more likely under acidic conditions (Figure 11C), whereas the 5' overhang is more likely at neutrality, since the 5' third strand dC residue need not then be protonated (Figure 11B). As noted above, an equilibrium between these alternatives is consistent with the value of 5.5 calculated for Δn_2.

Figure 10: Comparison of CD spectra of the duplexes $d(A\text{-}G)_6 \cdot d(C^+\text{-}T)_6$ at pH 4.2 (—) and $d(A\text{-}G)_6 \cdot d(C\text{-}T)_6$ at pH 7.0 (···) in mixing buffer titrated to the indicated pH.

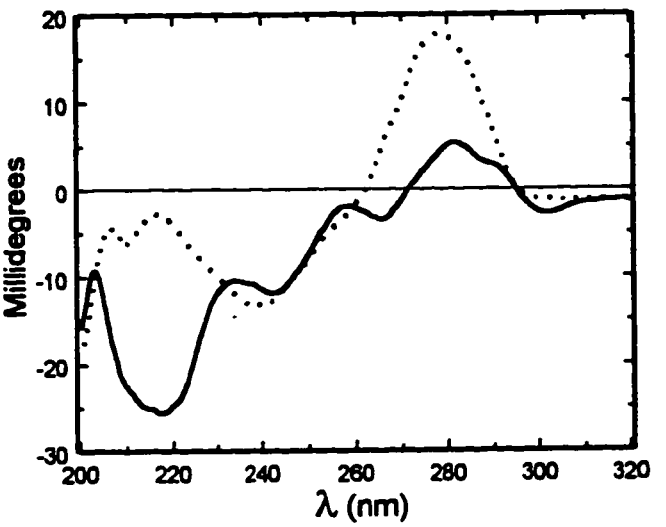
20
10
0
-10
-20
-30
Millidegrees
200
220
240
260
280
300
320
λ (nm)

Figure 11: Conceivable binding motifs of the third strand, shown as the top strand in italics.

(A) Third strand binding antiparallel requires reverse Hoogsteen base pairing.

(B) Third strand binding parallel with Hoogsteen base pairing and a 5' overhang.

(C) Third strand binding parallel with Hoogsteen base pairing and a 3' overhang. Strand orientation is expressed with reference to that of the homopurine strand (middle strand) of the target duplex.

```
   3'-TCTCTCTCTCTC-5'
   5'-AGAGAGAGAGAG-3'
A  3'-TCTCTCTCTCTC-5'
```

```
   5'-CTCTCTCTCTCT-3'
    5'-AGAGAGAGAGAG-3'
B   3'-TCTCTCTCTCTC-5'
```

```
    5'-CTCTCTCTCTCT-3'
   5'-AGAGAGAGAGAG-3'
C  3'-TCTCTCTCTCTC-5'
```

2.6 Conclusion

We have shown that protonation of third strand dC residues *is required* for $d(C\text{-}T)_6$ to interact with $[d(A\text{-}G)_6 \cdot d(C\text{-}T)_6]$ to form a triplex at neutrality or above. In this respect, formation of this triplex is mediated by a "proton switch". Not surprisingly, under such conditions third strand dissociation is cooperative, occurring with release of H^+ ions. An electrostatic rationale is provided for the essentiality of dC residue protonation. The reason is not so much the formation of the second H-bond per se, as it is to prevent the charge repulsion between the lone pair electrons at N3 of the third strand dC residues and those at N7 of the dG residues of the target Watson-Crick base pairs. The understanding developed here for the C^+:G•C base triplet should provide insights regarding the properties of other base triplets with analogous potential for ionizable third strand residues, as well as of other structures with base-base interactions involving ionized residues.

2.7 Footnotes

[1/] Our duplex and triplex length is ≅ 41Å (3.4Å x 12) which, for the ionic strengths studied here, is longer then the Debye length, κ^{-1}. Using [7] and [8]: κ^{-1} = 1.7Å (3M NaCl soln.); 7.3Å (*mixing buffer* soln.); 9.1 Å (0.1M NaCl soln.).

[2/] For both Na^+ and H^+ binding, $\frac{1}{\xi}$ must be dependent on the phosphate and third strand dC residue spacing. Equations [21] and [23] are still valid if the fraction of H^+ bound per third strand dC residue, θ_{H^+}, is not described by $1 - \frac{1}{\xi}$, but some other unknown function, 1 - fnc. That is,

$$\frac{\partial T_m}{\partial(\ln[H^+])} = \frac{1}{2}\frac{\Delta n_2}{Z_2}\frac{R(T_m)^2}{\Delta H_2} \quad \text{and} \quad \Delta n_2 = Z_2(\text{fnc}_{(S)} - \text{fnc}_{(T)}).$$

[3/] See (54,55) for comparison of the Poisson-Boltzmann equation and the Debye-Hückel approximation as applied to polyelectrolytes of the DNA type. The work of Bleam et al. (56) has shown that for DNA the fractional extent of neutralization ($\theta_{Na^+} = 0.75 \pm 0.1$) is in very good agreement with that predicted by counterion condensation theory (θ_{Na^+} = 0.76). Thus, in spite of the simple model used in counterion condensation theory, it gives accurate calculation of many polyelectrolyte phenomena for a variety of systems (56-59).

[4/] In this connection, we take issue with the notion that spectroscopically obtained enthalpy values must be incorrect when they are not similar to calorimetrically obtained

values. It is the prevailing view that calorimetrically obtained values are correct because they are obtained from a direct enthalpic measurement, whereas spectroscopically derived values require assumption of a model (37,60). However, these differences in mode of enthalpic estimation could mean that they measure different enthalpic events. The calorimetric measurement subtracts the enthalpic changes occurring in the reference solution (equivalent solution with no oligonucleotide) from those occurring in the sample. In the spectroscopic method the reference solution does not contribute to the absorbance difference at the wavelength of observation, in this case 255 nm, and therefore does not affect the transition curve. Different results from the two methods may also be due to the different oligomer concentrations used, calorimetry generally requiring 20x more concentrated solutions. Equivalent $\Delta H°$ values for third strand dissociation in solutions of very different oligomer concentration can only be expected if their water activity is the same and if water does not contribute to the enthalpy change on third strand dissociation; neither of these assumptions is correct. This has been confirmed by calorimetric studies showing a significant enthalpic contribution from reorganization of water during complexation in aqueous solution between protein-nucleotide, protein-peptide, protein-carbohydrate, and small molecule-small molecule systems (61). Also, we have shown that water plays an important role in triplex formation (62).

2.8 Acknowledgements

This work was supported by NIH grant (GM 42936) to J. R. F., and a Berlex Pre-Doctoral Fellowship from Berlex Corp., a Pre-Doctoral Traineeship from NIH grant (GM 08309), an Autodesk educational software grant from Autodesk Corp. and a gift of AXUM 3.0 from TriMetrix Corporation to L. L.

2.9 References

1. Wells, R. D., Collier, D. A., Hanvey, J. C., Shimizu, M. and Wohlrab, F. (1988) *Faseb. J.* **2**, 2939-49.
2. Htun, H. and Dahlberg, J. E. (1989) *Science.* **243**, 1571-6.
3. Moser, H. E. and Dervan, P. B. (1987) *Science.* **238**, 645-50.
4. Fresco, J. R. (1963) in *Informational Macromolecules* (Vogel, H. J., Bryson, V. and Lampen, J. O., Eds.) pp. 121-42, Academic Press, New York.
5. Lipsett, M. N. (1964) *J. Biol. Chem.* **239** No. 4, 1256-60.
6. Morgan, A. R. and Wells, R. D. (1968) *J. Mol. Biol.* **37**, 63-80.
7. Thiele, D. and Guschlbauer, W. (1971) *Biopolymers.* **10**, 143-57.
8. Arnott, S., Bond, P. J., Selsing, E. and Smith, P. J. C. (1976) *Nucleic. Acids. Res.* **3** No.10, 2459-70
9. Mirkin, S. M., Lyamichev, V. I., Drushlyak, K. N., Dobrynin, V. N., Filippov, S. A. and Frank-Kamenetskii, M. D. (1987) *Nature.* **330**, 495-7.
10. Letai, A. G., Palladino, M. A., Fromm, E., Rizzo, V. and Fresco, J. R. (1988) *Biochemistry.* **27**, 9108-12.
11. Xodo, L. E., Manzini, G., Quadrifoglio, F., van der Marel, G. A. and van Boom, J.H. (1991) *Nucleic. Acids. Res.* **19**, 5625-31.
12. Hanvey, J. C., Williams, E. M. and Besterman, J. M. (1991) *Antisense. Res. Dev.* **1**, 307-17.
13. Singleton, S. F. and Dervan, P. B. (1992) *Biochemistry.* **31**, 10995-1003.
14. Rajagopal, P. and Feigon, J. (1989) *Nature.* **339**, 637-40.

15. Rajagopal, P. and Feigon, J. (1989) *Biochemistry.* **28**, 7859-70.
16. Cheng, Y. K. and Pettitt, B. M. (1992) *Prog. Biophys. Mol. Biol.* **58**, 225-57.
17. Sklenár, V. and Feigon, J. (1990) *Nature.* **345**, 836-38.
18. AXUM 3.0, (1993) TriMetrix Corporation, 444 NE Ravenna Blvd., Suite 210, Seattle, WA 98115.
19. HyperChem 2.0 (1992) Autodesk Corporation, Scientific Modeling Division, 2320 Marinship Way, Sausalito, CA 94965.
20. Singh, U. C., Weiner, P. K., Caldwell, J. and Kollman, P. A. (1989) University of California, San Francisco, CA.
21. Manning, G. S. (1969) *J. Chem. Phys.* **51** No.3, 924-33.
22. Manning, G. S. (1972) *Biopolymers.* **11**, 937-49.
23. Record, M. T. Jr., Woodbury, C. P. and Lohman, T. M., (1976) *Biopolymers.* **15**, 893-915.
24. Adams, A., Lindahl, T. and Fresco, J. R. (1967) *Proc. Nat. Acad. Sci.* **57** No.6, 1684-91.
25. Akinrimisi, E. O., Sander, C. and Ts'o, P. O. P. (1963) *Biochemistry.* **2**, 340-4.
26. Inman, R. B. (1964) *J. Mol. Biol.* **9**, 624-37.
27. Liu, K., Miles, H. T., Frazier, J. and Sasisekharan, V. (1993) *Biochemistry.* **32**, 11802-9.
28. Hoogsteen, K. (1963) *Acta Crystallogr.* **16**, 907-16.
29. Ornstein, R. L. and Fresco, J. R. (1983) *Proc. Natl. Acad. Sci. U. S. A.* **80**, 5171-75.
30. Allen, L. C. (1975) *J. Am. Chem. Soc.* **97** No. 24, 6921-40.
31. Burstein, K. Y. and Isaev, A. N. (1984) *Theoret. Chim. Acta (Berl.)* **64**, 397-401.
32. Pullman, B., Claverie, P. and Caillet, J. (1967) *Proc. Nat. Acad. Sci.* **57**, 1663-9.
33. Elson, E. L., Scheffler, I. E. and Baldwin, R. L. (1970) *J. Mol. Biol.* **54**, 401-15.
34. Blake, R. D., Massoulié, J. and Fresco, J. R. (1967) *J. Mol. Biol.* **30**, 291-308.
35. Dove, W. F. and Davidson, N. (1962) *J. Mol. Biol.* **5**, 467-78.
36. Record, M. T., Jr. (1967) *Biopolymers.* **5**, 975-92.
37. Plum, G. E., Park, Y. W., Singleton, S. F., Dervan, P. B. and Breslauer, K. J. (1990) *Proc. Natl. Acad. Sci. U. S. A.* **87**, 9436-40.

38. Völker, J and Klump, H. H. (1994) *Biochemistry.* **33**, 13502-8.

39. Mirkin, S. M. and Frank-Kamenetskii, M. D. (1994) *Annu. Rev. Biophys. Biomol. Struct.* **23**, 541-76.

40. Holcomb, D. N. and Timasheff, S. N. (1968) *Biopolymers.* **6**, 513-29.

41. Antao, V. P. and Gray, D. M. (1993) *J. Biomol. Struct. Dyn.* **10**, 819-39.

42. Gehring, K., Leroy, J. L. and Gueron, M. (1993) *Nature.* **363**, 561-5.

43. Jaishree, T. N. and Wang, A. H. J. (1993) *Nucleic. Acids. Res.* **21**, 3839-44.

44. Leroy, J. L., Gehring, K., Kettani, A. and Gueron, M. (1993) *Biochemistry.* **32**, 6019- 31.

45. Manzini, G., Xodo, L. E., Gasparotto, D., Quadrifoglio, F., van der Marel, G. A. and van Boom, J. H. (1990) *J. Mol. Biol.* **213**, 833-43.

46. Xodo, L. E., Manzini, G. and Quadrifoglio, F. (1990) *Nucleic. Acids. Res.* **18**, 3557-64.

47. Rougée, M., Faucon, B., Mergny, J. L., Barcelo, F., Giovannangeli, C., Garestier, T. and Helene, C. (1992) *Biochemistry.* **31**, 9269-78.

48. Pilch, D. S., Brousseau, R. and Shafer, R. H. (1990) *Nucleic Acids Res.* **18**, 5743-50.

49. Wilson, W. D., Hopkins, H. P., Mizan, S., Hamilton, D. D. and Zon, G. (1994) *J. Am. Chem. Soc.* **116** No. 8, 3607-8.

50. Guschlbauer, W. (1967) *Proc. Nat. Acad. Sci.* **57** No. 5, 1441-48.

51. Michelson, A. M., Massoulié, J. and Guschlbauer, W. (1967) *Progr. Nucleic Acid Res.* **6**, 83-141.

52. Hamaguchi, K. and Geiduschek, E. P. (1962) *J. Am. Chem. Soc.* **84** No. 8, 1329-38.

53. Arnott, S. and Selsing, E., (1974) *J. Molec. Biol.* **88**, 509-21.

54. Frank-Kamenetskii, M. D., Anshelevich, V. V. and Lukashin, A. V. (1987) *Sov. Phys. Usp.* **30**, 317-30.

55. Anderson, C. F. and Record, M. T. Jr. (1990) *Annu. Rev. Biophys. Biomol. Struct.* **19**, 423-65.

56. Bleam, M. L., Anderson, C. F. and Record, M. T. Jr. (1980) *Proc. Nat. Acad. Sci.* **77**, 3085-89.

57. Granot, J. and Kearns, D. R. (1982) *Biopolymers.* **21**, 203-18.

58. Braunlin, W. H., Anderson, C. F. and Record, M. T. Jr. (1987) *Biochemistry.* **26**, 7724-31.

59. Padmanabhan, S., Richey, B., Anderson, C. F. and Record, M. T. Jr. (1987) *Biochemistry.* **27**, 4367-76.

60. Marky, L. A. and Breslauer, K. J. (1987) *Biopolymers.* **26**, 1601-20.

61. Chervenak, M. C. and Toone, E. J. (1994) *J. Am. Chem. Soc.* **116** No. 23, 10533-9.

62. Lavelle, L. and Fresco, J. R. In preparation.

III. Enhanced stabilization of the triplexes $d(C^+\text{-}T)_6$:$d(A\text{-}G)_6$·$d(C\text{-}T)_6$; $d(T)_{21}$:$d(A)_{21}$·$d(T)_{21}$ and Poly r(U:A·U) by various additives; evidence for a role for water in triplex stability

Laurence Lavelle and Jacques R. Fresco

in preparation

The stability of the triplexes $d(C^+\text{-}T)_6$:$d(A\text{-}G)_6$·$d(C\text{-}T)_6$, $d(T)_{21}$:$d(A)_{21}$·$d(T)_{21}$, Poly r(U:A·U) and their respective core duplexes, $d(A\text{-}G)_6$·$d(C\text{-}T)_6$, $d(A)_{21}$·$d(T)_{21}$, Poly r(A·U) has been studied in the presence of a variety of inorganic and organic anions and cations, cationic lipids, low molecular weight alcohols, SDS, coralyne, trehalose, glycerol, low molecular weight polyethylene glycols, and DMSO in otherwise aqueous solution. Triplex stability enhancement follows the Hofmeister series for anions, and similarly the water structure-making ability of the organic cations, the low molecular weight alcohols and other water structure-making solutes, whereas water structure-breaking solutes have the opposite effect. Water structure-making solutes appear to induce partial unwinding of target duplexes and removal of water therefrom, thereby facilitating the binding of a third strand in the major groove.

Abbreviations: MA-Cl, Methylammonium Chloride; DMA-Cl, Dimethylammonium Chloride; TriMA-Cl, Trimethylammonium Chloride; TMA-Cl, Tetramethylammonium Chloride; TMA-S, Tetramethylammonium Sulfate; TEA-Cl, Tetraethylammonium

Chloride; TPA-Cl, Tetrapropylammonium Chloride; CTriMA-Cl, Cetyltrimethylammonium Chloride; DidecylA-Cl, Didecylammonium Chloride; TridodecylMA-Cl, Tridodecylmethylammonium Chloride; DOSPA, 2,3-dioleyloxy-N-[2(sperminecarboxamido) ethyl]-N,N-dimethyl-1-propanaminium trifluoroacetate; SDS, Sodium Dodecylsulfate; MeOH, Methanol; EtOH, Ethanol; 2-PrOH, 2-Propanol; BuOH, 1-Butanol; Trehalose, α-D-glucopyranose α-D-glucopyranoside; DMSO, Dimethyl Sulfoxide; PEG200, poly(ethylene glycol) ave. MW200; PEG400, poly(ethylene glycol) ave. MW400; PEG600, poly(ethylene glycol) ave. MW600; NaCl, Sodium Chloride; Na_2HPO_4, Disodium Phosphate; $NaOOCCH_3$, Sodium Acetate; Na_2SO_4, Sodium Sulfate; $NaClO_4$, Sodium Perchlorate; NH_4Cl, Ammonium Chloride; $(NH_4)_2SO_4$, Ammonium Sulfate.

3.1 Introduction

Although triplexes have been studied extensively (see (1 - 6) for reviews), no study has systematically explored the broad range of solution conditions that affect their stability. Such an analysis has the potential to provide insights into the factors that determine both the stability of triplexes and the mechanism of their formation.

As polyanions, it is natural that the stability of nucleic acids is, in general, largely dependent on the concentration and type of cation in solution. Stabilization occurs by reducing the very high negative charge density of the phosphodiester backbone. However, the chemical nature of the cation can also determine other ways in which it can interact with nucleic acids. The triplex stabilizing effect of the group IA (e.g., Na^+, K^+) and group

IIA (e.g., Mg^{2+}) cations is well known, as is the ability of the transition metal cations to interact with the ring nitrogens and carbonyl groups of the purine and pyrimidine bases. [The ability of the transition metals to form organo-metallic complexes (e.g., square-planar, octahedral) is well known; and in the presence of nucleic acids the ligands are the purine and pyrimidine bases.] The positively charged organic polyamines, spermine and spermidine are also known to favor DNA triplex formation at neutral pH (7).

In this study the stabilizing effect of the organic cations MA^+, DMA^+, $TriMA^+$, TMA^+, TEA^+, and TPA^+ on triplex and duplex stability was first determined. As enhanced triplex stability was found in MA-Cl, DMA-Cl, TriMA-Cl, TMA-Cl, and TEA-Cl, the cationic lipids CTriMA (TriMA with one C_{16} tail), TridodecylMA (MA with three C_{12} tails) and DOSPA (essentially a spermine headgroup with two C_{18} tails, the headgroup has five positive charges at pH 7.0) were studied in an attempt to further increase triplex stability. Didecylamine, which has a positively charged NH_2^+ head group at pH 7 and two C_{10} tails, was also explored, but was found to be insoluble in water.

The foregoing examination of organic cation enhancement of triplex stability was complemented by experiments in which the nature of the anion was varied for particular sets of inorganic cations. This allowed a distinction to be made between the effect of cations which interact directly with the nucleic acid backbone, and the effect of anions which can affect the chemical potential and structure of water and thereby indirectly affect triplex stability.

The effect of another group of neutral additives capable of interacting with the aqueous solvent was also studied, including trehalose, glycerol, PEG and DMSO. Of

these, the disaccharide trehalose, is a well known stabilizer of proteins at high temperatures and is used in long-term storage of dried protein formulations (8, 9). This protein stabilizing ability is believed to be a combination of its own chemical stability (non-reducing disaccharide) and its glass forming (T_g 110 °C) and water replacing capacities (10). Glycerol is interesting in that it is a strong dehydrating compound, absorbing water up to 50% of its weight. PEG was selected for study because it facilitates crystallization of nucleic acids, and DMSO because it is a broad spectrum solvent of organic and inorganic compounds with a strong H-bonding ability.

3.2 Materials and Methods

Deoxyoligomers and Ribopolymers

$d(A\text{-}G)_6$ and $d(C\text{-}T)_6$ were synthesized, purified and analyzed as previously (11). Molar extinction coefficients determined after phosphodiesterase I digestion, $\varepsilon_{260} = 9890$ for $d(A\text{-}G)_6$ and $\varepsilon_{260} = 8510$ for $d(C\text{-}T)_6$ at 25 °C in 2.6 x 10^{-5} M Tris pH 7.4 / 2.4 x 10^{-5} M $MgCl_2$, were used to determine oligomer concentration. $d(T)_{21}$ and $d(A)_{21}$ were similarly synthesized and purified (Midland Certified Reagent Co., Midland, Texas) and analyzed for purity. The concentrations of these strands were calculated using the molar extinction coefficients for poly(dA) ($\varepsilon_{257} = 8600$) and for poly(dT) ($\varepsilon_{265} = 8700$) at 25 °C. Poly(A) and poly(U) were the same samples used in previous work from this laboratory (12);

concentrations of these strands were calculated using the molar extinction coefficients for poly(A) (ε_{280} = 2880) and for poly(U) (ε_{280} = 3140) at 25 °C.

Sample Preparation

Unless otherwise stated, triplexes were prepared in a *mixing buffer* (MB) of 0.15M NaCl/0.005M $MgCl_2$/0.01M cacodylate, titrated to the desired pH (± 0.1). Thermal stability of the triplexes and duplexes was compared with reference to their stability in MB at pH 7.0, which is considered a reasonable approximation of the physiological ionic and pH environment. Triplex mixtures were made with equimolar stocks of the two strands; after forming the duplex, a stoichiometric amount of the third strand was added. All samples were made with ddH_2O, buffered with 0.01M cacodylate, and titrated with HCl or NaOH. For many samples the pH was additionally checked after obtaining their melting profiles.

All additives were of the highest purity and purchased from the following sources. Aaper Alcohol and Chemical Co.: Ethanol; Aldrich: Methylammonium Chloride, Dimethylammonium Chloride, Trimethylammonium Chloride, Tetramethylammonium Chloride, Tetramethylammonium Sulfate, Tetraethylammonium Chloride, Tetrapropylammonium Chloride, Didecylamine, Cetyltrimethylammonium Chloride, Tridodecylmethylammonium Chloride, Poly(ethylene glycol) 200 (400, 600); J. T. Baker: Sodium Acetate, Ammonium Chloride, 1-Butanol; Baxter: Methanol; EM Science: Sodium Sulfate; Fisher: Dimethyl Sulfoxide; Kodak: Sodium Dodecylsulfate; Life Technologies: (DOSPA) 2,3-dioleyloxy-N-[2(sperminecarboxamido) ethyl]-N,N-

dimethyl-1-propanaminium trifluoroacetate; Merck: Ammonium Sulfate; Mallinckrodt: Disodium phosphate, 2-Propanol; Sigma: Trehalose, Sodium Chloride, Sodium Perchlorate.

UV Spectroscopy and Melting Profiles

Absorption spectra and thermal melting profiles were determined in a computer driven AVIV 14DS spectrophotometer equipped with a thermoelectrically controlled cell holder for cells of 1cm pathlength. Filtered, dry air was passed through the cell compartment to prevent condensation on the cell walls at low temperatures. The flow rate was set low enough so as not to create a temperature gradient between the sample and the cell holder, which was confirmed by monitoring the temperature in the sample and cell holder during trial melting profiles. For melting experiments, spectra were measured every 1 nm and 2 °C. Only triplex and duplex transitions that occur between 0 and 100 °C were observed. Care was taken to obtain true equilibrium melting profiles by recording scans only after a cuvette was allowed to reach the desired temperature (8 min). This ensured that the rate of temperature rise is less than the rate of the association-dissociation reaction under study, as confirmed by the absence of further absorbance change on longer incubation at some fixed temperature within the transition. These spectra were used to obtain melting profiles and their derivatives at appropriate wavelengths, from which melting transition temperatures, Tm values, were obtained from the midpoint of the transition. Tm values ($T_m \pm 0.5$ °C) were obtained by measuring each melting profile at least twice. Unless otherwise stated, Tm and % hyperchromism values were obtained from melting profiles

at 260 nm. All UV-melting profiles, wavelength scans and difference spectra are plotted using raw data. % Hyperchromism was calculated using:

$$\frac{Abs(duplex + coil)_{260} - Abs(triplex)_{260}}{Abs(duplex + coil)_{260}} X\ 100 \text{ for } 3 \rightarrow 2 + 1 \text{ triplex transitions; and}$$

$$\frac{Abs(coil)_{260} - Abs(triplex)_{260}}{Abs(coil)_{260}} X\ 100 \text{ for } 3 \rightarrow 1 + 1 + 1 \text{ triplex transitions; and}$$

$$\frac{Abs(coil)_{260} - Abs(duplex)_{260}}{Abs(coil)_{260}} X\ 100 \text{ for } 2 \rightarrow 1 + 1 \text{ duplex transitions.}$$

CD Spectroscopy

CD was measured every 0.2 nm (1 sec. average), with a 1.5 nm bandwidth, from 320 to 200 nm at 1 °C on a computer-driven AVIV 62DS CD spectrometer with a thermoelectrically-controlled cell holder. The cell compartment was continuously purged with dry N_2. The data was smoothed by a least-squares polynomial fit of 6th order.

3.3 Results

Tables 1 to 10 list the Tm values and the % hyperchromism obtained from the UV-melting profiles at 260 nm of the triplexes $d(C^+\text{-}T)_6$:$d(A\text{-}G)_6$·$d(C\text{-}T)_6$, $d(T)_{21}$:$d(A)_{21}$·$d(T)_{21}$, Poly r(U:A·U), and their respective core duplexes $d(A\text{-}G)_6$·$d(C\text{-}T)_6$, $d(A)_{21}$·$d(T)_{21}$, Poly r(A·U). These tables list ~450 transitions, which are not individually discussed. The first part of the Results section describes how the triplex and duplex were identified (Figures 1 to 10), while the second part (Figures 11 to 20) emphasizes the solution conditions that affect triplex stability.

Spectral identification of the triplexes

Triplex formation is often identified by the presence of two transitions in the UV-melting profile of a sample, e.g., Figures 9 and 16. The first transition generally represents the release of third strand from the core duplex while the second transition, at a higher temperature, results from dissociation of the remaining core duplex. One way to identify the duplex transition in the triplex mixture is to melt the equivalent duplex mixture and confirm that these transitions essentially coincide. Such confirmation was obtained for all second transitions so characterised. Triplex formation in some duplex mixtures as a consequence of duplex disproportionation will be discussed below.

$d(C^+\text{-}T)_6$:$d(A\text{-}G)_6$·$d(C\text{-}T)_6$. We have previously reported the unique difference spectrum for this triplex on dissociation of the third strand from its core duplex at neutral pH (11). Figure 1 shows the four possible difference spectra in mixing buffer (MB) at pH 7.0:

1. Difference spectrum for dissociation of the duplex in duplex mixture; 60 °C (single strands) - 40 °C (duplex), giving the difference spectrum for a 2 → 1 +1 transition.

2. Difference spectrum for dissociation of the duplex in triplex mixture; 60 °C (single strands) - 40 °C (duplex + single strand), giving the difference spectrum for a 1 + 2 → 1 +1 + 1 transition. The difference spectrum for dissociation of the duplex shows a main peak at 270 nm and a slightly lower intensity peak at 250 nm.

3. Difference spectrum for dissociation of the third strand from its core duplex; 20 °C (single strand + duplex) - 1 °C (triplex), giving the difference spectrum for a 3 → 2 + 1 transition. This difference spectrum shows a peak at 245 nm and a trough at 295 nm.

4. Difference spectrum for dissociation of all three strands; 60 °C (single strands) - 1 °C (triplex), giving the difference spectrum for a 3 → 1 + 1 + 1 transition. As expected, this difference spectrum has the characteristics of both third strand and duplex dissociation with peaks at ~247 and ~267 nm and a trough at 295 nm.

These unique spectral characteristics for dissociation of the third strand and dissociation of the duplex enable identification of the transitions obtained from UV-melting profiles. *All* the transitions for this triplex and its core duplex were analyzed in this manner; however, only specific examples are shown. The difference spectra in Figures 1 - 6 are included to illustrate the analysis that was performed for each transition. Figures 2 - 6 include examples of triplex identification that were especially difficult because of either of two factors, one being that the transition is 3 → 1 + 1 + 1, the other that some of the additives (e.g., CTriMA) undergo UV-sensitive transitions themselves. Non-triplex and non-duplex transitions were identified by melting the equivalent solution without nucleic acid. In addition, many triplex transitions were confirmed by demonstrating the expected pH dependence of triplex stability, as we prevously reported, and an absence of such increase in duplex stability above pH 4.2 (11).

In this way, it was shown for the triplex mixture in TriMA-Cl at pH 7.0 that the first transition (Tm = 28 °C) in 1.0 M TriMA-Cl represents the dissociation of third strand, while the second transition (Tm = 52 °C) is that for dissociation of the remaining core

duplex (peak at 270 nm and no trough at 245 nm). Similarly, the difference spectra for the triplex mixture in 3.0 and 4.0 M TriMA-Cl confirm that their monophasic melting profiles, with Tm = 50 and 53 °C, respectively, are due to direct melting of the triplex to its single strands.

The triplex mixture with 10^{-4} Wt% CTriMA-Cl (3 x 10^{-6} M), pH 7.0, with Tm of 20 °C was shown to represent (Figure 3) the dissociation of duplex, i.e., 1 + 2 → 1 + 1 + 1 transition. However, on increasing CTriMA-Cl to 10^{-2} Wt% (3 x 10^{-4} M), the triplex is formed, and displays a Tm = 28 °C at pH 7.0 for what is clearly a 3 → 2 + 1 transition; yet, a Tm value could not be obtained for the expected subsequent duplex transition (Table 2) because CTriMA undergoes its own phase transition with large near-UV changes that mask the duplex transition. The CTriMA transition is readily observable between 220 and 320 nm, whereas spectral transitions due to nucleic acids give a maximum hyperchromic change at ~260 nm but essentially no absorbance change above 300 nm. In addition, the difference spectrum of the CTriMA transition is distinctly different.

As shown in Table 2, CTriMA, TridodecylMA, and DOSPA all aggregate forming micelles due to their hydrophilic positively charged nitrogen at one end and a hydrophobic tail at the other.

The difference spectra for the triplex mixture in 10^{-3} and 10^{-4} Wt% (2 x 10^{-5} and 2 x 10^{-6} M respectively) TridodecylMA-Cl at pH 7.0 (Figure 4) confirm that no triplex forms. Instead, the observed transition is that of the duplex (1 + 2 → 1 + 1 + 1). However, on

lowering the pH to 6.0 for the 10^{-3} Wt% solution, triplex formation is observed and the difference spectrum is characteristic of a 3 → 1 + 1 + 1 transition, see Figure 1, plot 4.

Such data (Figure 5) also allowed confirmation that the single transition at 42 °C for the triplex mixture in 2.0 M $NaClO_4$ at pH 7.0 is only that for dissociation of duplex. Again, on lowering the pH to 6.0, the UV-melting profile shows two transitions with Tm = 18 and 43 °C. Moreover, the difference spectrum for the first transition is clearly characteristic of third strand release (3 → 2 + 1), while the difference spectrum for the second transition is the same as that for the difference spectrum at pH 7.0 (2.0 M $NaClO_4$) and for the difference spectrum of the duplex mixture in MB at pH 7.0 (Figure 1, plot 1). Thus, perchlorate ion is triplex destabilizing.

For the triplex mixture in 40% PEG200 + MB at pH 7.0 there is only one transition with Tm = 33 °C. Consistent with the significantly larger hyperchromic change (23%), the difference spectrum for this transition is characteristic of a direct 3 → 1 + 1 + 1 transition (Figure 6). For comparison, Figure 6 also shows the difference spectrum for the single transition of the triplex mixture in 5.0 M NaCl (51 °C, 10% hyperchromism). This difference spectrum is clearly that of a 1 + 2 → 1 + 1 + 1 transition, i.e., melting of duplex.

Figure 1: Difference spectra for the triplex $d(C^+\text{-}T)_6$:$d(A\text{-}G)_6$·$d(C\text{-}T)_6$ and duplex $d(A\text{-}G)_6$·$d(C\text{-}T)_6$ in mixing buffer (MB) at pH 7.0:

(2 → 1 +1) dissociation of the duplex in duplex mixture;

(1 + 2 → 1 +1 + 1) dissociation of the duplex in triplex mixture;

(3 → 2 + 1) dissociation of the third strand from its core duplex;

(3 → 1 + 1 + 1) dissociation of all three strands.

Figure 2: Difference spectra for the triplex $d(C^+\text{-}T)_6$:$d(A\text{-}G)_6$·$d(C\text{-}T)_6$ and duplex $d(A\text{-}G)_6$·$d(C\text{-}T)_6$ in TriMA-Cl at pH 7.0:

(3 → 2 +1) dissociation (first transition) of the third strand in 1.0 M TriMA-Cl;

(1 + 2 → 1 +1 + 1) dissociation (second transition) of the duplex in triplex mixture in 1.0 M TriMA-Cl;

(3 → 1 + 1 + 1) dissociation of triplex to single strands in 3.0 M TriMA-Cl;

(3 → 1 + 1 + 1) dissociation of triplex to single strands in 4.0 M TriMA-Cl.

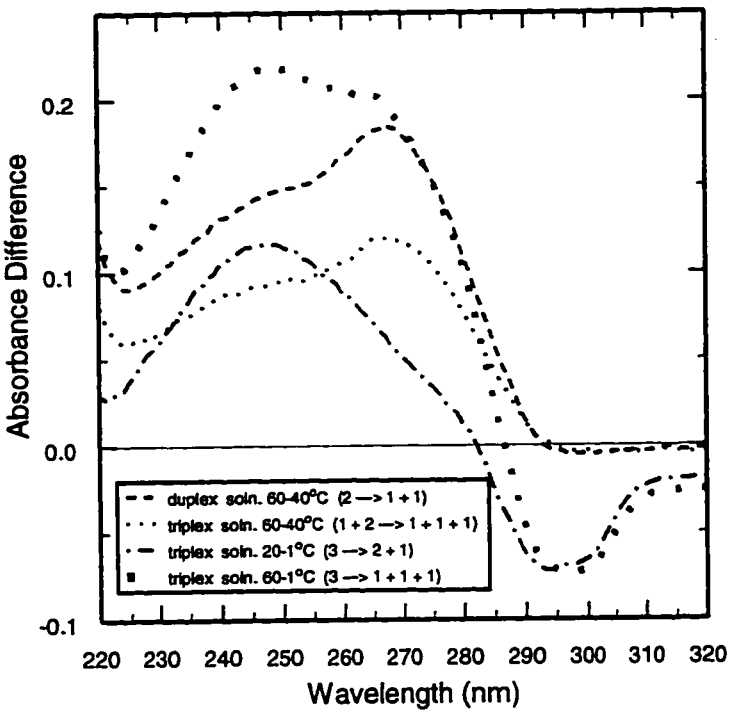
Absorbance Difference
0.2
0.1
0.0
-0.1
220 230 240 250 260 270 280 290 300 310 320
Wavelength (nm)
duplex soln. 60-40°C (2 —> 1 + 1)
triplex soln. 60-40°C (1 + 2 —> 1 + 1 + 1)
triplex soln. 20-1°C (3 —> 2 + 1)
triplex soln. 60-1°C (3 —> 1 + 1 + 1)

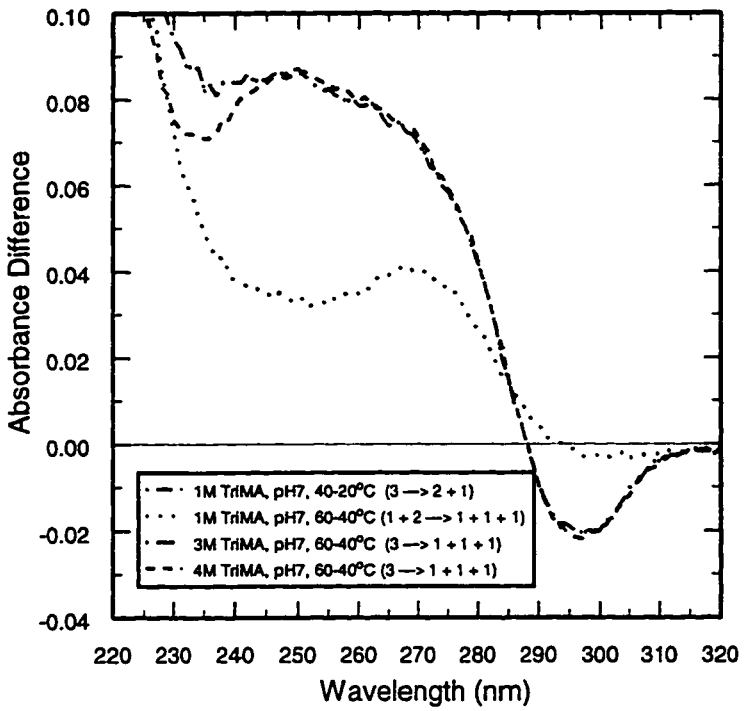
Absorbance Difference
0.10
0.08
0.06
0.04
0.02
0.00
-0.02
-0.04
220 230 240 250 260 270 280 290 300 310 320
Wavelength (nm)
1M TriMA, pH7, 40-20°C (3 —> 2 + 1)
1M TriMA, pH7, 60-40°C (1 + 2 —> 1 + 1 + 1)
3M TriMA, pH7, 60-40°C (3 —> 1 + 1 + 1)
4M TriMA, pH7, 60-40°C (3 —> 1 + 1 + 1)

Figure 3: Difference spectra for the triplex $d(C^+\text{-}T)_6$:$d(A\text{-}G)_6$·$d(C\text{-}T)_6$ and duplex $d(A\text{-}G)_6$·$d(C\text{-}T)_6$ in CTriMA-Cl at pH 7.0:

(1 + 2 → 1 + 1 + 1) dissociation of the duplex only in triplex mixture in 10^{-4} Wt% (3×10^{-6} M) CTriMA-Cl, i.e., no triplex formation;

(1 + 2 → 1 + 1 + 1) dissociation of the duplex in triplex mixture in 10^{-3} Wt% (3×10^{-5} M) CTriMA-Cl (There is possibly a very small amount of triplex present as indicated by a reduced peak at 270 nm and a very small trough at 295 nm.);

(3 → 2 + 1) dissociation of the third strand to duplex and single strand in triplex mixture in 10^{-2} Wt% (3×10^{-4} M) CTriMA-Cl.

Figure 4: Difference spectra for the triplex $d(C^+\text{-}T)_6$:$d(A\text{-}G)_6$·$d(C\text{-}T)_6$ and duplex $d(A\text{-}G)_6$·$d(C\text{-}T)_6$ in TridodecylMA-Cl at pH 6.0 and 7.0, respectively:

(1 + 2 → 1 + 1 + 1) dissociation of the duplex in triplex mixture in 10^{-3} Wt% (2×10^{-5} M) TridodecylMA-Cl at pH 7.0;

(1 + 2 → 1 + 1 + 1) dissociation of the duplex in triplex mixture in 10^{-4} Wt% (2×10^{-6} M) TridodecylMA-Cl at pH 7.0;

(3 → 1 + 1 + 1) dissociation of triplex to single strands in 10^{-3} Wt% (2×10^{-5} M) TridodecylMA-Cl at pH 6.0. See Figure 1, plot 4 for comparison.

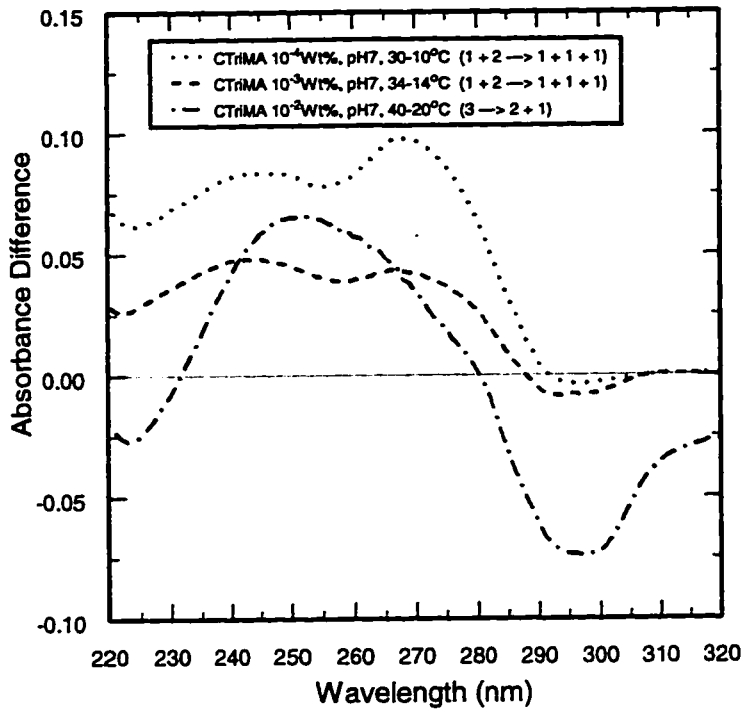
CTriMA 10⁻⁴Wt%, pH7, 30-10°C (1 + 2 —> 1 + 1 + 1)
CTriMA 10⁻³Wt%, pH7, 34-14°C (1 + 2 —> 1 + 1 + 1)
CTriMA 10⁻²Wt%, pH7, 40-20°C (3 —> 2 + 1)
Absorbance Difference
0.15
0.10
0.05
0.00
-0.05
-0.10
220 230 240 250 260 270 280 290 300 310 320
Wavelength (nm)

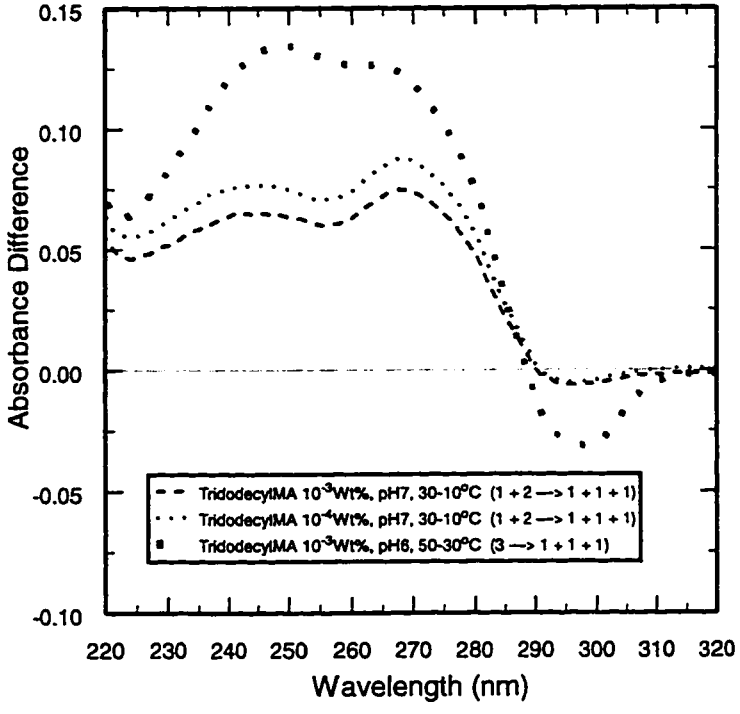
TridodecylMA 10⁻³Wt%, pH7, 30-10°C (1 + 2 —> 1 + 1 + 1)
TridodecylMA 10⁻⁴Wt%, pH7, 30-10°C (1 + 2 —> 1 + 1 + 1)
TridodecylMA 10⁻³Wt%, pH6, 50-30°C (3 —> 1 + 1 + 1)
Absorbance Difference
0.15
0.10
0.05
0.00
-0.05
-0.10
220 230 240 250 260 270 280 290 300 310 320
Wavelength (nm)

Figure 5: Difference spectra for the triplex $d(C^+\text{-}T)_6$:$d(A\text{-}G)_6$·$d(C\text{-}T)_6$ and duplex $d(A\text{-}G)_6$·$d(C\text{-}T)_6$ in 2.0 M $NaClO_4$ at pH 6.0 and 7.0, respectively:

(1 + 2 → 1 + 1 + 1) dissociation of the duplex in triplex mixture in 2.0 M $NaClO_4$ at pH 7.0;

(3 → 2 + 1) dissociation of the third strand to duplex and single strand in triplex mixture in 2.0 M $NaClO_4$ at pH 6.0;

(1 + 2 → 1 + 1 + 1) dissociation of the duplex in triplex mixture in 2.0 M $NaClO_4$ at pH 6.0.

Figure 6: Difference spectra for the triplex $d(C^+\text{-}T)_6$:$d(A\text{-}G)_6$·$d(C\text{-}T)_6$ in 40% PEG200 + MB at pH 7.0 and duplex $d(A\text{-}G)_6$·$d(C\text{-}T)_6$, in 5.0 M NaCl at pH 7.0:

(3 → 1 + 1 + 1) dissociation of triplex to single strands in triplex mixture, 40% PEG200 + MB at pH 7.0;

(1 + 2 → 1 + 1 + 1) dissociation of duplex in triplex mixture, 5.0 M NaCl at pH 7.0.

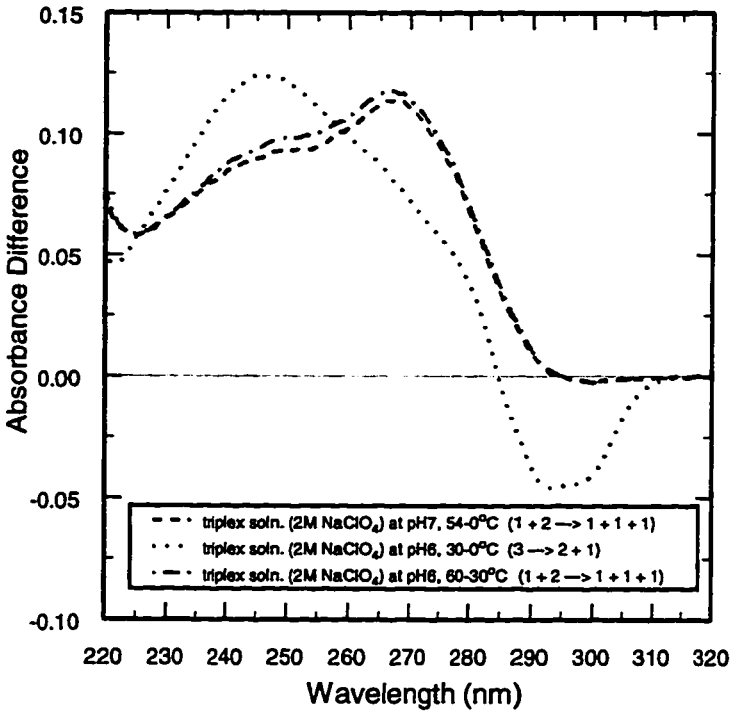
0.15
0.10
0.05
0.00
-0.05
-0.10
Absorbance Difference
220 230 240 250 260 270 280 290 300 310 320
Wavelength (nm)
triplex soln. (2M NaClO4) at pH7, 54-0°C (1 + 2 —> 1 + 1 + 1)
triplex soln. (2M NaClO4) at pH6, 30-0°C (3 —> 2 + 1)
triplex soln. (2M NaClO4) at pH6, 60-30°C (1 + 2 —> 1 + 1 + 1)

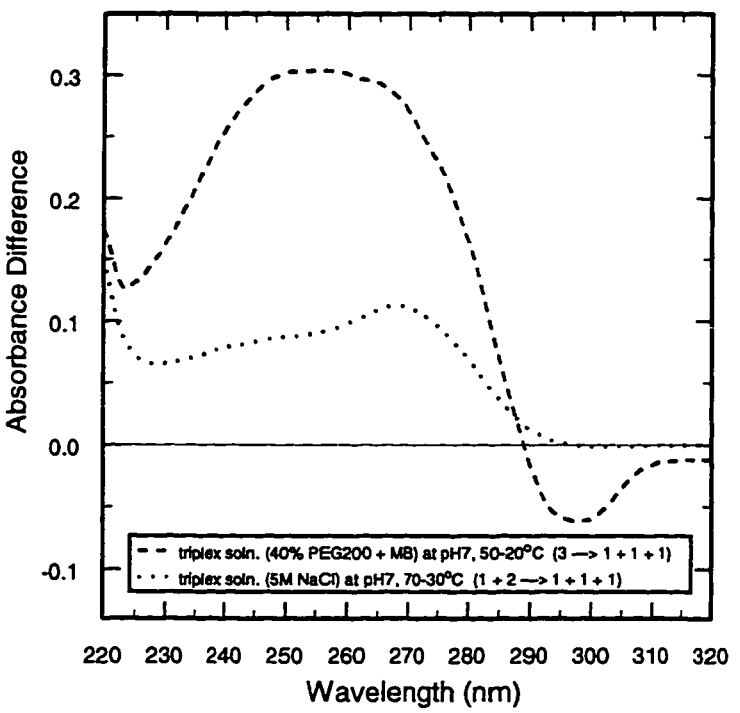
0.3
0.2
0.1
0.0
-0.1
Absorbance Difference
220 230 240 250 260 270 280 290 300 310 320
Wavelength (nm)
triplex soln. (40% PEG200 + MB) at pH7, 50-20°C (3 —> 1 + 1 + 1)
triplex soln. (5M NaCl) at pH7, 70-30°C (1 + 2 —> 1 + 1 + 1)

$d(T)_{21}$:$d(A)_{21}$·$d(T)_{21}$. Tables 8 and 9 list the Tm values for this triplex and for some of the target duplex mixtures. For these strands, because the difference spectrum for release of third strand from the core duplex $d(A)_{21}$·$d(T)_{21}$ is rather similar to the difference spectrum for dissociation of the core duplex, while the CD-spectra of the triplex and duplex are significantly different, CD spectroscopy was used to characterize the complexes formed under different conditions. In fact, the transitions in the UV-melting curves were characterized as triplex or duplex melting based upon: 1) the number of transitions observed; 2) % hyperchromism; 3) CD-spectra; and 4) the presence of one or more isosbestic points (see below).

Figure 7 shows the CD-spectra of the duplex mixture in MB and in 2.0 M TriMA-Cl + MB, and of the triplex mixture in MB and in 2.0 M TriMA-Cl + MB. The duplex in both solutions gives an intense positive band at 217 nm and an intense negative band at 247 nm. Between 235 nm and 320 nm the triplex in both solutions has a spectrum similar to that of the duplex, but below 235 nm it has an additional negative band at 209 nm. These CD-spectra are very similar to those reported in the literature for poly[d(T):d(A)·d(T)] and poly[d(A)·d(T)] (13). Thus, the single transition with Tm = 66 °C observed in the UV-melting profile of the triplex mixture in 2.0 M TriMA-Cl + MB is that of a 3 → 1 + 1 + 1 transition, and as is the case for all the 3 → 1 transitions for this triplex, one observes a significantly larger hyperchromic change (see Tables 8 and 9 for % hyperchromism).

Similarly, for the triplex mixture in 2.0 M $(NH_4)Cl$ (single transition with Tm = 71 °C, 36 % hyperchromism) and in 50 Vol% methanol + MB (single transition with Tm =

38 °C, 38 % hyperchromism) the CD-spectra confirm the formation of $d(T)_{21}$:$d(A)_{21}$·$d(T)_{21}$ (Figure 8).

The UV-spectra taken in the course of a melting experiment can also be analyzed to determine the number of equilibria in solution. Each species will have its own UV-spectrum and changing the temperature will change the ratio of those species, so at the wavelength where the two sets of spectra intersect an isosbestic point is obtained. Therefore, if there are three species in equilibrium, e.g., triplex, duplex and single strand, there should be a minimum of two isosbestic points corresponding to the wavelengths where the two families of spectra intersect. This type of analysis is possible for all the triplexes studied; the spectra for the triplex mixture $d(T)_{21}$:$d(A)_{21}$·$d(T)_{21}$ in 1.0 M TMA-Cl is shown as an example. Figure 9 shows the UV-melting profile at 260 nm and Figure 10 shows one 'family' of spectra with an isosbestic point at 284 nm that results from the equilibrium between the duplex and single strands. The equilibrium between the triplex and duplex + single strand gives an additional isosbestic point (data not shown).

Poly r(U:A·U). The melting temperatures of the triplex poly r(U:A·U) and of the duplex poly r(A·U) are given in Table 10. This triplex and duplex have been studied extensively (14). For triplex mixtures that gave two transitions in UV-melting profiles at 260 nm, the second transition was confirmed to be dissociation of the duplex by comparison with the melting profiles of the equivalent duplex mixture. For triplex mixtures that gave one transition, the % hyperchromism identified them as 3 → 1 + 1 + 1 transitions. For example, in varying the Vol% ethanol from 10 to 50, the % hyperchromism for the

duplex mixture remains constant at 26 % (2 → 1 + 1) while that for the triplex mixture with a 3 → 1 + 1 + 1 transition gives an increasing hyperchromic change from 37 to 54%.

Figure 7: CD-spectra at 1 °C, pH 7.0 of duplex mixture $d(A)_{21}{\cdot}d(T)_{21}$ in MB and in 2.0 M TriMA-Cl + MB ; and of triplex mixture $d(T)_{21}{:}d(A)_{21}{\cdot}d(T)_{21}$ in MB and in 2.0 M TriMA-Cl + MB.

Figure 8: CD-spectra at 1 °C, pH 7.0 of triplex mixture $d(T)_{21}{:}d(A)_{21}{\cdot}d(T)_{21}$ in 2.0 M $(NH_4)Cl$ and 50 Vol% methanol + MB.

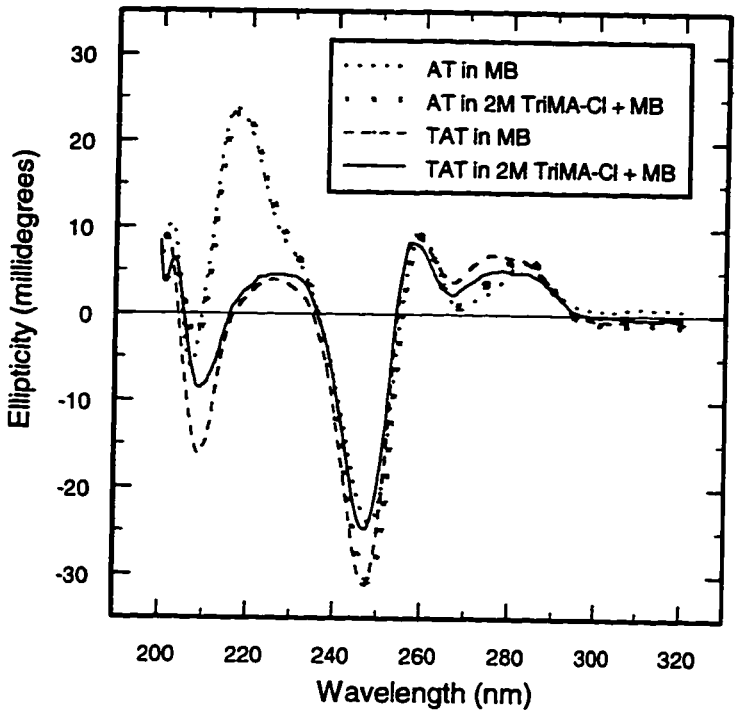
AT in MB
AT in 2M TriMA-Cl + MB
TAT in MB
TAT in 2M TriMA-Cl + MB
Ellipticity (millidegrees)
30
20
10
0
-10
-20
-30
200
220
240
260
280
300
320
Wavelength (nm)

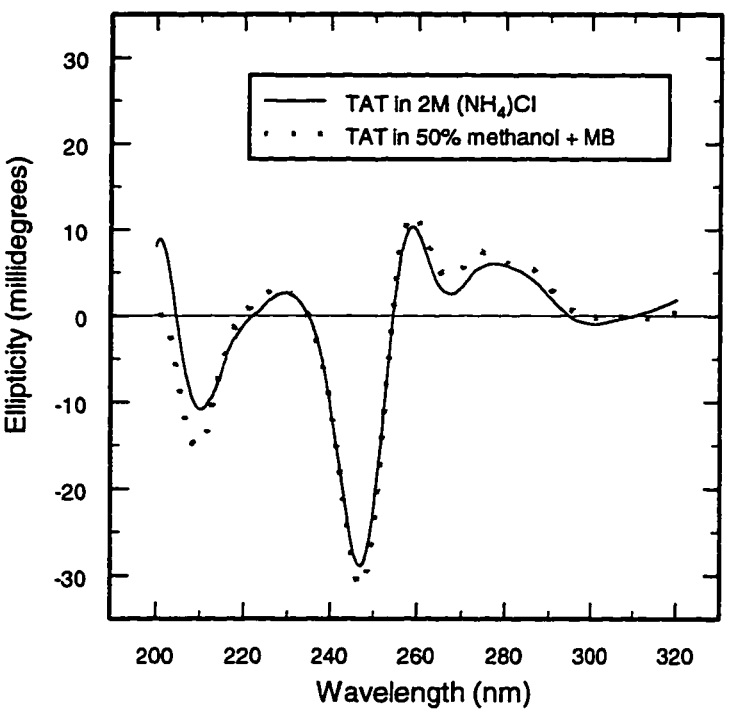
TAT in 2M (NH4)Cl
TAT in 50% methanol + MB
Ellipticity (millidegrees)
30
20
10
0
-10
-20
-30
200
220
240
260
280
300
320
Wavelength (nm)

Figure 9: UV-melting profile at 260 nm of triplex mixture $d(T)_{21}$:$d(A)_{21}$·$d(T)_{21}$ in 1.0 M TMA-Cl at pH 7.0.

Figure 10: UV-spectra between 58 and 74 °C of triplex mixture $d(T)_{21}$:$d(A)_{21}$·$d(T)_{21}$ in 1.0 M TMA-Cl at pH 7.0 showing an isosbestic point at 284 nm.

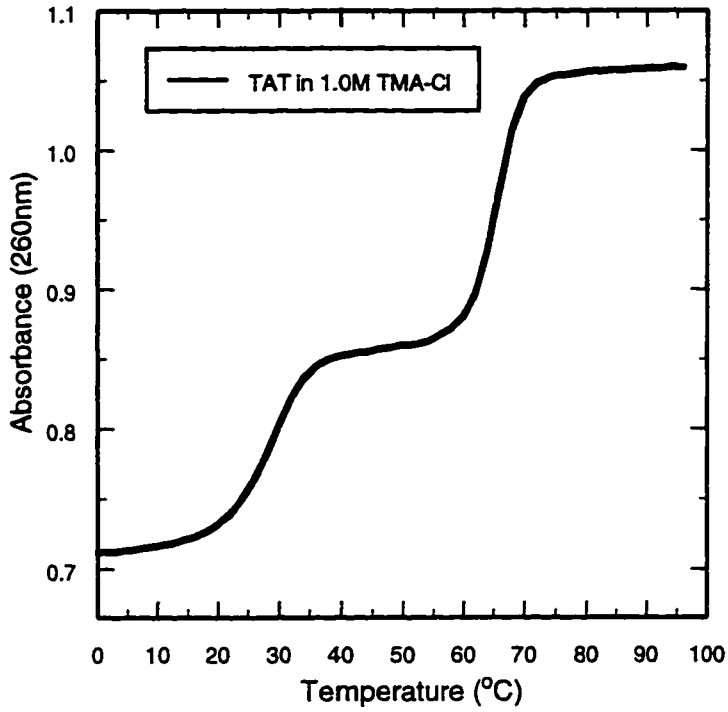
TAT in 1.0M TMA-Cl
Absorbance (260nm)
Temperature (°C)
1.1
1.0
0.9
0.8
0.7
0 10 20 30 40 50 60 70 80 90 100

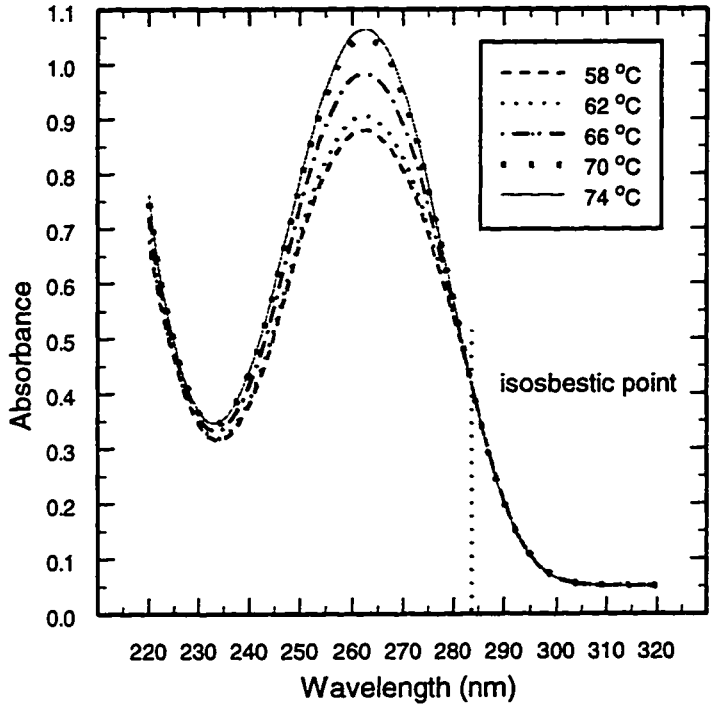
58 °C
62 °C
66 °C
70 °C
74 °C
isosbestic point
Absorbance
Wavelength (nm)
1.1
1.0
0.9
0.8
0.7
0.6
0.5
0.4
0.3
0.2
0.1
0.0
220 230 240 250 260 270 280 290 300 310 320

Triplex stability

The effect of the various additives on the stability (Tm value) of each triplex is discussed with respect to the stability of the triplex in MB at pH 7.0 (Tm = 11 °C, Table 4), unless stated otherwise.

$d(C^+\text{-}T)_6$:$d(A\text{-}G)_6$·$d(C\text{-}T)_6$. The organic salts MA-Cl, DMA-Cl, TriMA-Cl, TMA-Cl and TEA-Cl all enhance triplex stability (Tables 1 and 2, Figure 11). However, the organic salt TPA-Cl inhibits triplex formation at the concentrations studied ($\geq$ 0.1 M). Only TEA-Cl and TPA-Cl decrease duplex stability with increasing concentration, while the other organic salts have little effect on duplex stability (Table 6). At pH 7.0 all of these methyl-substituted nitrogen compounds are protonated: MA, pKa 10.7; DMA, pKa 10.7; TriMA, pKa 9.8 and the quaternary nitrogen compounds TMA, TEA and TPA are positively charged over a very wide pH range.

In addition to the triplex stabilizing ability of DMA-Cl, TMA-Cl and TEA-Cl, these organic cations also drive disproportionation of the duplex mixture to form a limited amount of triplex, as indicated by the low % hyperchromism. Table 6 tabulates the ability of these organic cations to promote triplex formation in the duplex mixture and their effect on duplex stability.

Since triplex stability is significantly enhanced by TriMA and TMA, it was rationalized that chemical species with a positive charge density and a molecular volume similar to these compounds at one end, but with a hydrophobic (hydrocarbon) tail may also enhance triplex stability. The underlying reasons for this expectation are: 1) the

positive charge neutralizes the high negative charge density of the three phosphodiester backbones of a triplex; 2) the TriMA or TMA headgroups have the correct steric volume and charge density to interact with the backbones; and 3) the hydrophobic tail will facilitate reactions driven by removal of water, in this case from the major groove (and possibly the minor groove) of the target duplex to allow for third strand binding. In this connection, since the hydrogen bonding of the nucleic acid bases with water and with each other is very similar, the process of base pairing occurs largely as a result of the bases preferring a hydrophobic environment.

Thus, the cationic lipids CTriMA, TridodecylMA and DOSPA were studied in an effort to further increase triplex stability. Even with the very low concentrations that are possible with these cationic lipids, a stabilizing effect was observed. At pH 7.0 triplex Tm was 28 °C (10^{-2} Wt% CTriMA-Cl (3 x 10^{-4} M)), 22 °C (10^{-3} Wt% DOSPA (7 x 10^{-6} M)), 27 °C (10^{-2} Wt% DOSPA (7 x 10^{-5})). Lowering the pH to 6.0 resulted in further enhancement of triplex stability, Tm = 41 °C (10^{-3} Wt% TridodecylMA-Cl (2 x 10^{-5} M)), 40 °C 10^{-4} Wt% and 10^{-3} Wt% DOSPA. The only additive effect observed was for 10^{-2} Wt% CTriMA-Cl + 0.1 M TMA-Cl + MB at pH 7.0, Tm = 45 °C. Table 2 lists the other combinations and the resultant effects on triplex stability.

Unfortunately, these cationic lipids are difficult to study for two reasons: 1) even at very low concentrations they show their own transitions in UV-melting profiles, which complicates analysis due to their masking of the triplex and duplex transitions; and 2) their limited solubility up to 10^{-5} or 10^{-4} M is not sufficient cation concentration to significantly stabilize the three negatively charged phosphodiester backbones. Addition of

MB to provide sufficient cations has two effects (Table 2): 1) the solubility of all the cationic lipids is further decreased; and 2) the limited stabilizing effect that most cationic lipids have on triplex stability is lost, with the triplex and duplex having similar Tm values with only MB in solution, e.g., 10^{-3} Wt% TridodecylMA-Cl + MB, triplex Tm = 11 °C and 10^{-3} Wt% DOSPA + MB, triplex Tm = 12 °C.

For these reasons it is difficult to fully elucidate the effect of changing the size and shape of the organic cation headgroup, and the length and number (orientation) of the lipid tails.

As expected for an anionic lipid, SDS appears to inhibit triplex formation (Table 3); however, the ability to observe transitions below 20 °C is obscured because the solution solidifies below ~20 °C.

Previous work has claimed that triplex stability is significantly enhanced (+25 °C) in the presence of coralyne, with maximum stability at 2 x 10^{-5} M (15). However, the triplex $d(C^{+}\text{-}T)_6$:$d(A\text{-}G)_6$·$d(C\text{-}T)_6$ does not show significantly enhanced stability in the presence of coralyne (Table 3), Tm = 14°C in 2 x 10^{-5} M coralyne + MB. In addition, the UV-melting profile of only coralyne in the presence of salt shows a highly cooperative transition (Tm = 58 °C, 40% hyperchromism at 260 nm), apparently due to stacking of this positively charged hetero-cycle. It is therefore likely that the observation of a transition at 260 nm may have been mistakenly identified as a triplex transition, especially since it shifts with salt and H^{+} ion concentration.

In spite of the extensive use of trehalose as a protein stabilizer, this sugar does not affect triplex stability (0.75, 1.5, 2.0 M in MB, T_m = 12, 12, 13 °C, respectively), though

it does destabilize the duplex (0.75, 1.5, 2.0 M in MB, T_m = 47, 44, 41 °C, respectively) (Figure 13 and Table 3). This indicates that general protein stabilizing agents such as trehalose, that are believed to enhance stability by virtue of their dehydrating ability, do not necessarily stabilize triplexes. In fact, they appear to destabilize duplexes.

Similar effects are seen with glycerol, which is known to absorb water up to 50% of its weight and is therefore a strong dehydrating compound. Thus, glycerol, too, does not affect triplex stability (10, 20, 30 Vol% in MB, T_m = 11, 12, 12 °C, respectively), while it does destabilize the duplex (10, 20, 30 Vol% in MB, T_m = 49, 45, 42 °C, respectively) (Figure 13 and Table 3). It is interesting to note that 30 Vol% glycerol + MB gives a Tm of 12 °C for dissociation of the third strand, which is essentially the same as MB alone (11 °C), whereas 30 Vol% glycerol + MB + 1.0 M TriMA-Cl gives a Tm of 19 °C, which is 9 °C less than in 1.0 M TriMA-Cl alone (28 °C). This is a clear example of a compound that has no effect on triplex stability by itself, yet counteracts the stabilizing effect of another compound.

PEG is often used to facilitate crystallization of nucleic acids, and DMSO is used as a broad spectrum solvent of organic and inorganic compounds and has strong H-bonding ability. Both PEG and DMSO enhance triplex stability (Figure 13, Table 3). For this triplex, increasing PEG molecular weight (20 Vol% PEG200, 400, 600) increases the stability of the triplex (Tm = 18, 22, 24 °C, respectively) and the duplex (Tm = 44, 48, 49 °C, respectively). Maximum stability with DSMO is obtained with 50 Vol% DMSO + MB (Tm = 27 °C), with decreasing stability both below and above 50 Vol%. In addition to the difference spectral analysis, as previously discussed, the single transition in 60

Vol% DMSO is sensitive to pH, a well known characteristic of this triplex (60 Vol% DMSO, pH 7.0 Tm = 15 °C, pH 6.0 Tm = 36 °C). Besides increasing triplex stability, DMSO decreases duplex stability (10, 20, 40 Vol%, Tm = 48, 45, 41 °C, respectively).

For the anion series and in comparison to the stability of the triplex in NaCl: Na_2HPO_4, $NaOOCCH_3$, Na_2SO_4, and $(NH_4)_2SO_4$ all enhance stability (Figure 12) of $d(C^+\text{-}T)_6$:$d(A\text{-}G)_6$·$d(C\text{-}T)_6$, whereas $NaClO_4$ and NH_4Cl destabilize it. $NaClO_4$ is the only inorganic salt that destabilizes the duplex.

As both the organic cation TMA^+ (with respect to Na^+) and the inorganic anion SO_4^{2-} (with respect to Cl^-) both significantly enhance triplex stability, it was thought that an additive effect might be obtained with $(TMA)_2SO_4$. However, this is not the case (Figure 11) as 1.0 M $(TMA)_2SO_4$ gives a Tm of 25 °C in comparison to 2.0 M TMA-Cl (29 °C).

Of the alcohols MeOH, EtOH, 2-PrOH and 1-BuOH (Figure 14), only 1-BuOH significantly destabilizes the triplex. Studies with 1-pentanol were attempted but resulted in phase separation of 1-pentanol and water. Maximum stability of the triplex is attained in 70 Vol% MeOH + MB (16 °C), 60 Vol% EtOH + MB (40 °C), and 50 Vol% 2-PrOH + MB (40 °C). Various combinations of EtOH and 2-PrOH with TMA-Cl and TriMA-Cl were evaluated, but no additive effects were observed (Table 5).

In addition to the triplex stabilizing ability of MeOH, EtOH and 2-PrOH, these alcohols also drive disproportionation of the duplex mixture to form triplex. Table 7 provides ample evidence for the ability of these alcohols to promote triplex formation in the duplex mixture. In the 1:1 strand mixture with 60 Vol% EtOH + MB, the extreme

case is observed with only triplex formation, i.e., $3 \rightarrow 1 + 1$ transition. As expected, duplex stability decreases with increasing triplex stability.

Figure 11: Plot of Tm vs organic salt concentration for melting of the triplex $d(C^{+}\text{-}T)_6$:$d(A\text{-}G)_6$·$d(C\text{-}T)_6$ at pH 7.0.

Figure 12: Plot of Tm vs inorganic salt concentration for the anion series Cl^{-}, HPO_4^{2-}, CH_3COO^{-}, SO_4^{2-}, for melting of the triplex $d(C^{+}\text{-}T)_6$:$d(A\text{-}G)_6$·$d(C\text{-}T)_6$ at pH 7.0.

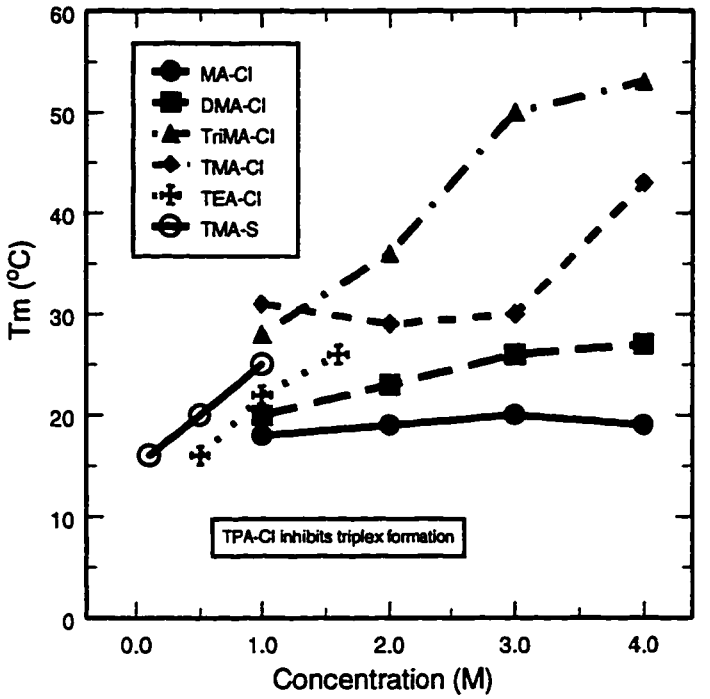
MA-Cl
DMA-Cl
TriMA-Cl
TMA-Cl
TEA-Cl
TMA-S
TPA-Cl inhibits triplex formation
Tm (°C)
Concentration (M)
0
10
20
30
40
50
60
0.0
1.0
2.0
3.0
4.0

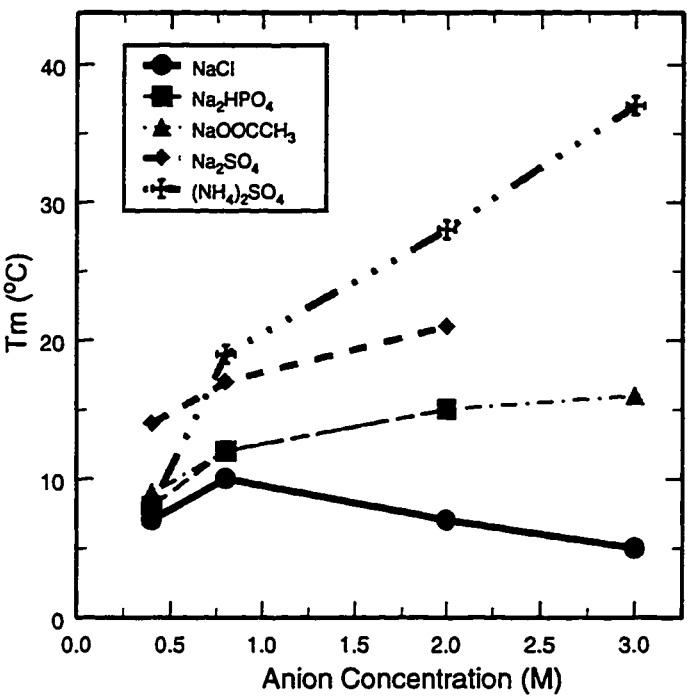
NaCl
Na_2HPO_4
$NaOOCCH_3$
Na_2SO_4
$(NH_4)_2SO_4$
Tm (°C)
Anion Concentration (M)
0
10
20
30
40
0.0
0.5
1.0
1.5
2.0
2.5
3.0

Figure 13: Plot of Tm vs % Vol(neutral organic molecule)/Vol(total) + MB and Tm vs trehalose concentration + MB, for melting of the triplex $d(C^+\text{-}T)_6$:$d(A\text{-}G)_6$·$d(C\text{-}T)_6$ at pH 7.0.

Figure 14: Plot of Tm vs % Vol(alcohol)/Vol(total) + MB for melting of the triplex $d(C^+\text{-}T)_6$:$d(A\text{-}G)_6$·$d(C\text{-}T)_6$ at pH 7.0.

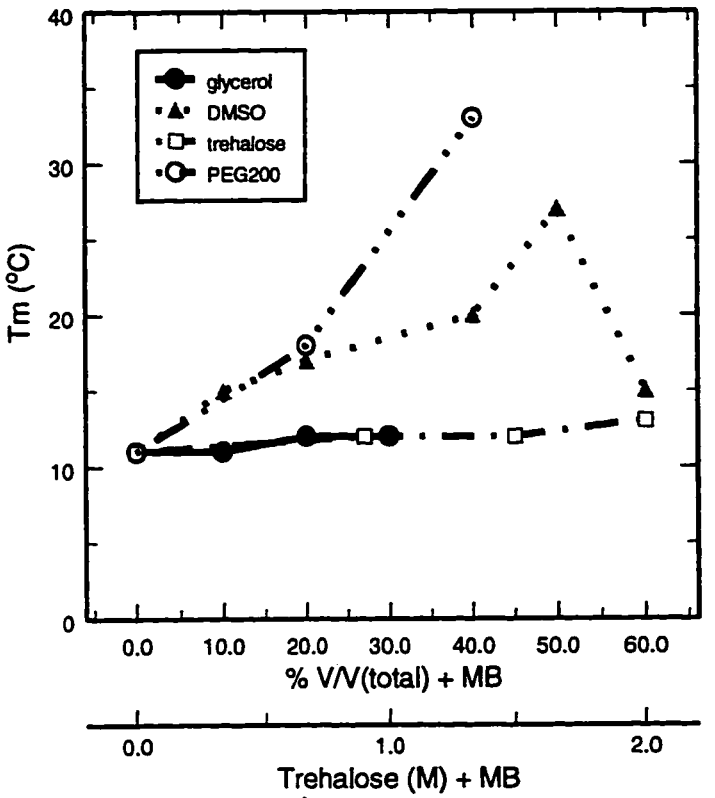
glycerol
DMSO
trehalose
PEG200
Tm (°C)
0
10
20
30
40
0.0
10.0
20.0
30.0
40.0
50.0
60.0
% V/V(total) + MB
0.0
1.0
2.0
Trehalose (M) + MB

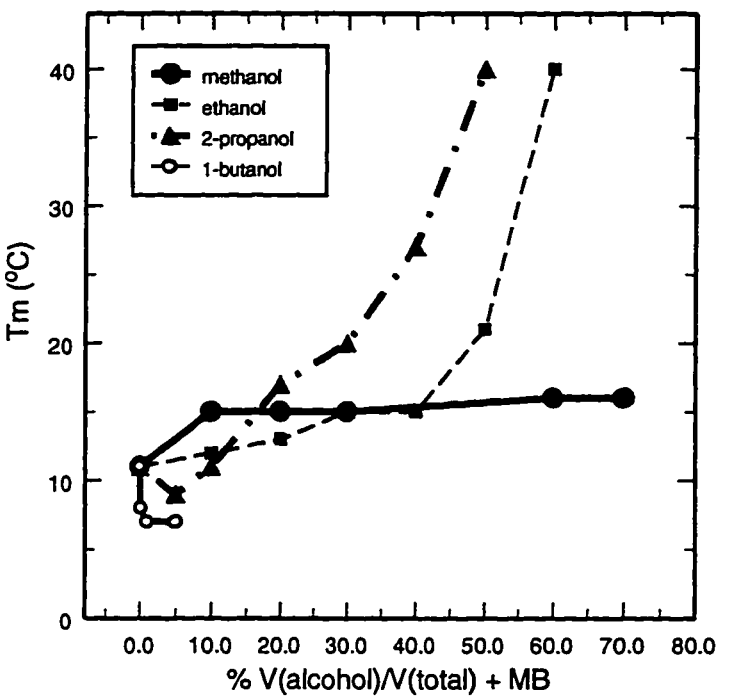
methanol
ethanol
2-propanol
1-butanol
Tm (°C)
0
10
20
30
40
0.0
10.0
20.0
30.0
40.0
50.0
60.0
70.0
80.0
% V(alcohol)/V(total) + MB

$d(T)_{21}$:$d(A)_{21}$·$d(T)_{21}$. Figure 15 shows the melting profiles for the triplex mixture at various NaCl concentrations. Three observations are apparent: 1) the melting profiles have two transitions at [NaCl] < 2.0 M and one transition at [NaCl] ≥ 2.0 M; 2) triplex stability is strongly dependent on [NaCl] < 2.0 M but less so at [NaCl] ≥ 2.0 M; and 3) unlike the triplex $d(C^+\text{-}T)_6$:$d(A\text{-}G)_6$·$d(C\text{-}T)_6$, which is destabilized at [NaCl] > 0.9 M (maximum Tm of 10 °C), this triplex is strongly stabilized with increasing [NaCl]. Figure 16 also shows the decreasing salt dependence of Tm at [NaCl] ≥ 2.0 M; but for the salts $(NH_4)Cl$ and $(NH_4)_2SO_4$, a strong salt dependence is still observed at concentrations > 2.0 M.

Relative to the stability of the triplex in NaCl, Na_2HPO_4, Na_2SO_4, $(NH_4)Cl$ and $(NH_4)_2SO_4$ all enhance stability, whereas $NaClO_4$ destabilizes. 2.0 M $NaOOCCH_3$ and 2.0 M NaCl have the same Tm of 66 °C for this triplex (Table 8).

The organic cations $TriMA^+$ and TMA^+ stabilize the triplex (Figure 17, Table 8), but less so than equivalent concentrations of NaCl, i.e., at 1.0 M TMA-Cl (Tm = 28 °C), TriMA-Cl (Tm = 39 °C), NaCl (Tm = 49 °C). However, as noted above, in NaCl triplex stability starts to plateau (Figure 16) at about 2.0 M, with a maximum Tm of 72 °C in 5.0 M NaCl, whereas in 6.0 M TMA-Cl triplex stability is increased to 95 °C. This behavior has two possible implications: 1) the charge density of the organic cations, $TriMA^+$ and TMA^+ is less than that of Na^+, and 2) charge screening is not the only mechanism by which these cations stabilize triplexes.

MeOH, EtOH and 1-PrOH also stabilize this triplex (in 50 Vol% + MB: MeOH (Tm = 38 °C), EtOH (Tm = 53 °C), 2-PrOH (Tm = 65 °C) (Figure 18), and to a greater extent than the shorter triplex $d(C^{+}\text{-}T)_6{:}d(A\text{-}G)_6{\cdot}d(C\text{-}T)_6$.

Again, contrary to previous reports (15) coralyne has no effect on the stability of this triplex, Tm = 23 °C in MB and 23 °C in 2 x 10^{-5} M coralyne + MB (Table 9).

Increasing stability is observed in PEG (Figure 18), and with increasing PEG molecular weight, Tm = 39 °C (PEG200) and Tm = 52 °C (PEG600) (Table 9).

DMSO also increases stability of this triplex, but maximum stability is obtained in 40 Vol% DMSO + MB (Tm = 38 °C), with decreasing stability both below and above 40 Vol% (Figure 18). For the triplex, $d(C^{+}\text{-}T)_6{:}d(A\text{-}G)_6{\cdot}d(C\text{-}T)_6$, maximum stability occurs in 50 Vol% DMSO.

Figure 15: UV-melting profiles at 260 nm of the triplex mixture $d(T)_{21}$:$d(A)_{21}$·$d(T)_{21}$ with increasing NaCl concentrations at pH 7.0.

Figure 16: Plot of Tm vs inorganic salt concentration for melting of the triplex $d(T)_{21}$:$d(A)_{21}$·$d(T)_{21}$ at pH 7.0.

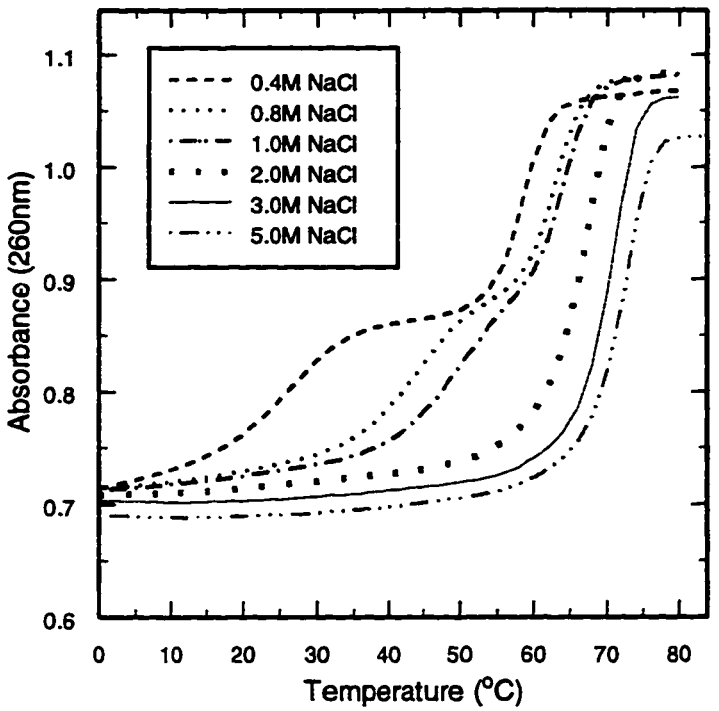
0.4M NaCl
0.8M NaCl
1.0M NaCl
2.0M NaCl
3.0M NaCl
5.0M NaCl
Absorbance (260nm)
Temperature (°C)
1.1
1.0
0.9
0.8
0.7
0.6
0
10
20
30
40
50
60
70
80

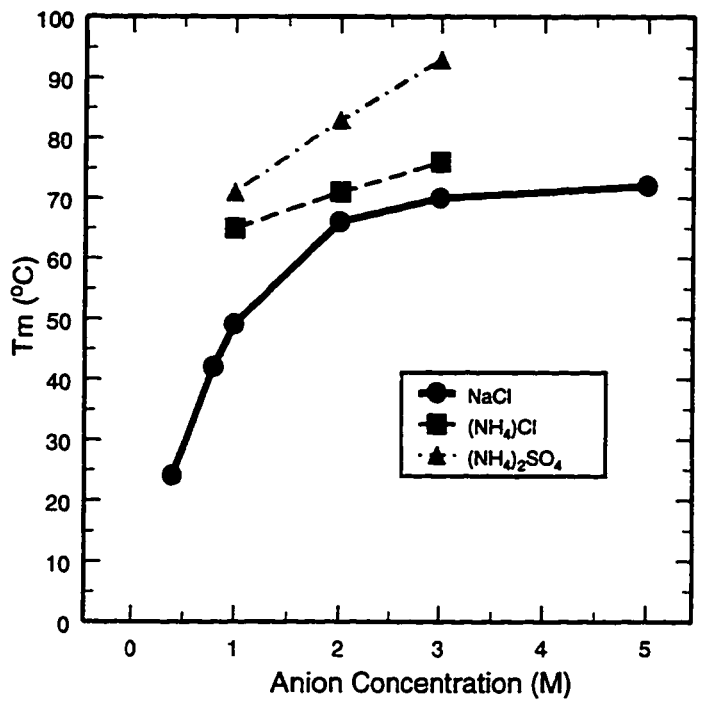
NaCl
(NH4)Cl
(NH4)2SO4
Tm (°C)
Anion Concentration (M)
100
90
80
70
60
50
40
30
20
10
0
0
1
2
3
4
5

Figure 17: Plot of Tm vs TriMA-Cl concentration + MB for melting of the triplex $d(T)_{21}$:$d(A)_{21}$·$d(T)_{21}$ at pH 7.0.

Figure 18: Plot of Tm vs % Vol(neutral organic molecule)/Vol(total) + MB for melting of the triplex $d(T)_{21}$:$d(A)_{21}$·$d(T)_{21}$ at pH 7.0.

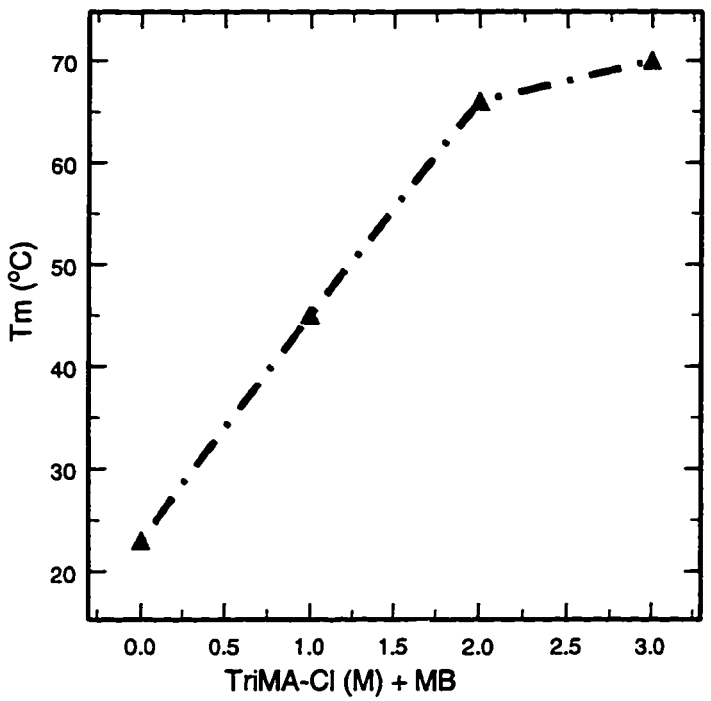
70
60
50
40
30
20
Tm (°C)
0.0
0.5
1.0
1.5
2.0
2.5
3.0
TriMA-Cl (M) + MB

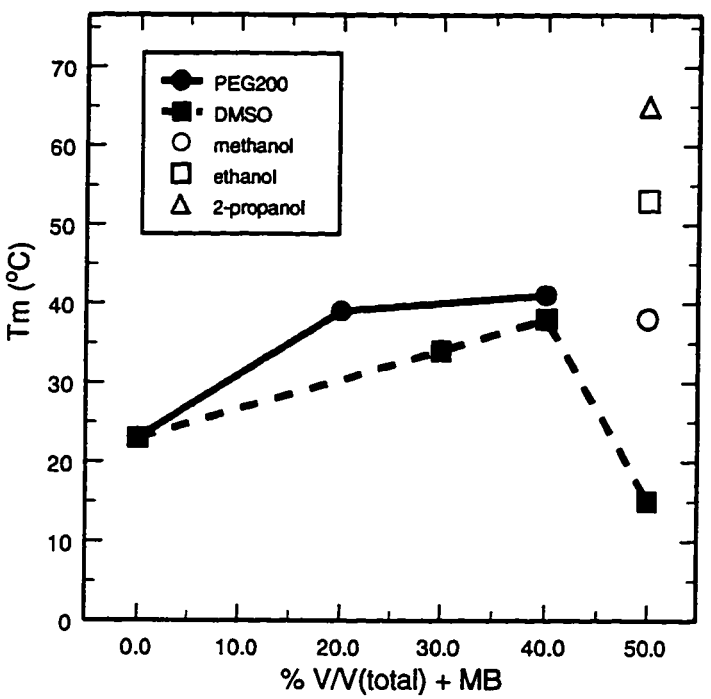
PEG200
DMSO
methanol
ethanol
2-propanol
70
60
50
40
30
20
10
0
Tm (°C)
0.0
10.0
20.0
30.0
40.0
50.0
% V/V(total) + MB

Poly r(U:A·U). The stability of this triplex and its core duplex in NaCl has been studied extensively (14). As expected for a triplex polymer that contains no C^+:G·C triplets, the stability of poly r(U:A·U) is very sensitive to ionic strength. Thus, although poly r(U:A·U) shows increased stability with increasing TriMA-Cl and TMA-Cl concentration, relative to comparable concentrations of NaCl there is no enhancement of stability. However, in 0.053 M TriMA + 0.016 M NaCl the triplex melts 3 → 1 + 1 + 1, whereas in 0.069 M NaCl (14) the triplex melts 3 → 2 + 1 and only at higher NaCl concentrations does it melt 3 → 1 + 1 + 1 (of course with higher Tm values).

Enhanced stability (Tm = 38 °C) in 10^{-3} Wt% CTriMA-Cl (3×10^{-15} M) + 0.016M NaCl is observed in comparison to 26 °C for the same NaCl concentration. Unfortunately, because CTriMA-Cl forms micelles, studies at higher concentrations are not possible.

Significant enhancement of stability in the presence of EtOH is observed (Figure 20).

The three triplexes studied all have homopyrimidine third strands, but they are otherwise different with respect to the presence or absence of protonated third strand C residues, the nature of their sugar or their length. Despite these differences the majority of observations are similar. The following are the only observed differences with these triplexes. NaCl and $(NH_4)Cl$ destabilize the triplex $d(C^+\text{-}T)_6$:$d(A\text{-}G)_6$·$d(C\text{-}T)_6$, but stabilize the triplex $d(T)_{21}$:$d(A)_{21}$·$d(T)_{21}$. 1.0 M TMA-S has less of a stabilizing effect on $d(C^+\text{-}T)_6$:$d(A\text{-}G)_6$·$d(C\text{-}T)_6$ but more so on $d(T)_{21}$:$d(A)_{21}$·$d(T)_{21}$ with respect to 2.0 M TMA-Cl.

Figure 19: Plot of Tm vs organic salt concentration + 0.016M NaCl for melting of the triplex poly r(U:A·U) at pH 7.0.

Figure 20: Plot of Tm vs ethanol concentration + 0.016M NaCl for melting of the triplex poly r(U:A·U) at pH 7.0.

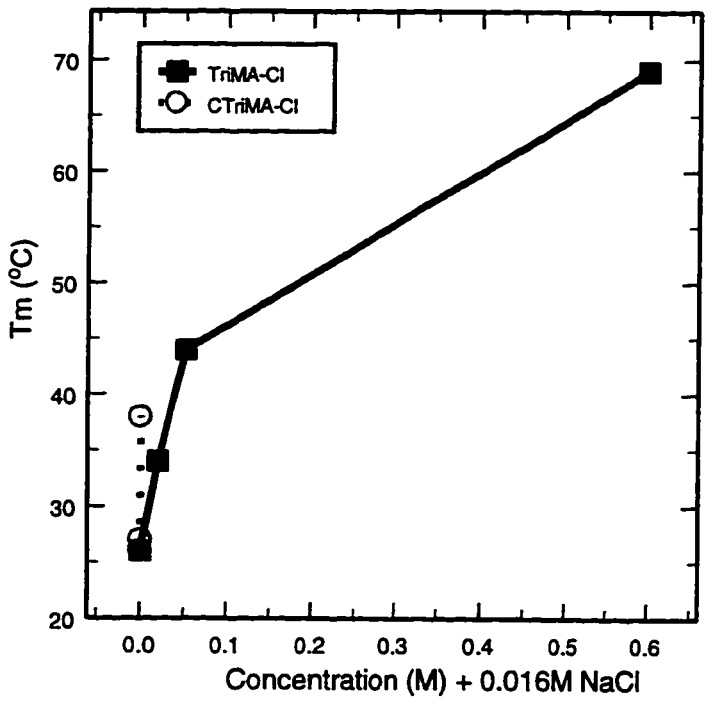
TriMA-Cl
CTriMA-Cl
Tm (°C)
70
60
50
40
30
20
0.0
0.1
0.2
0.3
0.4
0.5
0.6
Concentration (M) + 0.016M NaCl

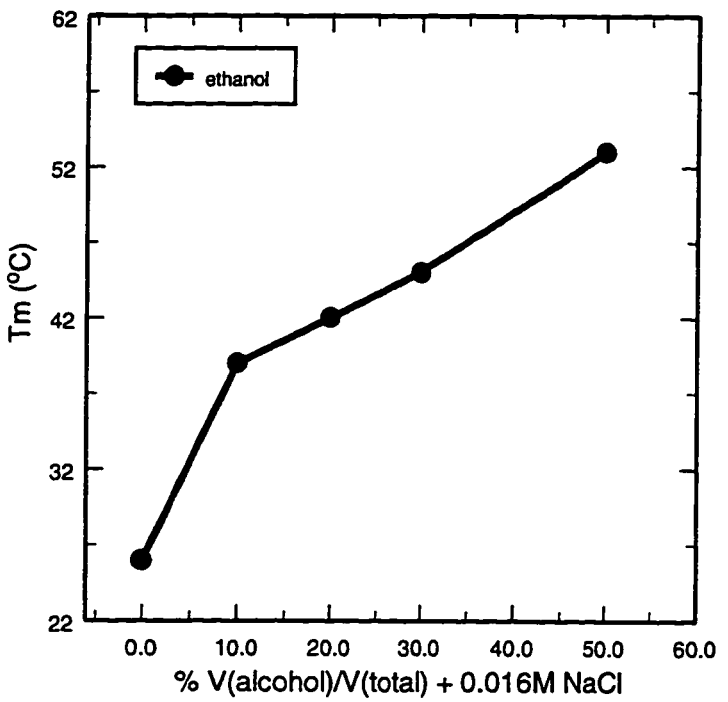
ethanol
Tm (°C)
62
52
42
32
22
0.0
10.0
20.0
30.0
40.0
50.0
60.0
% V(alcohol)/V(total) + 0.016M NaCl

Table 1: Melting Temperatures for the Triplex Mixture $d(C^+-T)_6$:$[d(A-G)_6 \cdot d(C-T)_6]$.

Conditions	1st Transition		2nd Transition	
pH 7.0 (or as stated) All chloride salts	Tm °C	Hyperchromism %	Tm °C	Hyperchromism %
1.0M Methylammonium	18	13	53	8
2.0M MA	19	12	53	8
3.0M MA	20	13	52	6
4.0M MA	19	11	51	8
1.0M Dimethylammonium	20	11	53	8
2.0M DMA	23	10	52	8
3.0M DMA	26	9	51	6
4.0M DMA	27	10	49	8
1.0M Trimethylammonium	28	10	52	6
2.0M TriMA	36	9	52	7
3.0M TriMA (pH 3.7)	72[a]	19	-	-
3.0M TriMA (pH 4.9)	67[a]	15	-	-
3.0M TriMA (pH 5.8)	58[a]	15	-	-
3.0M TriMA	50[a]	17	-	-
3.0M TriMA (pH 7.4)	36	8	51	7
3.0M TriMA (pH 7.8)	-	-	52	8
4.0M TriMA	53[a]	16	-	-
4.0M TriMA (pH 7.4)	36	8	50	6
1.0M Tetramethylammonium	31	10	54	9
2.0M TMA	29	9	55	7
3.0M TMA (pH 3.7)	75[a]	18	-	-
3.0M TMA (pH 4.9)	72[a]	16	-	-
3.0M TMA (pH 5.8)	61[a]	14	-	-
3.0M TMA	30	10	56	9
4.0M TMA	43	9	59	7
6.0M TMA	50[a]	23	-	-
6.0M TMA (pH 6.0)	67[a]	23	-	-
0.5M Tetraethylammonium	16	10	43	6
1.0M TEA	22	13	43	10
1.6M TEA	26	9	37	7
2.0M TEA	insoluble			
0.1M Tetrapropylammonium	-	-	29	8
0.5M TPA	-	-	31	8
0.9M TPA	-	-	28	8
0.9M TPA (pH 8.5)	-	-	27	8
1.0M TPA	insoluble			

[a] Melting temperature of triplex with a 3 → 1 transition.

Table 2: Melting Temperatures for the Triplex Mixture $d(C^+\text{-}T)_6$:$[d(A\text{-}G)_6 \cdot d(C\text{-}T)_6]$.

Conditions	1st Transition		2nd Transition	
pH 7.0 (or as stated)	Tm °C	Hyperchromism %	Tm °C	Hyperchromism %
10^{-4} Wt% CTriMA (3×10^{-6} M)	-	-	20	10
10^{-3} Wt% CTriMA (3×10^{-5} M)	-	-	23[a]	5
10^{-2} Wt% CTriMA (3×10^{-4} M)	28[b]	5	-	-
10^{-1} Wt% CTriMA (3×10^{-3} M)	insoluble, micelle formation			
10^{-4} Wt% CTriMA + MB	10	11	50	13
10^{-3} Wt% CTriMA + MB	22[c]	8	52	14
10^{-2} Wt% CTriMA + MB	insoluble, micelle formation			
10^{-3} Wt% CTriMA + 0.02M TMA + MB	12	8	51	10
10^{-3} Wt% CTriMA + 0.1M TMA + MB	14	11	51	9
10^{-3} Wt% CTriMA + 0.2M TMA + MB	15	10	52	8
10^{-3} Wt% CTriMA + 0.4M TMA + MB	16	11	52	8
10^{-2} Wt% CTriMA + 0.1M TMA + MB	45	11	64	11
10^{-2} Wt% CTriMA + 0.2M TMA + MB	insoluble, micelle formation			
DidecylA is insoluble in water (pH 7.0) at all concentrations.				
10^{-4} Wt% TridodecylMA (2×10^{-6} M)	-	-	20	10
10^{-3} Wt% TridodecylMA (2×10^{-5} M)	-	-	20	10
10^{-3} Wt% TridodecylMA (pH 6.0)	41[d]	14	-	-
10^{-2} Wt% TridodecylMA (2×10^{-4} M)	insoluble, micelle formation			
10^{-4} Wt% TridodecylMA + MB	10	10	51	11
10^{-3} Wt% TridodecylMA + MB	11	9	51	10
10^{-2} Wt% TridodecylMA + MB	insoluble, micelle formation			
10^{-4} Wt% DOSPA (7×10^{-7} M)	-	-	21	11
10^{-4} Wt% DOSPA (pH 6.0)	40[d]	10	-	-
10^{-3} Wt% DOSPA (7×10^{-6} M)	22[d]	7	-	-
10^{-3} Wt% DOSPA (pH 6.0)	40	6	79	7
10^{-2} Wt% DOSPA (7×10^{-5} M)	27	6	77	25[e]
10^{-1} Wt% DOSPA (7×10^{-4} M)	insoluble, micelle formation			
10^{-4} Wt% DOSPA + MB	10	11	50	16
10^{-3} Wt% DOSPA + MB	12	7	50	15
10^{-2} Wt% DOSPA + MB	insoluble, micelle formation			

MB, Mixing Buffer (0.15M NaCl; 0.005M $MgCl_2$); CTriMA, Cetyltrimethylammonium; DidecylA, Didecylammonium; TridodecylMA, Tridodecylmethylammonium; DOSPA, 2,3-dioleyloxy-N-[2(sperminecarboxamido)ethyl]-N,N-dimethyl-1-propanaminium trifluoroacetate.

[a] See Figure 3, duplex melting but possibly a very small amount of triplex melting.

[b] $3 \rightarrow 2 + 1$ transition (see Figure 3), phase transition of CTriMA masks duplex transition.

[c] Very broad transition (3-40°C). [d] Melting temperature of triplex with a $3 \rightarrow 1$ transition.

[e] Significant overlap with phase transition of DOSPA.

Table 3: Melting Temperatures for the Triplex Mixture $d(C^+\text{-}T)_6$:$[d(A\text{-}G)_6 \cdot d(C\text{-}T)_6]$.

Conditions pH 7.0 (or as stated)	1st Transition Tm °C	1st Transition Hyperchromism %	2nd Transition Tm °C	2nd Transition Hyperchromism %
0.1 Wt% SDS (4×10^{-3} M) + MB	-[a]	-	51	12
1 Wt% SDS (4×10^{-2} M) + MB	-[a]	-	51	11
10 Wt% SDS (4×10^{-1} M) + MB	-[a]	-	54	12
0.1M Tetramethylammonium Sulfate	16	7	48	21
0.5M TMA-S	20	17	56	11
1.0M TMA-S	25	14	57	11
1.5M TMA-S	TMA-S precipitates out of solution			
2×10^{-5} M Coralyne in H_2O (*no triplex*)	no cooperative transitions			
2×10^{-5} M Coralyne + MB (*no triplex*)	Coralyne has a highly cooperative transition at 58 °C with 40% hyperchromism (260 nm)			
2×10^{-5} M Coralyne + MB	14	14	54	13
2×10^{-5} M Coralyne + 0.075M NaCl + 0.0025M $MgCl_2$	16	10	49	10
0.75M Trehalose + MB	12	7	47	10
1.5M Trehalose + MB	12	4	44	10
2.0M Trehalose + MB	13	4	41	9
10 Vol% glycerol + MB	11	9	49	10
20 Vol% glycerol + MB	12	9	45	10
30 Vol% glycerol + MB	12	6	42	12
30 Vol% glycerol + MB + 1.0M TriMA	19	8	45	9
20 Vol% PEG200 + MB	18	11	44	10
40 Vol% PEG200 + MB	33[b]	23	-	-
20 Vol% PEG400 + MB	22	22	48	17
20 Vol% PEG600 + MB	24	15	49	14
10 Vol% DMSO + MB	15	12	48	12
20 Vol% DMSO + MB	17	11	45	12
40 Vol% DMSO + MB	20	12	41	12
50 Vol% DMSO + MB	27[b]	17	-	-
60 Vol% DMSO + MB	15[b]	12	-	-
60 Vol% DMSO + MB (pH 6.0)	36[b]	24	-	-

MB, Mixing Buffer (0.15M NaCl; 0.005M $MgCl_2$); SDS, Sodium Dodecylsulfate; Trehalose, α-D-glucopyranose α-D-glucopyranoside; PEG200, poly(ethylene glycol) ave. MW 200; PEG400, poly(ethylene glycol) ave. MW 400; PEG600, poly(ethylene glycol) ave. MW 600; DMSO, Dimethyl Sulfoxide. [a] SDS appears to inhibit triplex formation, however, transitions below 20°C may be occurring but are not observed as the solution solidifies below ~20°C.
[b] Melting temperature of triplex with a 3 → 1 transition.

Table 4: Melting Temperatures for the Triplex Mixture $d(C^+-T)_6$:[$d(A-G)_6$·$d(C-T)_6$].

Conditions	1st Transition		2nd Transition	
pH 7.0 (or as stated)	Tm °C	Hyperchromism %	Tm °C	Hyperchromism %
0.15M NaCl; 0.005M $MgCl_2$ (pH 4.2)	32	9	62[a]	13
0.15M NaCl; 0.005M $MgCl_2$ (pH 5.0)	29	12	50	9
0.15M NaCl; 0.005M $MgCl_2$ (pH 7.0)	**11**	**12**	**50**	**10**
0.15M NaCl; 0.005M $MgCl_2$ (pH 7.5)	1	4	50	10
0.4M NaCl	7	7	53	12
0.5M NaCl	8	14	54	10
0.8M NaCl	10	16	56	11
0.9M NaCl	10	17	56	11
1.0M NaCl	9	17	54	12
2.0M NaCl	7	13	54	12
3.0M NaCl	5	2	57	7
5.0M NaCl	-	-	51	10
6.0M NaCl	NaCl crystallizes out of solution			
0.4M Na_2HPO_4	8	9	54	12
0.8M Na_2HPO_4	12	11	56	11
2.0M Na_2HPO_4	15	11	57	11
2.0M Na_2HPO_4 (pH 6.5)	29	14	59	11
3.0M Na_2HPO_4	Na_2HPO_4 crystallizes out of solution			
0.4M $NaOOCCH_3$	9	12	53	11
0.8M $NaOOCCH_3$	12	12	56	11
2.0M $NaOOCCH_3$	15	13	55	11
3.0M $NaOOCCH_3$	16	13	54	12
0.4M Na_2SO_4	14	12	54	10
0.8M Na_2SO_4 (pH 7.2)	9	8	56	11
0.8M Na_2SO_4	17	13	55	12
2.0M Na_2SO_4	21	14	58	11
3.0M Na_2SO_4	Na_2SO_4 crystallizes out of solution			
2.0M $NaClO_4$	-	-	42	11
2.0M $NaClO_4$ (pH 6.0)	18	12	43	10
0.4M NH_4Cl	8	5	56	12
0.8M NH_4Cl	-	-	54	12
2.0M NH_4Cl	-	-	58	12
0.4M $(NH_4)_2SO_4$	8	4	55	12
0.8M $(NH_4)_2SO_4$	19	13	57	12
2.0M $(NH_4)_2SO_4$	28	13	58	11
3.0M $(NH_4)_2SO_4$	37[b]	14	60[b]	10

[a] See Discussion in text. [b] Overlapping transitions.

Table 5: Melting Temperatures for the Triplex Mixture $d(C^+\text{-}T)_6$:$[d(A\text{-}G)_6 \cdot d(C\text{-}T)_6]$.

Conditions pH 7.0 (or as stated) $V_{alcohol}/V_{total}$	1st Transition Tm °C	1st Transition Hyperchromism %	2nd Transition Tm °C	2nd Transition Hyperchromism %
10% methanol + MB	15	13	51	11
20% methanol + MB	15	14	48	11
30% methanol + MB	15	12	44	12
60% methanol + MB	16	7	37	7
70% methanol + MB	16	7	35	7
80% methanol + MB	soluble, no transitions			
10% ethanol + MB	12	12	48	10
20% ethanol + MB	13	12	44	11
30% ethanol + MB	15	6	41	11
40% ethanol + MB	15	7	36	10
50% ethanol + MB	21	23	38	8
60% ethanol + MB	40[a,c]	31	-	-
70% ethanol + MB	soluble, no transitions			
5% 2-propanol + MB	9	7	49	7
10% 2-propanol + MB	11	14	47	12
20% 2-propanol + MB	17	9	43	13
30% 2-propanol + MB	20	11	40	12
40% 2-propanol + MB	27[b]	31	39[b]	15
50% 2-propanol + MB	40[c]	38	-	-
60% 2-propanol + MB	insoluble			
0.1% 1-butanol + MB	8	10	51	9
1% 1-butanol + MB	7	9	50	9
5% 1-butanol + MB	7	10	47	9
10% 1-butanol + MB	phase separation			
30% 2-propanol + 20% ethanol + 3M TMA	32[c]	10	-	-
40% 2-propanol + 3M TMA	phase separation			
50% 2-propanol + 3M TMA	insoluble			
50% ethanol + 1.5M TriMA	30[c]	16	-	-

Mixing Buffer (MB): 0.15M NaCl; 0.005M $MgCl_2$

[a] Broad transition (20-60°C). [b] Overlapping transitions.

[c] Melting temperature of triplex with a 3 → 1 transition.

Table 6: Melting Temperatures for the Duplex Mixture [d(A-G)$_6$·d(C-T)$_6$].

Conditions	1st Transition		2nd Transition	
pH 7.0 (or as stated) All chloride salts	Tm °C	Hyperchromism %	Tm °C	Hyperchromism %
1.0M Methylammonium	-	-	52	16
2.0M MA	-	-	52	16
3.0M MA	-	-	52	16
4.0M MA	-	-	50	15
1.0.M Dimethylammonium	-	-	51	16
2.0M DMA	-	-	51	16
3.0M DMA	23	2	50	15
4.0M DMA	-	-	48	16
1.0M Trimethylammonium	-	-	50	14
2.0M TriMA	-	-	52	16
3.0M TriMA	-	-	51	17
4.0M TriMA	-	-	52	19
1.0M Tetramethylammonium	33	2	54	14
2.0M TMA	33	2	57	14
3.0M TMA	33	2	55	17
4.0M TMA	43	3	58	15
0.5M Tetraethylammonium	-	-	41	13
1.0M TEA	23	3	40	13
1.6M TEA	26	4	36	10
0.1M Tetrapropylammonium	-	-	29	13
0.5M TPA	-	-	30	15
0.9M TPA	-	-	27	16
0.9M TPA (pH 8.5)	-	-	26	16
MB (pH 4.2)	-	-	57[a]	23
MB (pH 5.0)	-	-	48	18
MB (pH 7.0)	-	-	**48**	**15**
MB (pH 7.5)	-	-	48	15
0.4M NaCl	-	-	51	15
0.5M NaCl	-	-	52	15
0.8M NaCl	-	-	54	15
0.9M NaCl	-	-	54	16
1.0M NaCl	-	-	53	16
2.0M NaCl	-	-	52	16
3.0M NaCl	-	-	52	15

Mixing Buffer (MB): 0.15M NaCl; 0.005M $MgCl_2$

[a] See Discussion in text.

Table 7: Melting Temperatures for the Duplex Mixture $[d(A\text{-}G)_6 \cdot d(C\text{-}T)_6]$.

Conditions pH 7.0 (or as stated) $V_{alcohol}/V_{total}$	1st Transition Tm °C	1st Transition Hyperchromism %	2nd Transition Tm °C	2nd Transition Hyperchromism %
10% methanol + MB (pH 6.7)	20	8	48	15
10% methanol + MB	13	5	47	17
20% methanol + MB	15	5	45	18
30% methanol + MB	15	5	42	18
60% methanol + MB	17	7	38	13
70% methanol + MB	17	6	35	12
80% methanol + MB	soluble, no transitions			
10% ethanol + MB	-	-	46	20
20% ethanol + MB	-	-	41	20
30% ethanol + MB	-	-	38	21
40% ethanol + MB	20[a]	7	38[a]	7
50% ethanol + MB	19	11	39	12
60% ethanol + MB	42[b]	30	-	-
70% ethanol + MB	soluble, no transitions			
5% 2-propanol + MB	-	-	48	19
10% 2-propanol + MB	-	-	46	19
20% 2-propanol + MB	-	-	42	20
30% 2-propanol + MB	-	-	39	20
40% 2-propanol + MB	21[c]	4	41[c]	15
50% 2-propanol + MB	32[c]	16	44[c]	10
60% 2-propanol + MB	insoluble			
0.1% 1-butanol + MB	-	-	50	17
1% 1-butanol + MB	-	-	49	17
5% 1-butanol + MB	-	-	44	17
10% 1-butanol + MB	phase separation			

Mixing Buffer (MB): 0.15M NaCl; 0.005M $MgCl_2$

[a] Broad and overlapping transitions. [b] Melting temperature of triplex with a 3 → 1 transition. [c] Significant overlap of transitions resulting in possible overestimation of 2nd transition Tm.

Table 8: Melting Temperatures for the Triplex Mixture $d(T)_{21}$:[$d(A)_{21}$·$d(T)_{21}$].

Conditions pH 7.0	1st Transition		2nd Transition	
	Tm °C	Hyperchromism %	Tm °C	Hyperchromism %
MB	**23**	**18**	**53**	**15**
0.4M NaCl	24	17	58	19
0.8M NaCl	42	18	62	17
1.0M NaCl	49[a]	18	64[a]	18
2.0M NaCl	66[b]	33	-	-
3.0M NaCl	70[b]	33	-	-
5.0M NaCl	72[b]	33	-	-
6.0M NaCl	NaCl crystallizes out of solution			
2.0M Na_2HPO_4	80[b]	33	-	-
2.0M $NaOOCCH_3$	66[b]	33	-	-
2.0M Na_2SO4	80[b]	33	-	-
2.0M $NaClO_4$	44[b]	30	-	-
1.0M $(NH_4)Cl$	65	36	-	-
2.0M $(NH_4)Cl$	71	36	-	-
3.0M $(NH_4)Cl$	76	36	-	-
1.0M $(NH_4)_2SO_4$	71	36	-	-
2.0M $(NH_4)_2SO_4$	83	36	-	-
3.0M $(NH_4)_2SO_4$	93	36[c]	-	-
1.0M TriMA-Cl + MB	45	16	61	11
2.0M TriMA-Cl + MB	66[b]	27	-	-
3.0M TriMA-Cl + MB	70[b]	26	-	-
1.0M TriMA-Cl	39	17	63	18
1.0M TMA-Cl	28	17	65	19
6.0M TMA-Cl	95[b]	33[c]	-	-
1.0M TMA-S	54	10	74	13
1.5M TMA-S	TMA-S precipitates out of solution			

Mixing Buffer (MB): 0.15M NaCl; 0.005M $MgCl_2$

[a] Overlapping transitions. [b] Melting temperature of triplex with a 3 → 1 transition.

[c] Obtained by extrapolation.

Table 9: Melting Temperatures for the Triplex Mixture $d(T)_{21}$:$[d(A)_{21}{\cdot}d(T)_{21}]$ and for the Duplex Mixture $[d(A)_{21}{\cdot}d(T)_{21}]$.

Conditions pH 7.0	1st Transition Tm °C	1st Transition Hyperchromism %	2nd Transition Tm °C	2nd Transition Hyperchromism %
$d(T)_{21}$:$[d(A)_{21}{\cdot}d(T)_{21}]$				
50 Vol% methanol + MB	38[a]	38	-	-
50 Vol% ethanol + MB	53[a]	74	-	-
50 Vol% 2-propanol + MB	65[a]	74	-	-
2 x 10^{-5} M Coralyne in H_2O (*no triplex*)	no cooperative transitions			
2 x 10^{-5} M Coralyne + MB (*no triplex*)	Coralyne has a highly cooperative transition at 58 °C with 40% hyperchromism (260nm)			
2 x 10^{-5} M Coralyne + MB	23	5	59	33
2 x 10^{-5} M Coralyne + 0.075M NaCl + 0.0025M $MgCl_2$	23	3	54	28
20 Vol% PEG200 + MB	39[a]	25	-	-
40 Vol% PEG200 + MB	41[a]	45	-	-
20 Vol% PEG600 + MB	52[a]	54	-	-
30 Vol% DMSO + MB	34[b]	18	44[b]	16
40 Vol% DMSO + MB	38[a]	35	-	-
50 Vol% DMSO + MB	15	9	34	28
$[d(A)_{21}{\cdot}d(T)_{21}]$				
MB	-	-	**53**	**28**
1.0M TriMA-Cl + MB	-	-	60	23
2.0M TriMA-Cl + MB	-	-	65	25
3.0M TriMA-Cl + MB	-	-	70	23

Mixing Buffer (MB): 0.15M NaCl; 0.005M $MgCl_2$

[a] Melting temperature of triplex with a 3 → 1 transition. [b] Overlapping transitions.

Table 10: Melting Temperatures for the Triplex Mixture Poly(rU):Poly(rA)·Poly(rU) and for the Duplex Mixture Poly(rA)·Poly(rU).

Conditions pH 7.0 All chloride salts	1st Transition Tm °C	 Hyperchromism %	2nd Transition Tm °C	 Hyperchromism %
Poly(rU):Poly(rA)·Poly(rU)				
0.016M NaCl	26	17	40	23
0.020M TriMA + 0.016M NaCl	34	21	42	18
0.053M TriMA + 0.016M NaCl	44[a]	37	-	-
0.600M TriMA + 0.016M NaCl	69[a]	41	-	-
0.020M TMA + 0.016M NaCl	31	18	40	17
10^{-4} Wt% CTriMA (3×10^{-6}M) + 0.016M NaCl	27	16	40	20
10^{-3} Wt% CTriMA (3×10^{-5}M) + 0.016M NaCl	38[b]	12	63[b]	18
10^{-2} Wt% CTriMA (3×10^{-4}M) + 0.016M NaCl	insoluble, micelle formation			
10 Vol% ethanol + 0.016M NaCl	39[a]	37	-	-
20 Vol% ethanol + 0.016M NaCl	42[a]	39	-	-
30 Vol% ethanol + 0.016M NaCl	45[a]	40	-	-
50 Vol% ethanol + 0.016M NaCl	53[a]	54	-	-
60 Vol% ethanol + 0.016M NaCl	insoluble			
Poly(rA)·Poly(rU)				
0.016M NaCl	-	-	40	25
0.020M TriMA + 0.016M NaCl	-	-	41	25
0.053M TriMA + 0.016M NaCl	-	-	45	24
0.600M TriMA + 0.016M NaCl	-	-	69	28
10 Vol% ethanol + 0.016M NaCl	-	-	39	26
20 Vol% ethanol + 0.016M NaCl	-	-	42	26
30 Vol% ethanol + 0.016M NaCl	-	-	46	26
50 Vol% ethanol + 0.016M NaCl	-	-	58	26
60 Vol% ethanol + 0.016M NaCl	insoluble			

[a] Melting temperature of triplex with a 3 → 1 transition. [b] Overlapping transitions.

3.4 Discussion

Enhancement of stability of triplex varies with triplex length. It is apparent that the stabilizing effect of DMSO, ethanol and CTriMA-Cl increases with triplex length. Examples are: 1) a maximum effect is observed with 50 Vol% DMSO for $d(C^+\text{-}T)_6$:$d(A\text{-}G)_6$·$d(C\text{-}T)_6$ and 40 Vol% with $d(T)_{21}$:$d(A)_{21}$·$d(T)_{21}$; 2) for $d(C^+\text{-}T)_6$:$d(A\text{-}G)_6$·$d(C\text{-}T)_6$ in ethanol a significant effect is observed at 50 Vol% and above, whereas for poly r(U:A·U); a significant effect is observed at 10 Vol% and above; and 3) 10^{-3} Wt% CTriMA-Cl does not enhance the stability of $d(C^+\text{-}T)_6$:$d(A\text{-}G)_6$·$d(C\text{-}T)_6$ but does so for poly r(U:A·U); however, here two factors are different, length and the presence of a positively charged triplet repeat, C^+:G·C.

There are two reasons for believing that the mechanism by which the organic salts MA-Cl, DMA-Cl, TriMA-Cl, TMA-Cl and TEA-Cl enhance the stability of the triplex $d(C^+\text{-}T)_6$:$d(A\text{-}G)_6$·$d(C\text{-}T)_6$ does not involve raising the pKa of the dC residues. Firstly, these salts also enhance to a greater extent then NaCl, the stability of the triplex $d(T)_{21}$:$d(A)_{21}$·$d(T)_{21}$, which contains no protonated residues in its T:A·T triplets. The stability of this triplex reaches a plateau at 3.0 M NaCl, with a maximum Tm of 72 °C at 5.0 M NaCl (Figure 17), whereas in 6.0 M TMA-Cl Tm = 95 °C (Table 8). Secondly, for the triplex $d(C^+\text{-}T)_6$:$d(A\text{-}G)_6$·$d(C\text{-}T)_6$, if the pKa of the dC residues was raised in the presence of these organic salts, then lowering the pH would not increase triplex stability; in fact it should decrease it. This too is not observed; rather, the stability of this triplex

increases substantially with decreasing pH, e.g., from a Tm in 3.0 M TMA-Cl of 30 °C at pH 7.0 to 75 °C at pH 3.7.

A model for interpreting the findings. The physical and chemical properties of water have been extensively studied (for example, 16, 17, 18), and it is known that when a salt is dissolved in water, different anions and cations are observed to decrease, increase or have little effect on the volume of the solution. These alternative effects have been explained in terms of the interaction of the anion or cation with water molecules according to what is often called the multilayer hydration model (17). Briefly, this model of ion-water interaction divides the volume of an ion in solution, V_{ion}, into four components:

$$V_{ion} = V_{cryst} + V_{elect} + V_{disord} + V_{caged}$$

where: V_{cryst} is the volume of the ion based on its crystal radius; V_{elect} is the electrostriction volume (stronger ion-H_2O interaction decreases volume); V_{disord} is the disordered or void-space volume (weaker ion-H_2O interaction increases volume); and V_{caged} is the caged or structured volume (that occurs when a hydrophobic ion (organic cation) interacts with H_2O molecules, which decreases volume).

Although these ion volume factors are interdependent, the observed solution volume changes on addition of ions is readily explained by this descriptive model[1/]. Using this model, ions can be divided into three classes: 1) electrostrictive "structure-making" ions when V_{elect} is dominant; 2) disordered "structure-breaking" ions when V_{disord} is dominant; and 3) hydrophobic "structure-making" ions when V_{caged} is dominant.

The volumes, V_{elect}, V_{disord} and V_{caged} have been calculated for each anion and cation for which a listing is given in (17). As these volumes are additive, predictions of the solution volume effect of a particular salt can be made. It is interesting that the structure-making or structure-breaking tendency of anions based upon this model follows the rank order of the Hofmeister series, which is the relative tendency of anions to stabilize and solubilize proteins. These effects (reviewed in 19) were first noted by Hofmeister in his classic 1888 paper in which he listed the effect of anions on protein solubility. A partial rank order follows:

(destabilize proteins) $ClO_4^- < Cl^- < CH_3COO^- < HPO_4^{2-} \leq SO_4^{2-}$ (stabilize proteins)

This rank order has subsequently been called the "chaotropic series", as extensive studies have shown Cl^- to have little effect on water-structure, whereas anions to the left of Cl^- are water structure-breakers (V_{disord} is dominant) called chaotropes (from the Greek, meaning disorder (*chao*)) because they destabilize proteins, while anions to the right of Cl^- are water structure-makers (V_{elect} is dominant) called kosmotropes (from the Greek, meaning order (*kosmos*)) because they stabilize proteins. Thus, polar or charged chaotropes "disrupt" the structure of water because they interact with water less strongly, while polar or charged kosmotropes interact with water more strongly than bulk water molecules with each other.

Previous work (20) has shown that the effect of various salts on the stability of duplex DNA also follows the Hofmeister series. In that work, the only minor exception to the Hofmeister series occurred with CH_3COO^-, which was ranked one before Cl^- instead

of one after Cl^-. For sea urchin DNA (37 % GC) in 4.0 M salt at pH 7.0, rank order according to duplex Tm values (°C) for the various sodium salts was (20):

(destabilize duplex DNA)ClO_4^- (74°) < CH_3COO^- (84°) < Cl^- (90°)(stabilize duplex DNA)

Although the effect on duplex stability of many salts was studied by Hamaguchi and Geiduschek (20), HPO_4^{2-} and SO_4^{2-} were not. In the same study it was concluded that at the very high concentrations needed to observe the anion effects, there were only minor differences observed when the cations Li^+, Na^+, K^+, and TMA^+ were varied.

The results obtained in this work show that the effect of anions on triplex stability follows the Hofmeister series. For the triplex $d(C^+\text{-}T)_6$:$d(A\text{-}G)_6$·$d(C\text{-}T)_6$ in 2.0 M anion at pH 7.0, rank according to triplex Tm values (°C) for the various salts is:

$NaClO_4$ (inhibits triplex formation) < NaCl (7°) < $NaOOCCH_3$ (15°); Na_2HPO_4 (15°) < Na_2SO_4 (21°) < $(NH_4)_2SO_4$ (28°).

For the triplex $d(T)_{21}$:$d(A)_{21}$·$d(T)_{21}$ in 2.0 M anion at pH 7.0, rank according to triplex Tm values (°C) for the various salts is:

$NaClO_4$ (44°) < NaCl (66°); $NaOOCCH_3$ (66°) < Na_2HPO_4 (80°); Na_2SO_4 (80°) < $(NH_4)_2SO_4$ (83°).

Whereas duplex DNA stability is not greatly affected by cations in general when at very high concentration, *the results obtained in this work show that organic cations have a strong effect on triplex stability.* Their stabilizing ability can also be explained by the ion-water model. Thus, for these organic cations V_{caged} is dominant, and in this case water "structure-making" occurs as a result of the hydrophobic cation. That is, the organic

cation (kosmotrope) interacts much less strongly with water, and in so doing orders the water molecules around them (the effect on the interfacial water surrounding the nonpolar solute is that it becomes more ordered).

Generally, for the triplex $d(C^{+}\text{-}T)_6$:$d(A\text{-}G)_6$·$d(C\text{-}T)_6$ at pH 7.0:

TPA-Cl (inhibits triplex formation) < NaCl < MA-Cl < DMA-Cl < TEA-Cl < TMA-Cl ≤ TriMA-Cl.

For the triplex $d(T)_{21}$:$d(A)_{21}$·$d(T)_{21}$ at pH 7.0, the highest obtainable Tm is 72 °C in 5.0 M NaCl, while the highest obtainable Tm is 95 °C in 6.0 M TMA-Cl[2/].

As both triplexes and duplexes have a very high negative charge density, cations of sufficient positive charge density are required to stabilize them. Therefore, although V_{caged} is negative for the organic cations (because of their water structure-making nature, i.e., decreased volume), TMA^+ (-21 $cm^3.mole^{-1}$), TEA^+ (-18 $cm^3.mole^{-1}$), and TPA^+ (-24 $cm^3.mole^{-1}$), TPA^+ must not have sufficient positive charge density. Thus, it is possible that the size (and hence charge density) of these organic cations also plays a role in their ability to stabilize triplexes. At pH 7.0 they all have one positive charge and therefore their charge density will scale with their surface area (calculated using ChemPlus in HyperChem (21)): MA^+ (178 $Å^2$), DMA^+ (208 $Å^2$), $TriMA^+$ (232 $Å^2$) TMA^+ (252 $Å^2$), TEA^+ (325 $Å^2$), and TPA^+ (383 $Å^2$). This would imply that $TriMA^+$ and TMA^+ have the optimum size and charge density to stabilize triplexes. However, as observed, their decreasing charge density also makes them less soluble in H_2O, and this may also have an effect.

It should be noted that TEA^+ and TPA^+ have a significant destabilizing effect on the duplex $d(A\text{-}G)_6 \cdot d(C\text{-}T)_6$ (Table 6).

The observations for the stability of the triplexes in the alcohols, PEG, and DMSO are the following.

Generally, for the triplex $d(C^+\text{-}T)_6 : d(A\text{-}G)_6 \cdot d(C\text{-}T)_6$ at pH 7.0:

MeOH < EtOH < 2-PrOH > 1-BuOH.

For the triplex $d(T)_{21} : d(A)_{21} \cdot d(T)_{21}$ in 50 Vol% alcohol + MB at pH 7.0, rank according to triplex Tm values (°C):

0 %, MB only (23°) < MeOH (38°) < EtOH (53°) < 2-PrOH (65°).

For the triplex poly r(U:A·U) in Vol% EtOH + 0.016 M NaCl at pH 7.0:

0 % (26°) < 10 % (39°)< 20 % (42°) < 30 % (45°) < 50 % (53°).

For the triplex $d(C^+\text{-}T)_6 : d(A\text{-}G)_6 \cdot d(C\text{-}T)_6$ in 20 Vol% PEG(ave. molecular weight) + MB at pH 7.0:

0 %, MB only (11°) < PEG200 (18°) < PEG400 (22°) < PEG600 (24°).

For the triplex $d(C^+\text{-}T)_6 : d(A\text{-}G)_6 \cdot d(C\text{-}T)_6$ in Vol% DMSO + MB at pH 7:

0 %, MB only (11°) < 10 % (15°) < 20 % (17°) < 40 % (20°) < 50 % (27°) > 60 % (15°).

For the triplex $d(T)_{21} : d(A)_{21} \cdot d(T)_{21}$ in Vol% DMSO + MB at pH 7.0:

0 %, MB only (23°) < 30 % (34°) < 40 % (38°) > 50 % (15°).

Aqueous neutral polar organic solutes can also be classified as water structure-breaking (chaotropes) or water structure-making (kosmotropes) (19). The low molecular

weight alcohols are water structure-making, as is the neutral hydrophilic polymer PEG and the potent H-bond acceptor DMSO.

It would appear therefore that solutes that are water structure-making enhance the stability of triplexes. Conversely, no water structure-breaking solute has been observed to enhance triplex stability. This thermodynamic model of ion-water interaction has given a thermodynamic answer. We now attempt to relate this thermodynamic understanding of how "altered water structure" may influence the conformation of DNA to the molecular mechanism for triplex formation.

The result of the water-alcohol or PEG or DMSO interaction is that there is less water available to hydrate other 'solutes'. This is a well known observation for DNA in water/ethanol mixtures. The higher the proportion of ethanol, the less the proportion of water available for hydration of DNA (i.e., dehydration), and in 60 to 70 % ethanol there is sufficient dehydration to induce a conformational change from B to A or Z. Such conformational changes require varying degrees of unwinding the DNA with resultant changes in rotation of the nucleotide residues from 36 - 45 ° to 30 - 33 ° in the case of B to A, and even *anti* to *syn* isomerization in the case of B to Z.

In this connection, the unwinding of duplex DNA has been observed to increase in the presence of MeOH, EtOH, ethylene glycol and DMSO but not glycerol (22). It was also observed that the degree of unwinding is a continuous process in response to the concentration of organic solvent. The Vol % required for unwinding increases in the order: DMSO < MeOH ≤ EtOH < ethylene glycol.

As glycerol does not enhance triplex formation, it is likely that MeOH, EtOH, 2-PrOH, PEG and DMSO all enhance triplex stability by facilitating unwinding of the duplex. In fact, it would make sense that all compounds that facilitate both a B to A/Z transition and dehydration also enhance binding of third strands that must enter the major groove of the duplex. Clearly, third strand binding must require displacement of water from the major groove of the duplex to accommodate this extra strand. This is further supported by the observation that RecA facilitates third strand binding, since the hydrophobic environment created by the protein must facilitate removal of water (23).

Thus, it would appear that solutes that are water structure-making enhance the stability of triplexes by facilitating the unwinding of the duplex to the extent needed to accommodate the third strand and this need not necessarily involve a B to A transition. And since water structure-makers may also be good dehydrating agents, this also facilitates the removal of water that must be required to allow for third strand binding.

Given that a triplex has essentially the same cylindrical diameter as a duplex, it is understandable why triplexes are far more sensitive to solution conditions than duplexes, a fact that the present work confirms. This understanding of the solution conditions that significantly impact on triplex stability should prove useful in efforts to obtain crystals of a triplex in a well-ordered lattice, currently a major obstacle in obtaining highly ordered single crystals for structure analysis.

3.5 Footnotes

[1/] This is a thermodynamic model, in that it is able to describe observations made. This model ignores the 'chemical details' that clearly give each anion and cation its chemical identity. For example, inorganic cations are known to form unique structures with water, where water molecules are acting as ligands via their oxygen atoms to form coordination complexes.

[2/] TMA could be used as a model 'solvent' to mimic the environment of DNA *in vivo*. DNA is in a highly compact 'condensed phase' when interacting with histone proteins that are essentially highly positively charged organic electrolytes. DNA concentration *in vivo* is very high, 70-80% w/v in sperm heads, virus capsids, bacterial nucleoids (24,25). A comparable TMA concentration is 6.4M (70% w/v). It is therefore interesting to note that TMA significantly enhances triplex stability.

3.6 Acknowledgments

This work was supported by NIH grant (GM 42936) to J. R. F., and a Pre-Doctoral Traineeship from NIH grant (GM 08309) and a gift of AXUM 4.0 from TriMetrix Corporation to L. L.

3.7 References

1. Wells, R. D., Collier, D. A., Hanvey, J. C., Shimizu, M. and Wohlrab, F. (1988) *Faseb. J.* **2**, 2939-2949.
2. Htun, H. and Dahlberg, J. E. (1989) *Science.* **243**, 1571-1576.
3. Helene. C. (1994) *European J. Cancer* **30A**, 1721-1726.
4. Plum, G. E., Pilch, D. S., Singleton, S. F. and Breslauer, K. J. (1995) *Annu. Rev. Biophys. Biomol. Struct.* **24**, 319-350.
5. Stull, R. A. and Szoka, F. C. (1995) *Pharmaceutical. Res.* **12**, 465-483.
6. Frank-Kamenetskii, M. D. and Mirkin, S. M. (1995) *Annu. Rev. Biochem.* **64**, 65-95.
7. Hampel, K. J., Crosson, P. and Lee, J. S. (1991) *Biochemistry.* **30**, 4455-4459.
8. Crow, J. (1987) *J. Biochem.* **242**, 1.
9. Colaco, C. (1992) *Biotechnology.* **10**, 1007.
10. Colaco, C. (1994) Formulations and Delivery of Proteins and Peptides, Cleland, J.L. and Langer, R. Eds. American Chemical Society Symposia Series No. 567, 222.
11. Lavelle, L., Fresco, J. R. (1995) *Nucleic. Acids. Res.* **23**, No.14, 2692-2705.
12. Broitman, S. L., Im, D. D. and Fresco, J. R. (1987) *Proc. Natl. Acad. Sci. U. S. A.* **84**, 5120-5124.
13. Johnson, K. H., Gray, D. M. and Sutherland, J. C. (1991) *Nucleic. Acids. Res.* **19**, No.9, 2275-2280.
14. Blake, R. D., Massoulie, J. and Fresco, J. R. (1967) *J. Mol. Biol.* **30**, 291-308.
15. Lee, J. S., Latimer, L. J. P. and Hampel, K. J. (1993) *Biochemistry.* **32**, 5591-5597.
16. Eisenberg, D. and Kauzmann, W. (1969) The Structure and Properties of Water, Oxford University Press, UK.
17. Horne, R. A. (Ed.) (1972) Water and Aqueous Solutions, Wiley-Interscience, NY.
18. Franks, F. (Ed.) (1973) Thermodynamic Properties. Water. A Comprehensive Treatise, Plenum Press, NY.
19. Collins, K. D. and Washabaugh, M. W. (1985) *Q. Rev. Biophysics.* **18**, 323-422.

20. Hamaguchi, K. and Geiduschek, E. P. (1962) *J. Am. Chem. Soc.* **84** No. 8, 1329-38.

21. HyperChem 4.0 (1994) Hypercube Corporation, Waterloo, Ontario, Canada.

22. Lee, C. H., Mizusawa, H. and Kakefuda, T. (1981) *Proc. Natl. Acad. Sci. U. S. A.* **78**, 2838-2842.

23. Iyer, M., Norton. J. C. and Corey. D. R. (1995) *J. Biol. Chem.* **270**, 14712-14717.

24. Rill, R. L. (1986) *Proc. Natl. Acad. Sci. U. S. A.* **83**, 342-346.

25. Strzelecka, T. E., Davidson, M. W. and Rill, R. L. (1988) *Nature* **331**, 457-460.

IV. α-DNA, a single-stranded secondary structure stabilized by ionic and hydrogen bonds: $d(A^+\text{-}G)_n$

Mary Claire Shiber, Laurence Lavelle*, John A. Fossella, and Jacques R. Fresco

published in Biochemistry (1995) **34**, 14293-14299

A novel nucleic acid secondary structure, exemplified by $d(A^+\text{-}G)_{10}$, is formed by an intramolecular, cooperative, acid-induced, coil → helix transition. The helix is apparently left-handed, lacks base stacking and pairing, and is maintained by hydrogen and ionic bonds between dA^+ "side chain" residues (with electropositive hydrogens $-N_6H_2$, $-N_1{}^+H$) and the phosphodiester backbone. Modeling indicates that those dA^+ residues lie approximately parallel to the helix axis, interacting with the n-1 backbone phosphates (with electronegative oxygens), somewhat like the -C=O···H-N- longitudinal interactions in a protein α-helix. Moreover, the intervening dG side chain residues are extrahelical, as are amino acid side chains of an α-helix.

* As I was responsible for the modeling, Chapter IV contains only the modeling section of this paper.

4.1 Introduction

All currently recognized types of nucleic acid secondary structure involve helical stacks of bases. Such stacks occur in single strands, in base pairs of hairpins formed by single strands, in base pairs of two-stranded complexes, in base triplets of three-stranded structures, and in base quartets of four-stranded complexes.

This chapter describes an entirely different type of nucleic acid helical secondary structure, one that does not depend for its stabilization on helically wound stacks of bases or base pairs. Rather, this novel type of secondary structure encompasses single strands of the repeating homopurine doublet sequence $d(A\text{-}G)_n$ helically twisted by an unusual combination of ionic and hydrogen (H-) bonds essentially parallel to the helix axis.

Previous studies (1,2) had shown $d(A\text{-}G)_{10}$ to display unusual properties under acidic conditions. That is, an intense differential absorption of circularly polarized light (CD) without concomitant development of hypochromism in the near-ultraviolet (UV) (1). Additional observations (2) enabled attribution of this unusual dichotomy in optical properties to a single-stranded helical secondary structure stabilized largely by Coulombic interactions between negatively charged backbone phosphates and distal protonated dA (dA^+) residues that do not overlap with their nearest neighbor dG residues.

4.2 Methods

Modeling was on an IBM PC, Intel 486DX, 66 MHz, 24 MB RAM with AMBER as part of HyperChem (3). Parameters are those of AMBER 3.0A (4), using the standard unmodified all-atom force field. Base charges for dA^+ are those for dA but with a proton

on N_1 with bond length of 1.1 Å (force constant of 14 kcal·mol^{-1}·Å^{-2}), bond angle of 117.4° and torsion angle of 0.0° (force constants of 125 and 16 kcal·mol^{-1}·degree^{-2}, respectively) to maintain the proton in the plane of the purine ring. All calculations were done with a 0.5 fs time step (integration step) as the hydrogen atoms were not constrained. The initial conformation was generated by putting d(A$^+$-G)$_5$, a tractable length of oligomer, in the helical conformation of one of the strands of a B-DNA duplex, and rotating every dA$^+$ residue ~180° to obtain an unstacked single strand.

In order to generate various conformations, a 22 ps, constant energy, constant volume (microcanonical ensemble), high temperature molecular dynamics simulation of d(A$^+$-G)$_5$ was performed. No cutoff distance was used for nonbonded interactions and a distance dependent dielectric constant, ε, [ε = (permittivity of free space) x (scale factor) x (interatomic separation)] was used as a model solvent. For a highly charged system such as this, a dielectric constant scale factor of 4.0 was used (5), and 1-4 scale factors were set at 0.5 for electrostatic and Van der Waals interactions. Previous simulations using scale factors of 1 and 2 resulted in the dA$^+$ residues remaining in close proximity to the electronegative backbone oxygens, thereby restraining the conformational search. The starting temperature of the simulation was 0 °K with temperature steps of 10 °K taking the system to 3000 °K in 0.15 ps, conformations (snapshots) were stored at 4000 time step intervals resulting in eleven conformations at 2 ps intervals.

To obtain a low energy conformation, simulated annealing was done on the high temperature 2 ps conformation by cooling slowly from 3000 to 300 °K in 0.5 °K steps,

with conformations stored every 0.25 ps. Conditions used were those of the high temperature molecular dynamics.

Room temperature molecular dynamics was used to obtain the most favorable conformation. The structure obtained from the simulated annealing was placed in a periodic box, 26 x 26 x 56.1 Å [~1110 H_2O, TIP3P model (equilibrated at 300 °K and 1 atm) (6)]. At this stage, the 5' dA residue was found to be non-interacting and set neutral; hence, 5 Na^+ ions were placed 1.7 Å equidistant from the oxygen atoms of the non-interacting phosphates and constrained to each oxygen with a force constant of 14 $kcal \cdot mol^{-1} \cdot Å^{-2}$. Using the AMBER protocol with explicit water molecules, the dielectric constant scale factor was set at 1.0 and 1-4 scale factors were set at 0.5 for electrostatic and Van der Waals interactions. Nonbonding interactions were limited by a switched cutoff, with outer and inner radii of 13 and 9 Å, respectively. To allow for stable trajectories, this system was first energy minimized to an rms gradient of 10.
A 10.625 ps constant temperature (300 °K), constant volume (canonical ensemble) molecular dynamics simulation was performed to search for a low energy conformation using a bath coupling constant of 0.1 ps and conformations stored every 0.125 ps.

4.3 Results

The low energy conformation obtained at the end of the room temperature simulation was energy minimized (with the same parameters) using a conjugate gradient method (Polak-Robiere) and convergence set at 0.1 $kcal \cdot Å^{-1} \cdot mol^{-1}$ for the rms gradient. The resultant structure had a non-regular "bent" backbone conformation with the following

characteristics: ~13 Å diameter, ~51 Å length, formed by a lattice of unstacked dA^+ residues lying more or less parallel to the long axis, each translated ~12 Å and linked to its n-1 phosphate by both ionic and H-bond interactions from which protrude non-interacting dG residues.

The above protocols (simulated annealing, room temperature molecular dynamics, energy minimization) were performed on the 4, 6 and 8 ps conformations obtained from the high temperature molecular dynamics simulation. In these cases, the resultant structures showed the dA^+ residues interacting with the oxygens of the phosphodiester backbone, but with various non-regular backbone conformations.

After building a physical model that was adjusted to fit the above energy minimized models, it became apparent that the dA^+- phosphate binding motif allows for conformational freedom between each "dinucleotide unit":

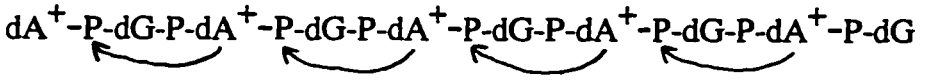

where the - bond indicates the site of conformational freedom (in particular, the α-torsion angle O3'-P-O5'-C5'). We therefore chose the above 2 ps energy minimized structure and changed the α-torsion angles (-) so as to obtain a more regular, non-bent backbone conformation. To remove any unfavorable interactions, a room temperature molecular dynamics simulation (canonical ensemble, with the same parameters) was performed and terminated after 3 ps with the potential energy (Ep) reaching a plateau at -20572

kcal·mol^{-1}. The low energy conformation obtained at the end of this simulation was energy minimized (with the same parameters, rms of 0.1 kcal·Å^{-1}·mol^{-1} etc., with a resultant Ep = -24307 kcal·mol^{-1}) and is the model discussed below and shown in Figures 1 and 2 with Na^+ and H_2O removed.

The model derived for d(A$^+$-G)$_5$ (Figures 1 and 2) reveals a helical structure ~12 Å in diameter and ~54 Å in length. It is formed by a lattice of unstacked dA$^+$ residues lying more or less parallel to the long axis, linked to the n-1 phosphate oxygens, i.e., one phosphate upstream, by strong ionic and H-bonds mediated by A-N$_1$H$^+$ and A-N$_6$H, while the non-interacting dG residues protrude from the helix. The backbone conformation of this novel secondary structure is unlike any known duplex conformation. However, the CD spectrum of d(A$^+$-G)$_{10}$ is remarkably like that of Z-DNA (1), and the model does indicate a left-handed helical sense of backbone twist (Figure 2).

With the exception of dA$_1$, which is displaced due to the absence of an upstream phosphate with which to bond (Figure 2), the dA$^+$ residues are held very close and parallel, rather than perpendicular, to the backbone. The distance between the N9 atoms of successive dA$^+$ residues is ~12 Å. While there is some variation in orientation about the glycosyl bonds, the torsion angle, χ, indicates an anti or high-anti conformation for all the residues. In this connection, it is important to note that the modeling was done with no constraints, and that UV resonance Raman (UVRR) observations confirm that all the residues are in an anti type conformation (7). There is no apparent interaction between the dG residues and any other component of the helix; rather, they are unrestricted and accessible to bulk solvent, just as indicated by the results of UVRR and solvent

perturbation spectroscopies. In this regard, conformational heterogeneity is expected for the first (5') dA residue (which lacks an upstream phosphate partner) and the dG residues, as they are relatively free to rotate about their glycosyl bond.

In sum, the calculations reveal a stable structure maintained by H-bond and Coulombic interactions between the dA^+ residues and the oxygens of the phosphodiester backbone. In the absence of the more typical base stacking and H-bonded base pairing, these must be the major interactions that stabilize the structure.

Figure 1: Five center residues of d(A^+-G)5, i.e., 5'-d($pA^+_5pG_6pA^+_7pG_8pA^+_9$)-3' showing ionic and H-bonds as indicated by dashed lines in wire representation (H_2O and Na^+ omitted for clarity). All structures are oriented 5' → 3' top to bottom.

First panel: space filling representation. Atom colors: C, green; N, blue; O, red; P, yellow; H, white.

Second panel: wire representation (same perspective).

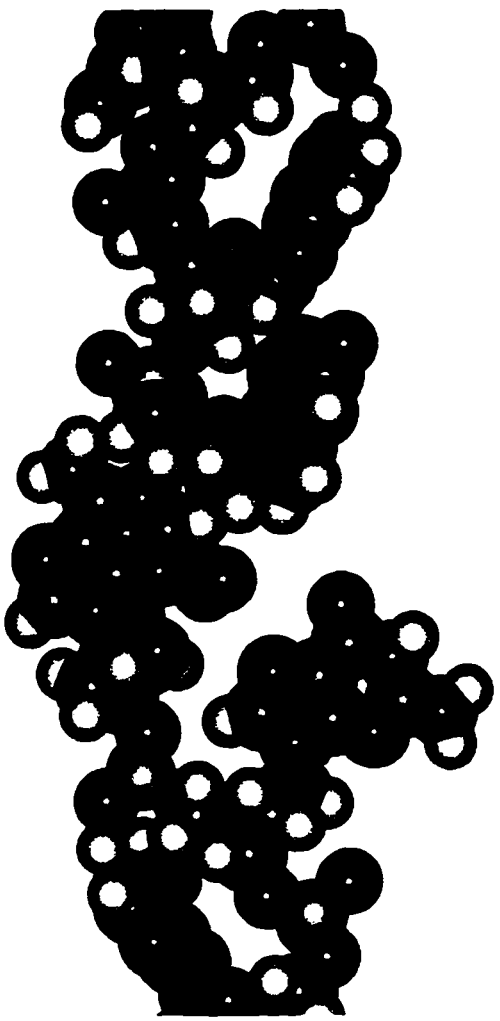

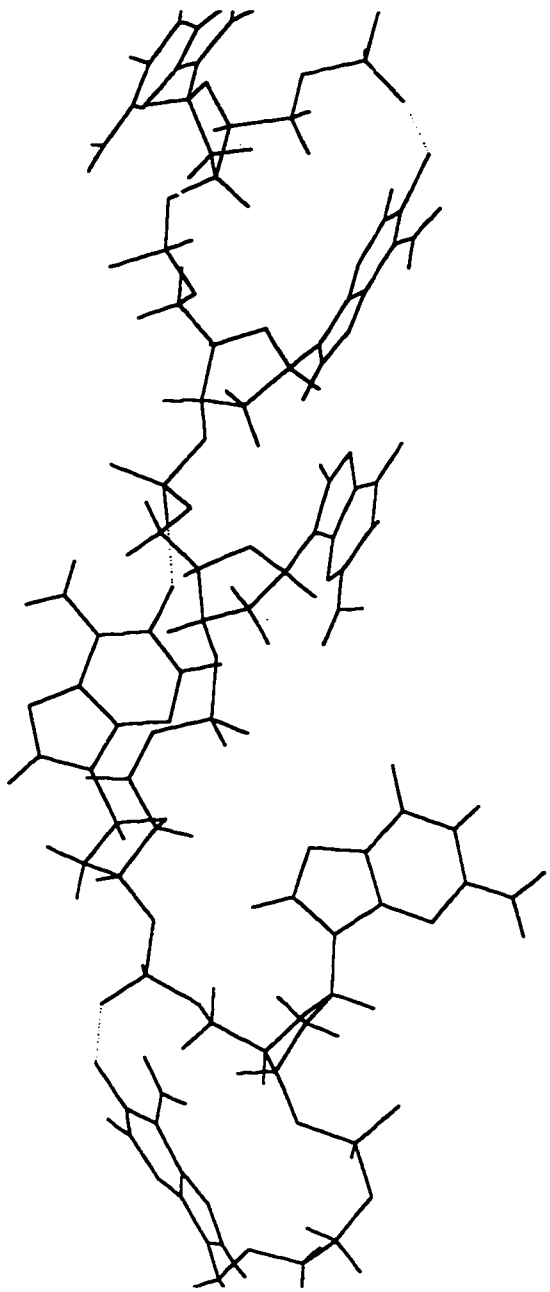

Figure 2: Stereo view of d(A^+-G)5.

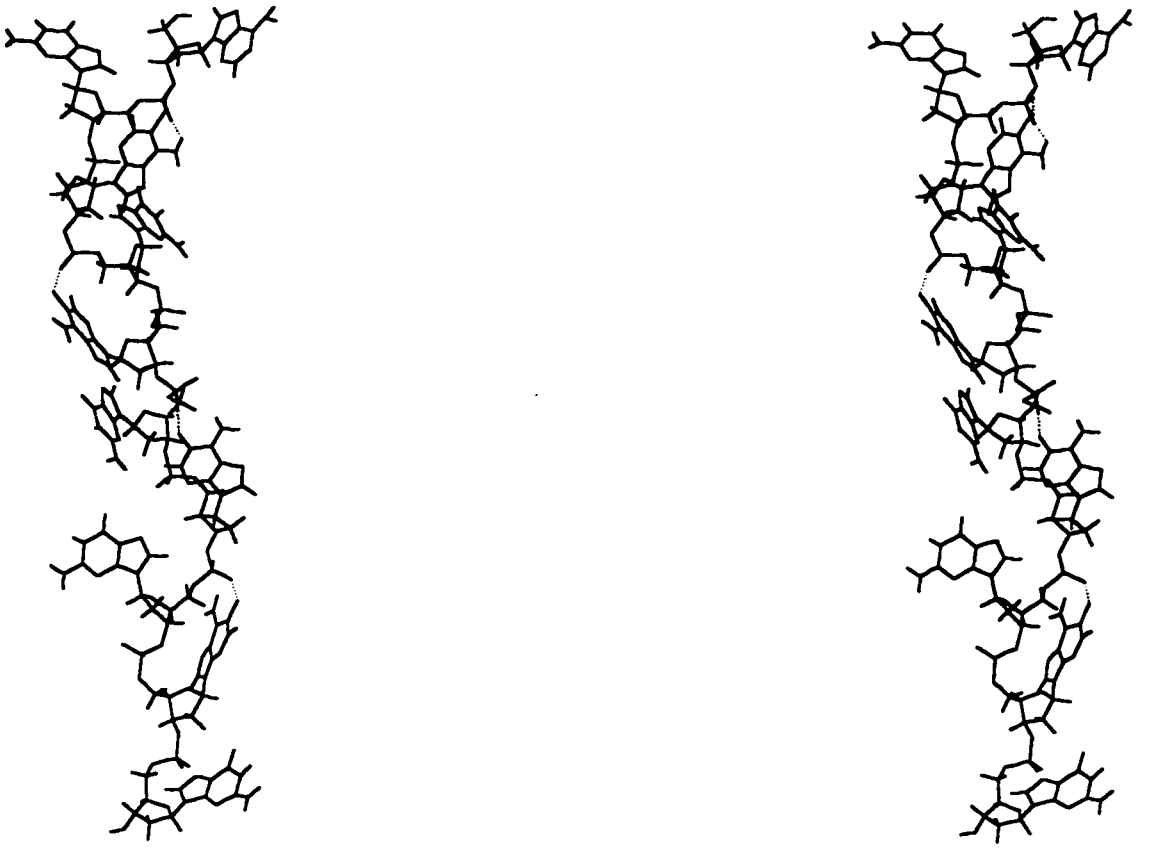

4.4 Discussion

The molecular modeling gives a clearer definition of the secondary structure first glimpsed indirectly from solution studies. It is particularly impressive that the energy minimized structure contains the full variety of non-covalent interactions, base dispositions and left-handed helical sense, independently demonstrated by the various spectroscopic observations (1,2,7).

In comparing $d(A^+\text{-}G)_{10}$ to other biopolymers, one is struck by its similarity in both structural organization and physical properties to α-helical polypeptides. For hydrophilic polypeptides such as polylysine and polyglutamic acid, the optical changes accompanying their pH and thermally induced helix → coil transitions are not unlike those observed for the comparable transition for $d(A^+\text{-}G)_{10}$ (2) which, different from other types of nucleic acid helices, exhibits no evidence of base stacking or base pairing (1). Rather, $d(A^+\text{-}G)_{10}$ is a single-stranded helical oligomer whose dA^+ side chain residues and backbone provide a helical core with stabilizing interactions approximately parallel to the helix axis, and whose dG constituents protrude into the surrounding solvent. The analogy with the properties of the protein α-helix is also indicated by the moderate cooperativity in proton uptake, partially melted intermediate states, and rise in apparent pK_a with oligomer length shown by $d(A^+\text{-}G)_{10}$ (2).

Possible biological roles for the single-stranded helix of $d(A^+\text{-}G)_{10}$ have previously been suggested (1,2) and that protein binding could stabilize the structure under physiological conditions. In fact, the new type of secondary structure described here need not be restricted to the alternating d(A-G) sequence, nor to the deoxyribo- backbone, so

there are likely to be sequence-specific variants, i.e., a family of such structures, just as there are α, π and 3_{10} polypeptide helices. In fact, additional modeling of $d(C^{+}\text{-}T)_n$ indicates that the interactions stabilizing the helical structure are capable of greater sequence versatility than has been tested with the simple alternating A-G sequence. In this respect, C and T residues possess the chemical features to serve analogously to the A and G residues of $d(A^{+}\text{-}G)_{10}$, i.e., to form ionic bonds with backbone phosphates (essentially at neutrality (8)), and to serve as "spacers", respectively. Thus, we can imagine other sequences, particularly repetitive ones, with even all four bases, for which some type of single-stranded helical array stabilized by longitudinal rather than horizontal interactions relative to the helix axis, represents the optimal energy minimum. Such sequences abound in eukaryotic genomes, and their extension has in some cases been associated with a number of genetic diseases (9,10,11). So it would not surprise us if they are found to exhibit a variety of structural and functional consequences in biological systems.

4.5 Acknowledgements

This work was supported by a grant from the National Institutes of Health to J. R. F. (GM42936). L. L. was supported by a predoctoral training grant from the National Institutes of Health (GM08309) and aided by an Autodesk educational software grant.

4.6 References

1. Dolinnaya, N. G., & Fresco, J. R. (1992) *Proc. Natl. Acad. Sci. U.S.A.* **89**, 9242-9246.
2. Dolinnaya, N. G., Braswell, E. H., Fossella, J. A., Klump, H., & Fresco, J. R. (1993) *Biochemistry* **32**, 10263-10270.
3. HyperChem 4.0 (1994) Hypercube Corporation, Waterloo, Ontario, Canada.
4. Weiner, S. J., Kollman, P. A., Nguyen, D. T., & Case, D. A. (1986) *J. Comp. Chem.* **7**, 230-252.
5. Weiner, S. J., Kollman, P. A., Case, D. A., Singh, U. C., Ghio, C., Alagona, G., Profeta, S., Jr., & Weiner, P. (1984) *J. Am. Chem. Soc.* **106**, 765-784.
6. Jorgensen, W. L., Chandrasekhar, J., Madura, J. D., Impey, R. W., & Klein, M. L. (1983) *J. Chem. Phys.* **79**, 926-935.
7. Mukerji, I., Shiber, M. C., Spiro, T. G., & Fresco, J. R. (1995) *Biochemistry*, In press.
8. Lavelle, L., & Fresco, J. R. (1995) *Nucleic Acids Res.* **23**, 2692-2705.
9. Verkerk, A. J. M. H., et al. (1991) *Cell* **65**, 905-914.
10. Miwa, S. (1994) *Nature Genetics* **6**, 3-4.
11. Sutherland, G. R., & Richards, R. I. (1994) *American Scientist* **82**, 157-163.

V. Other possible α-DNA analogs, e.g., $d(C^+-T)_n$

5.1 Introduction, Results and Discussion

It may be said that to some degree it is unfortunate that the first nucleic acid structure was that of the regular double helix. Like an energy landscape that remains frustrated in a local minimum, the double helix "domain" has frustrated exploration of the nucleic acid structural landscape. More recently however, progress has been made in exploring this structural landscape as nucleic acids have been shown to adopt a wider variety of structures, such as quadruplexes, triplexes, parallel duplexes and uniplexes. The Fresco laboratory has in the past and continues to explore this less traveled structural landscape. This brief chapter will discuss the feasibility of additional uniplexes (α-DNA analogs) that are stereochemically possible and energetically feasible. Whether such structures play a role in the structural landscape of biological functionality remains to be determined.

The model derived for $d(A^+-G)_5$ in chapter 4 (1) revealed a helical structure ~12 Å in diameter and ~54 Å in length, maintained by unstacked dA^+ residues lying more or less parallel to the long axis, and linked to the n-1 phosphate oxygens, i.e., one phosphate upstream, by strong ionic and H-bonds mediated by A-N_1H^+ and A-N_6H, while the non-interacting dG residues protrude from the helix. As dC residues have a higher pKa (4.6 for dCMP) than dA residues (pKa = 4.2 for dAMP), it would appear that $d(C^+-T)_n$, with dT residues acting as spacer analogs of dG, may be capable of forming a similar α-

helical type uniplex at a higher pH, and possibly at neutrality (2). The major difference is the shorter length of the structural unit dC^+ in comparison to dA^+:

dC^+, N1 to N4H = 4.6 Å and N1 to $N3H^+$ = 3.2 Å;

dA^+, N9 to N6H = 5.6 Å and N9 to $N1H^+$ = 5.3 Å.

Nonetheless, dA^+ was replaced by dC^+, and dG was replaced by dT, i.e., only the bases were replaced (the existing conformation of the phosphodiester backbone and the deoxyribose moieties was maintained). After all the bases were replaced, they were energy minimized (to remove bad contacts) with respect to the phosphodiester backbone and sugars that were maintained in their original positions, i.e., a rigid lattice with respect to the energy minimizing bases.

Prior to the above base substitutions and energy minimization, a physical model of $d(C^+\text{-}T)_5$ built with unstacked dC^+ residues lying more or less parallel to the long axis, and linked to the n-1 phosphate oxygens was found to be structurally similar to $d(A^+\text{-}G)_5$.

As described in the Methods section below, Na^+ counterions and water were added to this energy minimized structure and placed in a periodic box, and all atoms were minimized (Ep = - 23035 $kcal \cdot mol^{-1}$). The resultant model is discussed below and shown in Figures 1 and 2 with Na^+ and H_2O removed for clarity.

The model obtained for $d(C^+\text{-}T)_5$ reveals a helical structure ~12 Å in diameter and ~51 Å in length, just 3 Å shorter than the $d(A^+\text{-}G)_5$ equivalent. It is formed by a lattice of unstacked dC^+ residues lying more or less parallel to the long axis, linked to the n-1 phosphate oxygens, i.e., one phosphate upstream, by strong ionic and H-bonds mediated

by C-N3H$^+$ and C-N4H, while the non-interacting dT residues protrude from the helix. With the exception of dC_1, which is displaced due to the absence of an upstream phosphate with which to bond (Figure 2), the dC$^+$ residues are held very close and parallel, rather than perpendicular, to the backbone. The distance between the N_1 atoms of successive dC$^+$ residues is ~11 Å. There is no apparent interaction between the dT residues and any other component of the helix; rather, they are unrestricted and accessible to bulk solvent.

In spite of the significant difference between the larger (two ring) purine dA$^+$ and dG residues and the smaller (single ring) pyrimidine dC$^+$ and dT residues, there is a remarkable structural similarity between d(A$^+$-G)5 (Figure 3) and d(C$^+$-T)5 (Figures 1 and 2). The minor differences between d(C$^+$-T)5 and d(A$^+$-G)5 are:

1) the distance between successive dC$^+$ residues is ~11 Å, while for the dA$^+$ residues it is ~12 Å;

2) the overall length of d(C$^+$-T)5 is 51 Å, while for d(A$^+$-G)5 it is 54 Å.

It is important to note that the resultant conformation of d(C$^+$-T)5 in H_2O was obtained with no constraints, as is made evident by the conformational differences between d(C$^+$-T)5 and d(A$^+$-G)5. In this regard, conformational heterogeneity is expected for the first (5') dC residue (which lacks an upstream phosphate partner) and the dT residues, as they are relatively free to rotate about their glycosyl bond.

In sum, the calculations reveal a stable structure maintained by H-bond and Coulombic interactions between the dC$^+$ residues and the oxygens of the phosphodiester backbone.

In the absence of the more typical base stacking and H-bonded base pairing, these must be the major interactions that stabilize the d(C^+-T)5 structure.

The intramolecular binding motif involving protonated base - phosphodiester backbone interaction mediated by ionic and H-bonds has been shown to be stereochemically possible and energetically feasible for both d(C^+-T)5 and d(A^+-G)5. It is therefore reasonable to imagine other sequences, particularly repetitive ones, with even all four bases, for which some type of single-stranded helical array stabilized by longitudinal rather than horizontal interactions relative to the helix axis, represents the optimal energy minimum.

Figure 1: Seven center residues of d(C^+-T)5,

i.e., 5'-d($pC^+_3pT_4pC^+_5pT_6pC^+_7pT_8pC^+_9$)-3' showing ionic and H-bonds as indicated by dashed lines in wire representation (H_2O and Na^+ omitted for clarity). All structures are oriented 5' → 3' top to bottom.

First panel: space filling representation. Atom colors: C, green; N, blue; O, red; P, yellow; H, white.

Second panel: wire representation (same perspective).

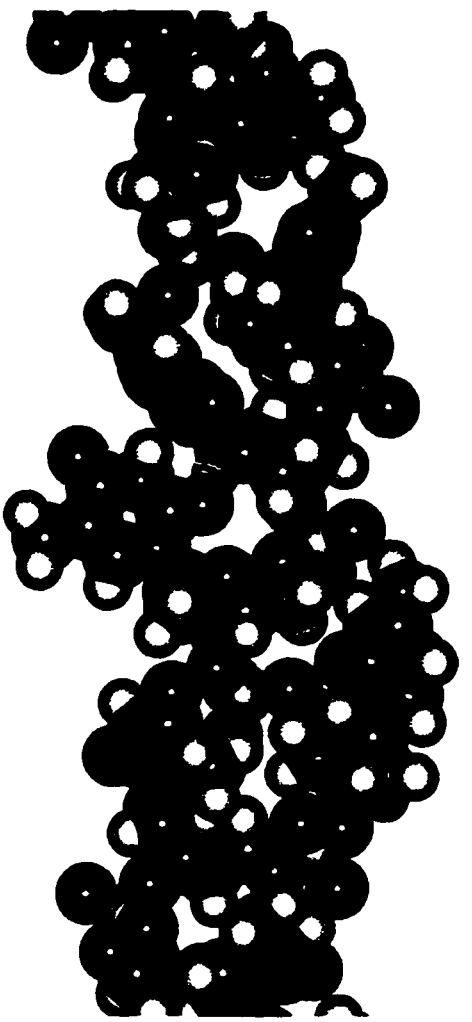

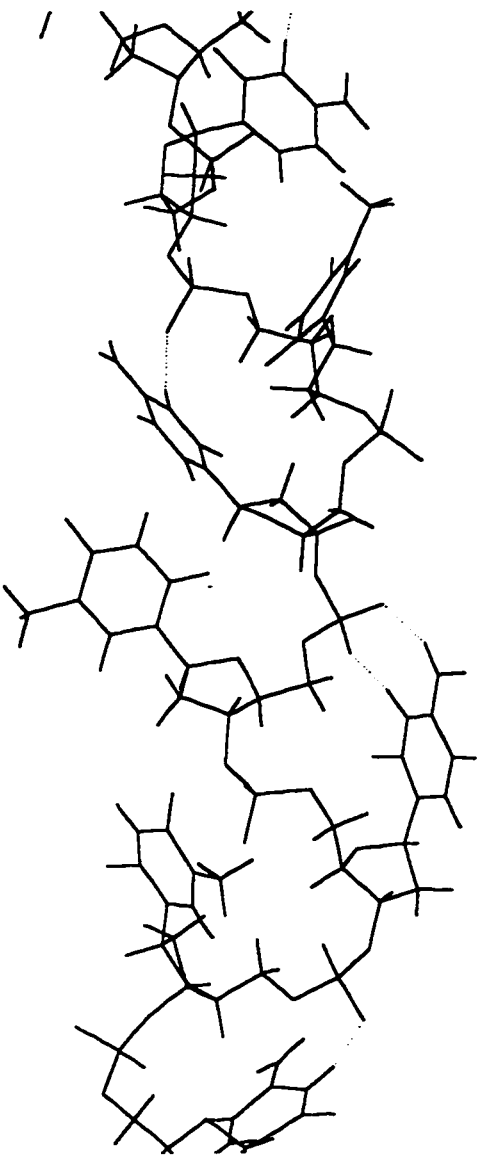

Figure 2: Stereo view of d(C^+-T)5.

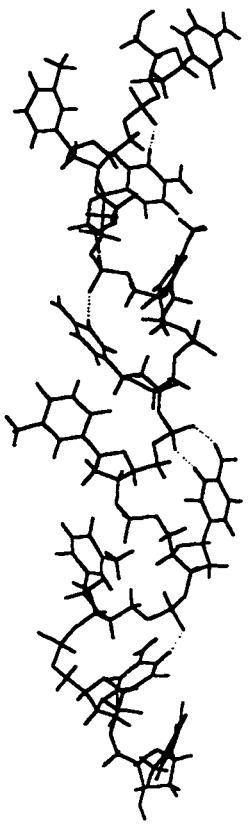

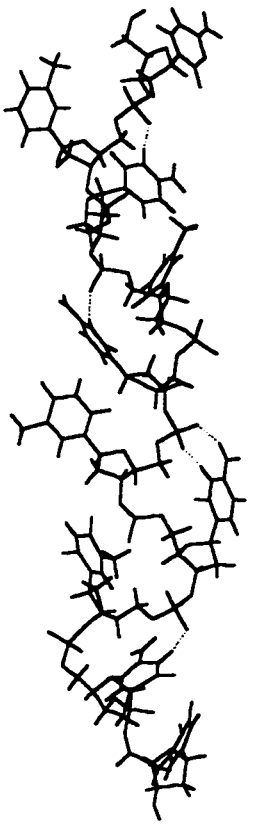

Figure 3: Stereo view of d(A^+-G)5.

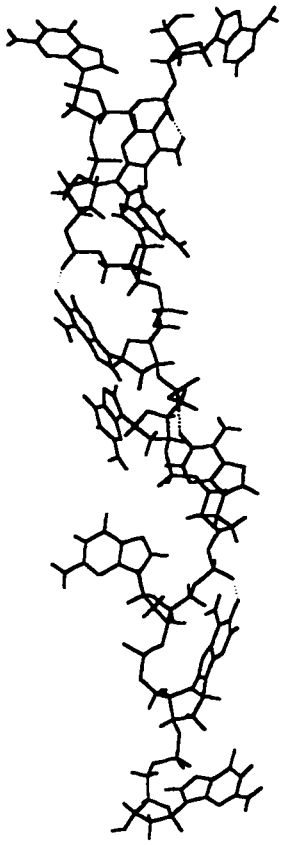

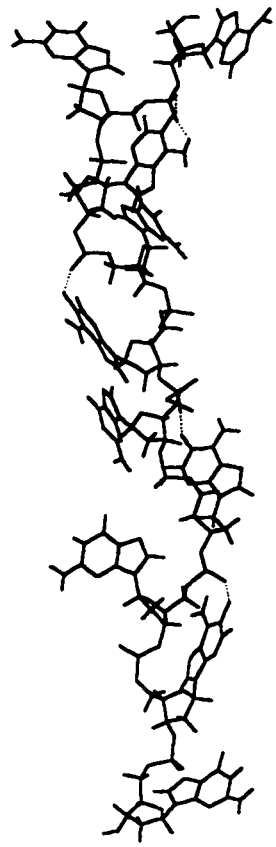

5.2 Methods

The programs and protocols used in the above calculations were the same as those used in chapter 4 (1). Modeling was on an IBM PC, Intel 486DX, 66 MHz, 24 MB RAM with AMBER as part of HyperChem (3). Parameters are those of AMBER 3.0A (4), using the standard unmodified all-atom force field. Base charges for dC^+ are those for dC but with a proton on N3 with bond length of 1.1 Å (force constant of 14 kcal·mol^{-1}·Å^{-2}), bond angle of 117.4° and torsion angle of 0.0° (force constants of 125 and 16 kcal·mol^{-1}·degree^{-2}, respectively) to maintain the proton in the plane of the purine ring. All calculations were done with a 0.5 fs time step (integration step) as the hydrogen atoms were not constrained.

For initial energy minimization of the newly replaced bases, dC^+ and dT, no cutoff distance was used for nonbonded interactions and a distance dependent dielectric constant, ε, [ε = (permittivity of free space) x (scale factor) x (interatomic separation)] was used as a model solvent. For a highly charged system such as this, a dielectric constant scale factor of 4.0 was used (5), and 1-4 scale factors were set at 0.5 for electrostatic and Van der Waals interactions. A conjugate gradient method (Polak-Robiere) was used and convergence set at 0.1 kcal·Å^{-1}·mol^{-1} for the rms gradient. To this energy minimized structure 5 Na^+ ions were placed 1.7 Å equidistant from the oxygen atoms of the non-interacting phosphates and constrained to each oxygen with a force constant of 14 kcal·mol^{-1}·Å^{-2}.

The above structure was then placed in a periodic box, 26 x 26 x 56.1 Å, resulting in a total of 3686 atoms [~1123 H_2O, TIP3P model (equilibrated at 300 °K and 1 atm) (6)]

and energy minimized (Polak-Robiere). Using the AMBER protocol with explicit water molecules, the dielectric constant scale factor was set at 1.0 and 1-4 scale factors were set at 0.5 for electrostatic and Van der Waals interactions. Nonbonding interactions were limited by a switched cutoff, with outer and inner radii of 13 and 9 Å, respectively.

5.3 References

1. Shiber, M.C., Lavelle, L., Fossella, J.A., Fresco, J.R. (1995) *Biochemistry.* **34**, 14293-14299.
2. Lavelle, L., & Fresco, J. R. (1995) *Nucleic Acids Res.* **23**, 2692-2705.
3. HyperChem 4.0 (1994) Hypercube Corporation, Waterloo, Ontario, Canada.
4. Weiner, S. J., Kollman, P. A., Nguyen, D. T., & Case, D. A. (1986) *J. Comp. Chem.* **7**, 230-252.
5. Weiner, S. J., Kollman, P. A., Case, D. A., Singh, U. C., Ghio, C., Alagona, G., Profeta, S., Jr., & Weiner, P. (1984) *J. Am. Chem. Soc.* **106**, 765-784.
6. Jorgensen, W. L., Chandrasekhar, J., Madura, J. D., Impey, R. W., & Klein, M. L. (1983) *J. Chem. Phys.* **79**, 926-935.